Inaugural dissertation

for

obtaining the doctoral degree

of the

Combined Faculty of Mathematics, Engineering and Natural Sciences

of the

Ruprecht - Karls - University

Heidelberg

Presented by

M.Sc. Julia Hermann

born in: Mutlangen, Germany

Oral examination: 13th December 2024

# The interplay between mTORC1 and tRNA wobble modification in generating the protein synthesis machinery

Referees: Prof. Dr. Michaela Frye

Dr. Wilhelm Palm

# I. Summary

The synthesis of cellular proteins requires a significant portion of energy and cellular resources. Thus, protein translation is highly regulated to adapt the proteome output to environmental changes. In mammalian cells, the kinase mTORC1 is activated by environmental inputs from growth factors and nutrients. In turn, mTORC1 enhances anabolic processes, such as synthesizing proteins and lipids, while suppressing protein catabolism. Although the molecular mechanisms by which mTORC1 regulates protein synthesis are well studied, it is still unclear how cells can adapt to the inactivation of mTORC1. In my PhD project, I performed genome-wide CRISPR screens to systematically identify genes crucial for adapting mammalian cells to the inactivation of mTORC1. Particularly striking hits were tRNA-modifying enzymes that form $mcm^5s^2$ modifications at wobble uridines of tRNAs ($U_{34}$-enzymes): Elongator and Ctu1/2. Under mTORC1 inhibition, Elongator and Ctu1/2 became essential for cell proliferation *in vitro* and in tumors *in vivo*. As the functional role of tRNA wobble modifications in mammalian cells was poorly understood, I first characterized the impact of $U_{34}$-enzymes on protein synthesis. By integrating nascent proteomics, steady-state proteomics, and ribosome profiling, I found that tRNA wobble modifications globally affect protein synthesis by promoting efficient decoding of VAA codons. Notably, $U_{34}$-enzymes enhanced the synthesis of ribosomal proteins, but steady-state protein levels were only slightly affected. Finally, I assessed the impact of mTORC1 inhibition in $U_{34}$-enzyme-deficient cells and found that the simultaneous suppression of mTORC1 and $U_{34}$-enzymes depleted cells of ribosomal proteins, resulting in global translation inhibition. Hence, my PhD project revealed a molecular mechanism by which mTORC1 and tRNA wobble modification cooperate to generate the protein synthesis machinery and thus maintain cellular translation capacity and cell proliferation.

# II. Zusammenfassung

Die Synthese von zellulären Proteinen erfordert einen erheblichen Anteil an Energie und zellulären Ressourcen. Daher wird die Proteintranslation stark reguliert, um das Proteom an Umweltveränderungen anzupassen. In Säugetierzellen wird die Kinase mTORC1 durch die Zufuhr von Wachstumsfaktoren und Nährstoffen aus der Umwelt aktiviert. Im Gegenzug fördert mTORC1 anabole Prozesse wie die Synthese von Proteinen und Lipiden, während der Proteinkatabolismus unterdrückt wird. Obwohl die molekularen Mechanismen, durch die mTORC1 die Proteinsynthese reguliert, gut erforscht sind, ist noch unklar, wie sich Zellen an die Inaktivierung von mTORC1 anpassen können. In meinem Promotionsprojekt habe ich genomweite CRISPR-Screens durchgeführt, um systematisch Gene zu identifizieren, die in Säugetierzellen für die Anpassung an die Inaktivierung von mTORC1 entscheidend sind. Besonders auffällige Treffer waren tRNA-modifizierende Enzyme, die $mcm^5s^2$-Modifikationen an Wobble-Uridinen von tRNAs bilden ($U_{34}$-Enzyme): Elongator und Ctu1/2. Unter Hemmung von mTORC1 wurden Elongator und Ctu1/2 für die Zellproliferation *in vitro* und in Tumoren *in vivo* essenziell. Da die funktionelle Rolle von tRNA-Wobble-Modifikationen in Säugetierzellen nur unzureichend verstanden war, charakterisierte ich zunächst die Auswirkungen von $U_{34}$-Enzymen auf die Proteinsynthese. Durch die Einbindung von neusynthetisierter Proteomik, Gleichgewichts-Proteomik und Ribosomen-*Profiling* konnte ich feststellen, dass tRNA-Wobble-Modifikationen die Proteinsynthese global beeinflussen, indem sie die effiziente Dekodierung von VAA-Codons fördern. Insbesondere verstärkten $U_{34}$-Enzyme die Synthese von ribosomalen Proteinen, während die Proteinkonzentrationen im stationären Zustand nur geringfügig beeinflusst wurden. Schließlich untersuchte ich die Auswirkungen einer mTORC1-Hemmung in Zellen defizient für $U_{34}$-Enzyme und stellte fest, dass die gleichzeitige Unterdrückung von mTORC1 und $U_{34}$-Enzymen den Zellen ribosomale Proteine entzieht, was zu einer globalen Translationshemmung führt. Mein Promotionsprojekt deckte somit einen molekularen Mechanismus auf, durch den mTORC1 und die tRNA-Wobble-Modifikation zusammenwirken, um die Proteinsynthesemaschinerie zu generieren und damit die zelluläre Translationskapazität und das Zellwachstum aufrechterhalten.

# Table of contents

# III. Acknowledgements

First, I am incredibly grateful to my supervisor, Dr. Wilhelm Palm, for the excellent support I received during my doctoral thesis. The opportunity to become part of the laboratory, work independently, and count on support at all times was not a matter of course. I am grateful for the attentive and constructive advice and discussions, which contributed significantly to the success of this thesis. Moreover, I thank Dr. Wilhelm Palm very much for his tireless work in optimizing the manuscript. I express my gratitude for the opportunity to cooperate with other working groups, which contributed significantly to the success of my project. Not least, participating in an international conference was a valuable experience for me, for which I am very grateful.

I want to thank the members of my PhD defense committee, Prof. Dr. Michaela Frye, Prof. Dr. Almut Schulze, and Prof. Dr. Bernd Bukau, for their participation and the evaluation of my work. I thank my thesis advisory committee members, Prof. Dr. Almut Schulze and Prof. Dr. Michael Knop, for their valuable contributions and support during my time as a doctoral student.

To Dr. Dominic Helm and Martin Schneider from the DKFZ Proteomics Core Facility, many thanks for the help with the experimental set-up and analysis of the proteomics experiments. I thank Prof. Dr. Jeroen Krijgsveld and Dr. Toman Borteçen, as well as Dr. Fabricio Loayza-Puch and Alexander Kowar, for their help with performing and analyzing nascent proteomics and ribosome profiling experiments, which are an essential part of my work. In addition, I want to thank Prof. Dr. Johannes Zuber and his lab members for performing the mouse experiments, providing resources, and helping with bioinformatic analyses. I want to thank all members of the Loayza-Puch lab, Simons lab, and Teleman lab for their feedback and insightful discussions during our meetings.

My sincere thanks to all former and current members of the Palm Lab for their help and support and the pleasant working atmosphere. I especially thank Dr. Catarina da Silva Pechincha, Dr. Edoardo Ratto, Rafael Paschoal de Campos, and Aslihan Inal for their friendly conversations, words of encouragement when needed, and the time spent together outside the lab.

I want to thank my dear family and friends from the bottom of my heart for their continuous support. Special thanks go to my parents, who have supported me along the way and have always been there for me. I want to thank my brother Chris for proofreading this thesis. I am incredibly grateful to my twin sister Tina and my partner Yannik for their unconditional support and for giving me the strength to walk this long path successfully.

From the bottom of my heart, I say: Thank you.

# IV. Disclaimer

The work described in my PhD thesis is part of the manuscript:

Julia Hermann, Toman Borteçen, Robert Kalis, Alexander Kowar, Catarina Pechincha, Vivien Vogt, Martin Schneider, Dominic Helm, Jeroen Krijgsveld, Fabricio Loayza-Puch, Johannes Zuber, Wilhelm Palm. mTORC1 cooperates with tRNA wobble modification to sustain the protein synthesis machinery.

The manuscript is currently being revised by a peer-reviewed journal.

Most of the content in my PhD thesis is described and shown in this manuscript. The study was initially designed and conceived by me and Wilhelm Palm, with contributions from all authors, as described in chapter *4 Results*. For details, see *V. Contributions.*

The method sections describing steady-state proteomics (chapter 3.2.22) and related analyses (chapter 3.2.23) contain protocols Dominic Helm and Martin Schneider kindly provided from the DKFZ Proteomics Core Facility. The method sections describing nascent proteomics (chapters 3.2.24 and 3.2.25) and related analyses (chapters 3.2.26 and 3.2.27) contain protocols that Toman Borteçen kindly provided. The method sections describing ribosome profiling (chapters 3.2.16 and 3.2.17) and related analyses (chapter 3.2.18) contain protocols that Alexander Kowar kindly provided. Robert Kalis and Vivien Vogt kindly provided the method section describing animal experiments (chapter 3.2.28).

Figure 1 has been adapted from (McMahon & Ruggero, 2018) and figure 2 from (Sabatini, 2017).

# V. Contributions

The inducible Cas9 (iCas9) cell lines were generated by Catarina Pechincha and Melanie de Almeida.

Robert Kalis performed the initial steps of the screen sequencing analysis, and I performed further read count analysis.

I prepared samples for steady-state proteomics; Dominic Helm and Martin Schneider at the DKFZ Proteomics Core Facility performed further processing and analyses.

I did the initial steps of sample preparations for nascent proteomics, and further sample preparations and statistical analyses were done by Toman Borteçen.

Alexander Kowar and I prepared samples for ribosome profiling; Alexander Kowar generated ribosome profiling libraries and conducted statistical analyses.

Robert Kalis and Vivien Vogt performed mice experiments.

A detailed description of contributions is mentioned in chapter *3.2 Methods* as well as in chapter *4 Results* in the main text and figure legends.

# VI. List of abbreviations

| | |
|---|---|
| **ATF4** | activating transcription factor 4 |
| **A site** | aminoacyl site |
| **AMPK** | AMP-activated protein kinase |
| **BSA** | bovine serum albumin |
| **Ctu1/2** | cytosolic thiouridylase subunits 1/2 |
| **DEPTOR** | DEP-domain containing mTOR interacting protein |
| **DMSO** | dimethyl sulfoxide |
| **4E-BP1** | eIF4E Binding Protein 1 |
| **FBS** | fetal bovine serum |
| **dsgRNA** | dual small guide RNA |
| **eEF** | eukaryotic elongation factor |
| **eIF** | eukaryotic initiation factor |
| **Elp1-6** | Elongator complex subunits 1-6 |
| **ER** | endoplasmatic reticulum |
| **E site** | exit site |
| **FC** | fold change |
| **GAP** | GTPase-activating protein |
| **GCN2** | general control non-derepressible 2 |
| **GCN4** | general control non-derepressible 4 |
| **gDNA** | genomic DNA |
| **HEK** | human embryonic kidney |
| **HIF1α** | hypoxia-inducible factor 1α |
| **iCas9** | inducible Cas9 |
| **iDKO** | inducible double knockout |

| | |
|---|---|
| **IGF-1** | insulin-like growth factor-1 |
| **iKO** | inducible knockout |
| **IRES** | internal ribosome entry site |
| **ISR** | integrated stress response |
| **KO** | knockout |
| **$mcm^5s^2U_{34}$** | 5-methoxycarbonylmethyl-2-thiouridine |
| **MEF** | mouse embryonic fibroblast |
| **mLST8** | mammalian lethal with Sec13 protein 8 |
| **mRNA** | messenger RNA |
| **mTORC1** | mechanistic target of rapamycin complex 1 |
| **mTORC2** | mechanistic target of rapamycin complex 2 |
| **$m^1A$** | $N^1$-methyladenosine |
| **$m^6A$** | $N^6$-methyladenosine |
| **$m^5C$** | 5-methylcytosine |
| **$m^7G$** | 7-methylguanylate |
| **NGS** | next-generation sequencing |
| **PRAS40** | proline-rich Akt substrate of 40 kDa |
| **PIC** | 43S preinitiation complex |
| **PI3K** | phosphoinositide 3-kinase |
| **P site** | peptidyl site |
| **Raptor** | regulatory protein associated with mTOR |
| **REDD1** | regulated in DNA damage and development 1 |
| **Rictor** | rapamycin-insensitive companion of mTOR |
| **rRNA** | ribosomal RNA |
| **rtTA3** | reverse tetracycline transactivator 3 |

| | |
|---|---|
| **SD** | standard deviation |
| **SEM** | standard error of the mean |
| **sgRNA** | small guide RNA |
| **S6K1/2** | p70S6 Kinase 1/2 |
| **SREBP1/2** | sterol regulatory element-binding protein 1/2 |
| **TC** | ternary complex |
| **TFEB** | transcription factor EB |
| **TOP** | 5'-terminal oligopyrimidine |
| **TOS** | target of rapamycin signaling |
| **tRNA** | transfer RNA |
| **TSC** | tuberous sclerosis complex |
| **$U_{34}$** | wobble uridine |
| **ULK1** | unc-51-like kinase 1 |
| **UPR** | unfolded protein response |
| **5‘ UTR** | 5‘ untranslated region |
| **WT** | wildtype |

# VII. List of tables

# VIII. List of figures

# 1 Introduction

## 1.1 Protein synthesis in mammalian cells

Proteins account for more than 50 % of a mammalian cell's dry mass, and their synthesis requires significant energy and cellular resources (Buttgereit & Brand, 1995; Palm & Thompson, 2017). The protein synthesis machinery itself makes up a large proportion of total protein, including transfer RNAs (tRNAs), ribosomes, translation factors, and messenger RNAs (mRNAs) (Alberts *et al*, 2008; Preiss & Hentze, 2003). Specifically, ribosomal proteins account for about 4-6 % (Nagaraj et al, 2011; Wisniewski et al, 2014). Thus, the production and the activity of the protein synthesis machinery are regulated by various signaling pathways and covalent modifications to maintain normal cell function and homeostasis (An & Harper, 2020; Hershey et al, 2012).

During protein synthesis, a gene's mRNA sequence is translated into a protein's amino acid sequence on ribosomes in the cytoplasm of eukaryotic cells (Alberts *et al.*, 2008). Mechanistically, the tRNA acts as an adaptor molecule that reads the mRNA nucleotide sequence in triplets (codons) and incorporates the corresponding amino acid into the growing polypeptide chain (Agris, 2004; Alberts *et al.*, 2008). As there are only 20 proteinogenic amino acids but 64 different nucleotide combinations, most amino acids are encoded by several synonymous codons, known as the degeneracy of the genetic code (Crick, 1966b).

### 1.1.1 Components of the protein synthesis machinery

As described above, tRNAs deliver the amino acid encoded by the mRNA codon. tRNA molecules form a complex three-dimensional structure, including four short double-helical segments (Avcilar-Kucukgoze & Kashina, 2020). Aminoacyl-tRNA synthetases attach the cognate amino acid on the 3’ end of the tRNA molecule. An unpaired region of three nucleotides in the anticodon loop forms the anticodon that recognizes the codon in an mRNA sequence (Alberts *et al.*, 2008; Avcilar-Kucukgoze & Kashina, 2020). During the translation process, amino acids are stepwise added to the C-

terminus of the growing polypeptide chain through energetically favorable peptide bonds (Alberts *et al.*, 2008).

Ribosomes, along with tRNAs, are another critical component of the protein synthesis machinery (Dalla Venezia *et al*, 2019). In eukaryotes, the 80S ribosomes consist of ribosomal proteins and several ribosomal RNA (rRNA) molecules assembled into a 60S large subunit (5S, 5.8S, 28S rRNAs and 47 ribosomal L-proteins) and a 40S small subunit (18S rRNA and 33 ribosomal S-proteins) (Baßler & Hurt, 2019; Hurt *et al*, 2023). During translation, the small subunit serves as a scaffold, ensuring that tRNAs are correctly aligned with the mRNA codons (Alberts *et al.*, 2008). The large subunit facilitates the formation of peptide bonds that join amino acids into a polypeptide chain (Alberts *et al.*, 2008).

### 1.1.2 The translation process in mammalian cells

Protein translation in mammalian cells is a cycling process divided into initiation, elongation, termination, and recycling of ribosomes (Shu *et al*, 2020). The rate-limiting step is usually the initiation phase (Hinnebusch, 2014). In eukaryotic cells, most mRNAs carry a 7-methylguanylate ($m^7G$) cap at their 5‘ end (Furuichi, 2015). The eukaryotic initiation factor 4F (eIF4F) complex binds to the $m^7G$ cap during cap-dependent translation initiation (Shu *et al.*, 2020). The eIF4F complex consists of the eukaryotic initiation factors 4E (eIF4E), 4G (eIF4G), and 4A (eIF4A) (Bhat *et al*, 2015; Merrick, 2004; Shu *et al.*, 2020). Upon eIF4F binding, the 43S preinitiation complex (PIC) is assembled and attached to the mRNA to form the 48S complex (Bhat *et al.*, 2015; Shu *et al.*, 2020). The 43S PIC consists of the ternary complex (TC) containing aminoacylated initiator methionine tRNA, GTP, and eukaryotic initiation factor 2 (eIF2), the 40S ribosomal subunit, and the eukaryotic initiation factors 1 (eIF1), 1A (eIF1A), and F3 (eIF3) (Bhat *et al.*, 2015; Shu *et al.*, 2020). Then, the mRNA’s 5‘ untranslated region (5‘ UTR) is scanned for the first start codon, an ATG, in an appropriate context (Kozak, 1989). Besides canonical start codons, more up- or downstream initiation sites and non-ATG codons can serve as alternative start codons under certain conditions (Kearse & Wilusz, 2017; Lee *et al*, 2012). When the PIC identifies a start codon, the 60S ribosomal subunit is recruited while eIFs are released, yielding the mature 80S

ribosome, which starts the elongation process (Shu *et al.*, 2020). The eukaryotic elongation factors 1 (eEF1) and 2 (eEF2) mediate the translocation of tRNAs, carrying the respective amino acid encoded by the mRNA codon, to the aminoacyl site (A site) of the ribosome (Dever *et al*, 2018; Shu *et al.*, 2020). The elongation factors further catalyze the translocation of the ribosomal subunits along the mRNA, allowing the aminoacylated tRNA to reach the peptidyl site (P site) of the ribosome (Dever *et al.*, 2018). At the P site, amino acids form peptide bonds with the growing polypeptide chain before the tRNA moves to the exit site (E site) and gets released (Dever *et al.*, 2018). The ribosomes move at different elongation speeds over different codons, as rare codons slow the elongation process. Thus, the codon usage bias affects the translation efficiency of mRNAs (Saikia *et al*, 2016). Termination of translation occurs when the ribosome encounters a stop codon, triggering the coordinated action of the eukaryotic release factors 1 (eRF1) and 3 (eRF3) (Dever *et al.*, 2018; Shu *et al.*, 2020). The synthesized protein is released, tRNAs dissociate, and ribosomal subunits are recycled for the following mRNA sequence (Dever & Green, 2012).

## 1.2 RNA modifications

More than 170 RNA modifications have been identified to coordinate protein translation and mRNA metabolism. Although RNA modifications have been known for several years, many physiological roles remain to be determined, as genome-wide techniques only recently allow the detection and quantification of rare modifications with high resolution (whole paragraph according to (Frye et al, 2018)).

RNA modifications have been studied for the different RNA types involved in the translation process: mRNAs, rRNAs, and tRNAs. In general, RNA modifications are introduced, recognized, and erased by specific proteins to coordinate transcription and protein output and thus modulate cellular responses (Delaunay *et al*, 2024; Shi *et al*, 2020). Besides the 5‘ cap and 3‘ polyadenylation, the most abundant internal mRNA modification is $N^6$-methyladenosine ($m^6A$), which alters mRNA processing and transport and, thus, the turnover and translation of specific transcripts (Boulias & Greer, 2023). Human rRNAs mainly carry pseudouridines ($\Psi$), 2‘-O-methyls, and base methylations, essential for rRNA biogenesis (Roundtree *et al*, 2017). Besides

modifications in mRNAs and rRNAs, tRNAs carry more than 100 different types of modifications (Frye *et al.*, 2018). A human tRNA molecule carries between 11 to 13 modifications, ranging from isomerization and methylation events, such as 5-methylcytosine ($m^5C$), $N^1$-methyladenosine ($m^1A$), Ψ or inosine (I), to the complex addition of multistep modifications (Frye *et al.*, 2018; Schimmel, 2018). The tRNA modification functions, among others, affect tRNA stability, localization, and decoding efficiency (Roundtree *et al.*, 2017). However, relatively little is known about the mechanistic role of many tRNA modifications in RNA processing or protein synthesis.

### 1.2.1 tRNA wobble uridine-modifying enzymes ($U_{34}$-enzymes)

During protein synthesis, many tRNAs can recognize multiple codons that only differ in the last nucleoside of the codon at tRNA´s position 34, known as the wobble position (Figure 1). According to the wobble hypothesis, if there is uridine at the anticodon wobble position ($U_{34}$), the tRNA would recognize the cognate adenosine (A) and wobble to guanosine (G). However, chemical modifications at $U_{34}$ were identified, which restrict wobble base pairing and, thus, increase the accuracy and efficiency of anticodon-codon interactions (whole paragraph according to (Crick, 1966a; Schaffrath & Leidel, 2017)).

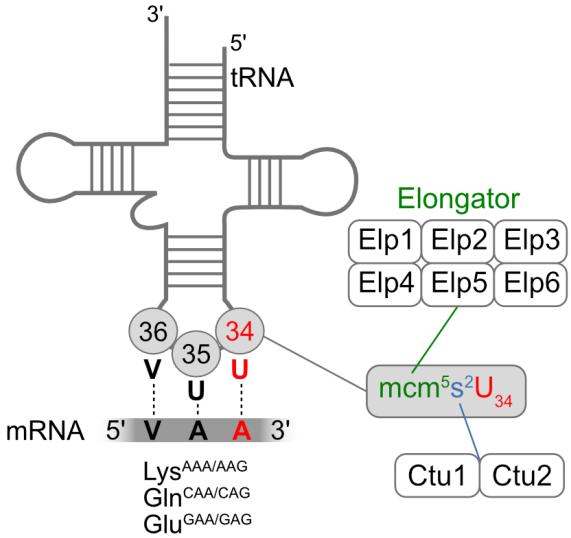


**Figure 1 – tRNA wobble modifications enhance the efficiency of VAA codon translation.**
Schematic representation of $mcm^5s^2$ modifications at the anticodon wobble uridine ($U_{34}$) catalyzed by the Elongator complex (Elp1-Elp6) and Cytosolic Thiouridylase (Ctu1/2). Amino acids that require modification for efficient translation are lysine (AAA), glutamine (CAA), and glutamate (GAA), referred to as VAA codons. Adapted from (McMahon & Ruggero, 2018).

A necessary $U_{34}$ modification in eukaryotic tRNAs is the 5-methoxycarbonylmethyl-2-thiouridine ($mcm^5s^2U_{34}$) (Figure 1). This tRNA wobble modification is highly conserved in humans, yeast, worms, and plants (Chen et al, 2009; Leimkuhler et al, 2017). Wobble uridines are modified by two tRNA wobble uridine-modifying enzymes ($U_{34}$-enzymes): the Elongator complex (Elp1-6) and the Cytosolic Thiouridylase Subunits 1/2 (Ctu1/2). The Elongator complex consists of two complexes of the six subunits Elp1-6 and catalyzes the formation of the $mcm^5$ group (Karlsborn *et al*, 2014). Ctu1-Ctu2 form a heterodimer and add a thiol group to form $mcm^5s^2U_{34}$ (Dewez *et al*, 2008). Amino acids that require $mcm^5s^2U_{34}$ for efficient translation are lysine (AAA), glutamine (CAA), and glutamate (GAA), collectively referred to as VAA (Figure 1). Those amino acids are also encoded by a second codon, VAG, that is efficiently translated without tRNA wobble modification (Dewez *et al.*, 2008; Huang *et al*, 2005; Karlsborn *et al.*, 2014; Schaffrath & Leidel, 2017). The tRNA wobble modification changes the physicochemical properties of uridine (Schaffrath & Leidel, 2017). The thiolation increases the conformational stability of uridine, which favors interactions with adenosine, while the $mcm^5$ group modulates the electrons in the ring to support hydrogen bonds with guanosine (Schaffrath & Leidel, 2017). In humans, mice, and *S. pompe*, the $mcm^5$ group is required to add a thiol group (Schaffrath & Leidel, 2017).

### 1.2.2 The physiological and pathological roles of tRNA $U_{34}$ wobble modifications

Defects in the formation of $mcm^5s^2U_{34}$ have been associated with various phenotypes in different organisms (Schaffrath & Leidel, 2017). In fission yeast, the loss of $U_{34}$-enzymes reduced the translation of the AAA-rich stress transcription factors Atf1 and Pcr1 (Fernández-Vázquez *et al*, 2013). Consequently, Elp3-deficient cells were hypersensitive to stresses, including elevated temperatures or oxidative stress (Fernández-Vázquez *et al.*, 2013). Furthermore, ribosome profiling experiments in $U_{34}$-enzyme-deficient budding yeast and worms showed a decreased translation speed, specifically at VAA codons (Nedialkova & Leidel, 2015; Zinshteyn & Gilbert, 2013). In some studies, overexpression of hypomodified tRNAs that decode lysine (AAA) or glutamine (CAA) rescued the decreased translation speed of the respective codons in $U_{34}$-enzyme-deficient yeast cells (Fernández-Vázquez *et al.*, 2013; Nedialkova &

Leidel, 2015). Moreover, the loss of $U_{34}$-enzyme triggered proteotoxic stress due to the aggregation of endogenous misfolded proteins (Nedialkova & Leidel, 2015). In another yeast study, the reduced translation efficiency at VAA codons did not affect global protein output but activated the integrated stress response (Zinshteyn & Gilbert, 2013).

Interestingly, in budding yeast, the thiolation status of tRNA $U_{34}$ was coupled with the availability of sulfur amino acids. The loss of tRNA thiolation reduced the synthesis of VAA-rich transcripts critical to adjust cell metabolism and growth accordingly. Thus, yeast cells adapted protein translation and metabolic output to the availability of methionine and cysteine (whole paragraph according to (Laxman *et al*, 2013)).

As described above, the loss of tRNA wobble modifications rendered yeast cells hypersensitive to environmental stresses such as elevated temperatures, oxidative stress, or nutrient starvation (Fernández-Vázquez *et al.*, 2013; Laxman *et al.*, 2013; Nedialkova & Leidel, 2015; Zinshteyn & Gilbert, 2013). Furthermore, yeast cells lacking $U_{34}$-enzymes became hypersensitive to inhibiting the kinase mechanistic target of rapamycin complex 1 (mTORC1), a central regulator of protein translation (Nedialkova & Leidel, 2015; Zinshteyn & Gilbert, 2013). As mTORC1 inhibition recapitulates a starvation-like phenotype, the hypersensitivity of $U_{34}$-enzyme-deficient yeast cells to mTORC1 inhibitors was also interpreted as increased stress sensitivity (Nedialkova & Leidel, 2015; Zinshteyn & Gilbert, 2013). In budding yeast, rapamycin sensitivity has been linked to a critical role of wobble tRNA modifications in TOR-dependent regulation of cell growth under various nitrogen levels (Scheidt *et al*, 2014). Moreover, in fission yeast, Elongator promoted the translation of TORC1 repressors and TORC2 components (Candiracci *et al*, 2019). Thus, Elongator has been mechanistically connected with the TORC signaling pathway to sustain cell differentiation under nutrient starvation (Candiracci *et al.*, 2019). Whether $U_{34}$-enzyme-deficient cells in higher eukaryotes are also hypersensitive to mTORC1 inhibitors was not shown.

Interestingly, several studies in mammalian cells and mouse models indicated that different cancer types depend on tRNA wobble modifications to translate VAA codon-rich oncoproteins (Delaunay *et al*, 2016; Ladang *et al*, 2015; Rapino *et al*, 2018; Xu *et al*, 2019). Mouse models of intestinal tumors revealed a critical role of Elp3 during tumor initiation by promoting codon-dependent Sox9 translation (Ladang *et al.*, 2015). Moreover, $mcm^5s^2U_{34}$ modifications were crucial for the translation of further

transcripts. DEK was identified as being enriched in VAA codons (Delaunay *et al.*, 2016). Consequently, Ctu1/2 and Elp3 were required for efficient DEK translation, which induced the synthesis of LEF1, a mediator of malignant breast cancer progression (Delaunay *et al.*, 2016). In a $BRAF^{V600E}$-driven melanoma model, tRNA wobble modifications maintained high protein levels of the VAA-rich transcription factor hypoxia-inducible factor 1α (HIF1α), resulting in critical metabolic adaptations in melanoma (Rapino *et al.*, 2018). Thus, the loss of Ctu1/2 or Elp3 decreased HIF1$\alpha$ levels and re-sensitized melanoma cells to targeted therapy (Rapino *et al.*, 2018). A genome-wide CRISPR screen in gallbladder cancer showed that the loss of Elp5 impaired the translation of the VAA-rich mRNA of hnRNPQ, which is critical to drive P53 (Xu *et al.*, 2019). Gallbladder cancer with low Elp5/ hnRNPQ/ P53 levels poorly responded to the standard treatment gemcitabine. Thus, in contrast to the melanoma study, an increased tRNA wobble modification activity would favor the treatment outcome in this case (Xu *et al.*, 2019).

As neurons are susceptible to changes in translation speed, it is not surprising that a defect in the formation of tRNA wobble modifications was associated with neurodegeneration (Hawer *et al*, 2018). The loss of Elp3 induced the unfolded protein response (UPR) in the ER of mouse brains due to a reduced translation speed, leading to neurological defects (Laguesse *et al*, 2015). Moreover, a critical role of $mcm^5s^2U_{34}$ was demonstrated for sporadic amyotrophic lateral sclerosis (ALS) patients (Bento-Abreu *et al*, 2018).

Taken together, as described above the loss of tRNA $U_{34}$ wobble modifications was associated with different phenotypes in yeast and mammals. Two models were developed to explain these phenotypes. The first model is based on the observation that an individual VAA-rich transcript is translated inefficiently without $U_{34}$-enzymes. As a result, less protein output mediates loss-of-function phenotypes. The second model explains the more pleiotropic phenotypes, such as protein aggregation and proteotoxic stress, observed in $U_{34}$-enzyme-deficient cells. The codon-specific defects in protein synthesis lead to an imbalance between protein synthesis and folding. Consequently, changes in proteome output and downstream cellular signaling trigger proteotoxic stress and protein aggregation (whole paragraph according to (Schaffrath & Leidel,

2017)). In the future, more studies are needed to understand how $U_{34}$-enzymes affect protein synthesis mechanistically.

## 1.3 Mechanistic target of rapamycin complex 1 (mTORC1)

Besides covalent modifications in components of the protein synthesis machinery, signaling pathways are central to regulate the synthesis of proteins, particularly the mTORC1 signaling pathway (Ben-Sahra & Manning, 2017; Saxton & Sabatini, 2017). Activated by environmental inputs from growth factors and nutrients, the kinase mTORC1 phosphorylates multiple effectors to enhance anabolic processes while blocking catabolic processes in the cell.

The serine/ threonine kinase mTOR, which belongs to the PI3K-related kinase family, is the catalytic subunit of mTORC1 and the mechanistic target of rapamycin complex 2 (mTORC2) (Guertin *et al*, 2006; Hara *et al*, 2002; Kim *et al*, 2002). Besides mTOR, mTORC1 consists of the regulatory protein associated with mTOR (Raptor) and the mammalian lethal with Sec13 protein 8 (mLST8) (Saxton & Sabatini, 2017). Raptor binds to the TOR signaling (TOS) motif present on mTORC1 substrates, which allows the recruitment of mTORC1 effectors (Nojima *et al*, 2003). mLST8 stabilizes the kinase via direct interaction with mTOR (Yang *et al*, 2013). Moreover, Raptor is regulated by the inhibitory components proline-rich Akt substrate of 40 kDa (PRAS 40) and the DEP-domain containing mTOR interacting protein (DEPTOR) (Haar *et al*, 2007; Peterson *et al*, 2009; Sancak *et al*, 2007). Additionally, the rapamycin-FKBP12 complex can bind the catalytic subunit of mTORC1 to exclude specific substrates from the catalytic cleft (Yang *et al.*, 2013). In contrast, mTORC2 is insensitive to the rapamycin-FKBP12 complex and, thus, not directly inhibited by rapamycin treatment (Saxton & Sabatini, 2017). mTORC2 also consists of mTOR and mLST8, but Rictor (rapamycin insensitive companion of mTOR) instead of Raptor (Jacinto *et al*, 2004). Besides DEPTOR, mTORC2 is regulated by mSin1 and Protor1/2 (Frias *et al*, 2006; Pearce *et al*, 2007).

### 1.3.1 Upstream activation of mTORC1

Various cellular pathways upstream of mTORC1 regulate the kinase activity in response to the availability of growth factors, energy, and nutrients (Figure 2). Several growth factor signaling pathways converge on inhibiting the tuberous sclerosis complex (TSC), a central negative regulator of mTORC1 (Figure 2) (Tee et al, 2002). TSC consists of TSC1, TSC2, and TBC1D7 and acts as the GTPase-activating protein (GAP) of the small GTPase Rheb, which interacts with mTORC1 and activates its kinase activity (Long et al, 2005; Tee et al., 2002). For example, the insulin/insulin-like growth factor-1 (IGF-1) induces the phosphorylation and, thus, inactivation of TSC via Akt (Manning *et al*, 2002). Additionally, receptor tyrosine kinases can activate Ras-MAPK signaling, which leads to mTORC1 activation through phosphorylation and inhibition of TSC (Roux *et al*, 2004). Besides growth factors, energy and oxygen levels regulate TSC and, thus, mTORC1 activity. A decrease in energy levels activates AMP-activated protein kinase (AMPK), which phosphorylates and activates TSC2 followed by reduced mTORC1 activity (Inoki *et al*, 2003). Moreover, a reduction in oxygen inhibits mTORC1 via activation of AMPK and REDD1 (Regulated in DNA damage and development 1), which induce TSC (Brugarolas *et al*, 2004). Taken together, various inputs from growth factors, energy, and oxygen converge on the activity of TSC, which negatively regulates mTORC1 via Rheb (Figure 2).

Apart from growth factors, energy, and oxygen, mTORC1 activity responds to levels of amino acids. Cells take up amino acids from the environment through transmembrane transporters or generate them through lysosomal digestion of extra- or intracellular proteins (Hsu & Sabatini, 2008; Palm & Thompson, 2017). mTORC1 senses levels of amino acids through the Rag GTPases (Kim et al, 2008). The heterodimers RagA/B and RagC/D are anchored to the lysosomal membrane via the ragulator complex (Figure 2) (Sancak et al, 2010). If amino acids are available, RagA/B is bound to GTP and RagC/D to GDP. In this active state, the Rags bind to Raptor and recruit mTORC1 to the lysosome (Sancak *et al.*, 2010). Thus, mTORC1 is activated by concerted inputs from amino acids and growth factors (Saxton & Sabatini, 2017). The Rags respond to cytosolic leucine and arginine availability to adapt mTORC1 activity accordingly. Both amino acids signal through inhibition of the negative mTORC1 regulator GATOR1 constituted of DEPDC5, Nprl2, and Nprl3 (Figure 2) (Bar-Peled et al, 2013). GATOR1

functions as the GAP for RagA/B, and the hydrolysis of GTP to GDP inhibits mTORC1 (Saxton & Sabatini, 2017). GATOR2 consists of Mios, WDR24, WDR59, Seh1L, and Sec13 and acts as a positive regulator of mTORC1 through interaction with GATOR1 (Saxton & Sabatini, 2017). The leucine sensor Sestrin2 was identified as a protein interacting with GATOR2 and inhibiting its function under leucine deprivation (Figure 2) (Chantranupong *et al*, 2014). Thus, if leucine is available, Sestrin2 dissociates from GATOR2 and positively regulates mTORC1 signaling (Chantranupong *et al.*, 2014). Similarly, CASTOR senses arginine and dissociates from GATOR2 in the presence of arginine (Figure 2) (Saxton *et al*, 2016). Moreover, the integrated stress response was directly linked to mTORC1 activity. The GCN2-ATF4 activation upon general amino acid deprivation upregulates Sestrin2 to sustain mTORC1 suppression (Ye *et al*, 2015). Further mechanisms by which mTORC1 signaling is regulated depending on the availability of amino acids are currently being investigated.

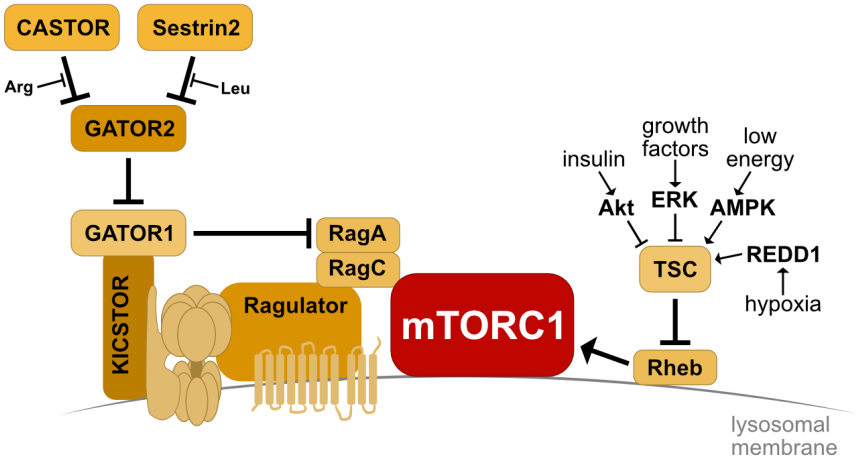


**Figure 2 – mTORC1 signaling network.**
Schematic representation of the signaling pathway upstream of mTORC1. mTORC1 integrates numerous environmental signals, including the availability of amino acids, growth factors, energy, and oxygen, to regulate anabolic and catabolic processes in the cell. Adapted from (Sabatini, 2017).

### 1.3.2 Downstream effectors of mTORC1

As described above, mTORC1 is finely regulated by concerted inputs from nutrients and growth factors. This regulation is critical as mTORC1 promotes energy-demanding processes that allow cells to grow and proliferate, such as synthesizing proteins, lipids, and nucleotides, while blocking catabolic processes, such as autophagy (Figure 3).

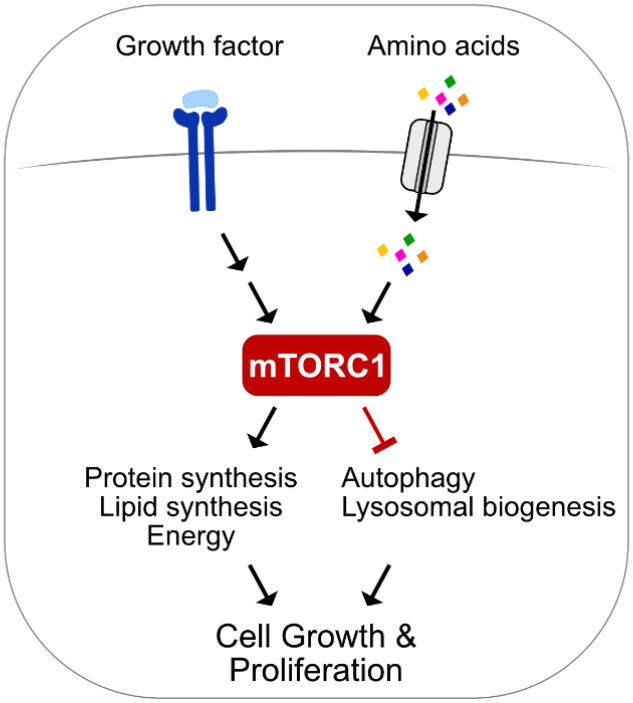


**Figure 3 – Cellular processes downstream of mTORC1.**
Schematic representation of cellular processes downstream of mTORC1. The kinase mTORC1 induces anabolic processes such as protein synthesis, lipid synthesis, and energy production while suppressing catabolic processes. mTORC1 maintains the balance between anabolism and catabolism according to environmental signals such as the availability of growth factors or nutrients.

## Protein synthesis

mTORC1 promotes the production of proteins mainly through two effectors, p70S6 Kinase 1/2 (S6K1/2) and eIF4E Binding Protein 1/2 (4E-BP1/2) (Saxton & Sabatini, 2017). S6K1 is directly phosphorylated and activated by mTORC1 at site Thr389 (Saxton & Sabatini, 2017). Upon activation, S6K1 phosphorylates and activates substrates that increase mRNA translation initiation and elongation, including eIF4B, which positively regulates the formation of the translation initiation complex (Holz *et al*, 2005). In contrast, 4E-BP1 inhibits translation by binding to eIF4E, which prevents the formation of the eIF4F complex (Gingras *et al*, 1999). Consequently, 4E-BP1 suppresses cap-dependent translation initiation. mTORC1 phosphorylates 4E-BP1 at several phosphorylation sites and induces its dissociation from eIF4E, thus promoting cap-dependent translation (Brunn *et al*, 1997).

Although mTORC1 regulates the global protein synthesis, a subset of mRNAs carrying 5'-terminal oligopyrimidine (TOP) motifs is particularly sensitive to mTORC1. TOP motifs consist of a cytosine followed by 4-14 pyrimidines (Hsieh *et al*, 2012; Jefferies *et al*, 1994; Thoreen *et al*, 2012). Global ribosome profiling analyses confirmed that acute mTORC1 inhibition strongly reduced the translation of mRNAs with TOP motifs, but only slightly reduced global translation (Thoreen *et al.*, 2012). mRNAs that carry TOP motifs encode ribosomal proteins and some translation factors (Jefferies *et al.*, 1994). Thus, mTORC1 contributes to the production of components of the protein synthesis machinery to increase the cellular translation capacity in the long term.

**Lipid synthesis**

Cells require *de novo* lipid synthesis to form the plasma membrane and organellar membranes to grow and proliferate. mTORC1 promotes lipid synthesis through the transcription factor sterol regulatory element-binding protein 1/2 (SREBP1/2) (Saxton & Sabatini, 2017). Inactivated SREBPs localize to the membrane of the endoplasmic reticulum (Eberlé *et al*, 2004). Upon translocation to the Golgi, the N-terminal domain is released by proteolytic cleavage and enters the nucleus (Eberlé *et al.*, 2004). The active SREBPs bind to sterol-regulatory DNA elements and induce the synthesis of enzymes required for sterol and fatty acid biosynthesis (Porstmann *et al*, 2008). mTORC1 suppresses Lipin-1, a negative SREBP regulator, to adapt *de novo* lipid synthesis to environmental signals (Peterson *et al*, 2011).

**Energy**

As the synthesis of proteins and lipids is energy-demanding, growing cells require more energy. mTORC1 promotes aerobic glycolysis to increase ATP and carbon intermediates through an increased translation of the transcription factor HIF1α (Ben-Sahra & Manning, 2017; Düvel *et al*, 2010). HIF1α increases the expression of glucose transporters and many enzymes required for glycolysis (Ben-Sahra & Manning, 2017; Düvel *et al.*, 2010). Moreover, mTORC1 modulates mitochondrial metabolism and the

TCA cycle through transcriptional regulation of mitochondrial genes (Cunningham *et al*, 2007).

**Protein catabolism**

Besides the previously described anabolic processes, mTORC1 inhibits protein catabolism, mainly through blocking autophagy (Saxton & Sabatini, 2017). The initial step of autophagosome initiation is forming a complex between ULK1 (unc-51-like kinase 1), ATG13 (autophagy-related protein 13) and FIP200 (Saxton & Sabatini, 2017). In mammalian cells, mTORC1 phosphorylates ULK1, disrupting the activation of ULK1 by AMPK (Kim *et al*, 2011). Thus, mTORC1 and AMPK regulate autophagy in reciprocal ways (Kim *et al.*, 2011). Moreover, mTORC1 regulates protein catabolism by phosphorylating and suppressing the nuclear translocation of the transcription factor EB (TFEB) (Martina *et al*, 2012; Settembre *et al*, 2012). TFEB promotes the expression of genes required for autophagy and lysosomal biogenesis. Thus, upon nutrient starvation, mTORC1 no longer phosphorylates TFEB, which is then translocated to the nucleus and promotes lysosomal biogenesis (Martina *et al.*, 2012; Settembre *et al.*, 2012).

### 1.3.3 The opposing effect of mTORC1 inhibition on cell proliferation

Cells take up nutrients from the extracellular space to support the synthesis of proteins and other macromolecules (Palm & Thompson, 2017). In mammalian cells, nutrient uptake through cell surface nutrient transporters and endolysosomal pathways is controlled by growth factors (Palm & Thompson, 2017). Moreover, mammalian cells can use macropinocytosis, a non-selective endocytic process by which soluble macromolecules are internalized and digested in the lysosome (Bloomfield & Kay, 2016; Palm, 2019). Interestingly, the Palm laboratory could show that mTORC1 reduces lysosomal degradation of proteins taken up from the extracellular space (Palm *et al*, 2015). Thus, mTORC1 suppresses the proliferation of cancer cells that rely on proteins as an amino acid source (Palm *et al.*, 2015). Mechanistically, mTORC1 suppresses V-ATPase assembly at lysosomal membranes, thus regulating lysosome's

pH and catabolic activity (Ratto *et al*, 2022). Consequently, the inhibition of mTORC1 results in opposing effects on cell proliferation: when cells rely on free amino acids, mTORC1 inhibition suppresses cell proliferation, but when cells acquire the amino acid source of proteins, mTORC1 inhibition promotes cell proliferation (Palm *et al.*, 2015). These findings reveal a novel critical role of mTORC1 in metabolic homeostasis and stress adaptation; the underlying molecular mechanisms remain to be studied.

## 1.4 Protein translation, mTORC1 and cancer

Many cancer-related mutations affect the protein synthesis machinery to promote aberrant cancer growth (Bhat *et al.*, 2015). As mTORC1 is a central regulator of protein translation, mutations that hyperactivate mTORC1 were associated with cancer development (Bhat *et al.*, 2015). For example, 4E-BP phospho-mutants that constitutively bind to eIF4E and prevent cap-dependent translation initiation suppressed Akt-mediated tumorigenesis in mice (Hsieh *et al*, 2010). Accordingly, the mTORC1-dependent inhibition of 4E-BP1 is critical for translating pro-tumorigenic genes and turning 4E-BPs into tumor suppressor genes (Martineau *et al*, 2013; Zoncu *et al*, 2011). Moreover, increased Akt-mTORC2 signaling was associated with tumorigenesis as mTORC2 activity was required for prostate tumor growth in mice deficient for the negative mTORC1 regulator PTEN (Guertin *et al*, 2009).

As the mode of action of mTORC1 in supporting cell proliferation was well established, the potential for the naturally occurring mTORC1 inhibitor rapamycin as an anti-cancer drug was expected to be high (Benjamin *et al*, 2011). Although rapamycin and its analogs (rapalogues) strongly suppressed cell proliferation *in vitro*, most clinical trials were disappointing (Sehgal, 2003; Zoncu *et al.*, 2011). This was explained, at least partially, by the insensitivity of 4E-BPs to rapamycin as well as by the activation of Akt through the decline in the negative feedback loops mTORC1-S6K-PI3K and mTORC1-GRB10 (Bhat *et al.*, 2015).

As described above, the Palm laboratory established the molecular mechanism by which mTORC1 inhibition promotes cancer cell proliferation when cells rely on extracellular proteins as a nutrient source (Palm *et al.*, 2015; Ratto *et al.*, 2022). In this

context, particularly KRas-driven pancreatic cancer cells exploit macropinocytosis to sustain proliferation within their vascularly compromised tumor environment (Commisso *et al*, 2013; Kamphorst *et al*, 2015; Palm *et al.*, 2015). Together, these data might explain why the efficiency of mTOR inhibitors was especially low in poorly vascularized tumors (Kim *et al*, 2017). Future studies should consider that mTORC1 plays context-dependent roles, and novel functions of mTORC1 signaling to sustain metabolic flexibility, especially in cancer cells, remain to be investigated.

# 2 Aims of the thesis

mTORC1 is a central regulator of protein synthesis. Upon nutrient abundance and growth factor availability, mTORC1 enhances anabolic processes while blocking protein catabolism. In contrast, when cells rely on proteins as an amino acid source, mTORC1 suppresses cell proliferation by negatively regulating lysosomal catabolic activity. The opposing effect of mTORC1 on cell proliferation depending on the nutrient environment indicates a critical role in stress adaptation, but underlying mechanisms remain to be investigated. In my PhD project, I aimed to systematically identify genes and critical pathways required for cell adaptation to the inactivation of mTORC1 when cells rely on either free amino acids or proteins as a nutrient source. First, I aimed to establish tools and methods for genome-wide CRISPR screens in the presence of the mTOR inhibitor torin 1 under different metabolic conditions. After conducting the CRISPR screens, I validated interesting screen hits. I found that tRNA-modifying enzymes that form $mcm^5s^2$ at wobble uridines of tRNAs ($U_{34}$-enzymes), Elongator and Ctu1/2, became selectively essential for cell proliferation under mTORC1 inhibition. As the functional role of $U_{34}$-enzymes in mammalian cells and their connection to mTORC1 signaling were unclear, I finally aimed to study the interplay between tRNA wobble modification and mTORC1 mechanistically and to clarify their relevance in cancer growth. My PhD study established a molecular mechanism by which mTORC1 and tRNA wobble modifications cooperate in generating the protein synthesis machinery. Consequently, mTORC1 inhibition suppressed $U_{34}$-enzyme-deficient tumor growth *in vivo,* suggesting that the combined inhibition of both pathways might be a potential target to suppress cancer growth.

# 3 Materials and Methods

## 3.1 Materials

### 3.1.1 Cell lines

**Table 1 – Cell lines used in this study.**

| Cell line | Source |
|---|---|
| Murine EPP2 | (Pechincha *et al*, 2022) |
| Murine KRPC | (Palm *et al.*, 2015) |
| SV40 large T antigen-immortalized MEFs (LSL-KRas$^{G12D}$) | (Palm *et al.*, 2015) |
| Murine KPC (LSL-KRas$^{G12D/+}$; LSL-Trp53$^{R172H/+}$; Pdx-1-Cre) | (Pechincha *et al.*, 2022) |
| Human T24 | ATCC HTB-4 |
| Human HEK 293T | ATCC CRL-3216 |

### 3.1.2 Cell culture reagents

**Table 2 – Cell culture reagents used in this study.**

| Cell culture reagents | Company | Catalogue number |
|---|---|---|
| DMEM | Gibco | 41965-039 |
| DMEM/F-12 | Gibco | 11320-074 |
| Dialyzed FBS (dFBS) | Gibco | 26400-044 |
| FBS | Gibco | 10270-106 |
| Glutamine | Gibco | 25030-024 |
| Puromycin | Santa Cruz Biotechnology | sc-108071A |
| Geneticin | Gibco | 10131-035 |
| Blasticidin | Santa Cruz Biotechnology | sc-495389 |
| Hygromycin | Gibco | 10687-010 |
| Doxycycline | Sigma Aldrich | J67043 |
| Amino acid-free, glucose-free DMEM/F-12 | US Biological | D9807-11 |
| Bovine Serum Albumin | Sigma Aldrich | A1470 |
| Albumin, Bovine Serum, fatty acid-poor | Sigma Aldrich | 126579 |
| Glucose | Sigma Aldrich | G7021 |
| Sodium bicarbonate | Sigma Aldrich | S5761 |

**Table 3 – List of amino acid concentrations used for DMEM/F-12 cell culture medium.**

| Amino acid | DMEM/F-12 concentration | Company | Catalogue number |
|---|---|---|---|
| Alanine | 50 µM | Sigma Aldrich | A0325000 |
| Arginine:HCl | 699 µM (SILAC: 480 µM) | Sigma Aldrich | A1271000 |
| Asparagine:H2O | 50 µM | Sigma Aldrich | Y0000305 |
| Aspartate | 50 µM | Sigma Aldrich | A9256 |
| Cysteine:HCl:H2O | 100 µM | Sigma Aldrich | C3290000 |
| Cystine:2HCl | 100 µM | Sigma Aldrich | C3300000 |

| | | | |
|---|---|---|---|
| Glutamate | 50 µM | Sigma Aldrich | G8415 |
| Glutamine | 2500 µM | Gibco | 25030 |
| Glycine | 250 µM | Sigma Aldrich | G5417 |
| Histidine:HCl:H2O | 150 µM | Sigma Aldrich | H0755000 |
| Isoleucine | 416 µM | Sigma Aldrich | I0460000 |
| Leucine | 450 µM | Sigma Aldrich | L0375000 |
| Lysine:HCl | 499 µM | Sigma Aldrich | L0900000 |
| Methionine | 116 µM | Sigma Aldrich | M0960000 |
| Phenylalanine | 215 µM | Sigma Aldrich | P1150000 |
| Proline | 150 µM | Sigma Aldrich | P3350000 |
| Serine | 250 µM | Sigma Aldrich | S0450000 |
| Threonine | 449 µM | Sigma Aldrich | T8441 |
| Tryptophan | 44 µM | Sigma Aldrich | T2610000 |
| Tyrosine:2Na:H2O | 248 µM | Sigma Aldrich | T1145 |
| Valine | 452 µM | Sigma Aldrich | V0030000 |
| Glucose | 17.5 mM | Sigma Aldrich | G7021 |
| Bicarbonate | 2.4 g/ L | Sigma Aldrich | S5761 |
| L-Lysine:2HCl (4,4,5,5-D4) | 499 µM | Cambridge Isotope Laboratories | DLM-2640-1 |
| L-Lysine:2HCl (D9) | 499 µM | Cambridge Isotope Laboratories | DLM-570-PK |
| L-Arginine:HCl (13C6) | 480 µM | Silantes | 201204102 |
| L-Arginine:HCl (13C6, 15N4) | 480 µM | Silantes | 201604102 |
| 4-Azido-L-homoalanine HCl (L-AHA) | 100 µM | Jena Bioscience | CLK-AA005 |

### 3.1.3 Primary antibodies

**Table 4 – Primary antibodies used in this study.**

| Antibody | Company | Catalogue number |
|---|---|---|
| Akt(pan) | Cell Signaling | 2920 |
| Phospho-Akt (Ser473) | Cell Signaling | 4060 |
| S6 Ribosomal Protein | Cell Signaling | 2217 |
| Phospho-S6 Ribosomal Protein (Ser240/244) | Cell Signaling | 2215 |
| p70 S6 Kinase | Cell Signaling | 2708 |
| Phospho-p70 S6 Kinase (Thr389) | Cell Signaling | 9234 |
| 4E-BP1 | Cell Signaling | 9452 |
| Elp3 | Cell Signaling | 5728 |
| Ribosomal Protein S3 | Cell Signaling | 9538 |
| Ribosomal Protein L29 | Proteintech | 15799-1-AP |
| HA-tag | Cell Signaling | 3724 |
| β-actin | Sigma Aldrich | A5441 |
| Puromycin | Sigma Aldrich | MABE343 |
| Cd9 Monoclonal Antibody KMC8, APC | Thermo Fisher Scientific | 17-0091-82 |

### 3.1.4 Secondary antibodies

**Table 5 – Secondary antibodies used in this study.**

| Antibody | Company | Catalogue number |
|---|---|---|
| HRP anti-mouse | Cytiva | NA931 |
| HRP anti-rabbit | Cytiva | NA9340 |

### 3.1.5 Chemicals and inhibitors

**Table 6 – Chemicals and inhibitors used in this study.**

| Inhibitor | Company | Catalogue number |
|---|---|---|
| Torin 1 | Tocris | 4247 |
| GDC-0941 | Cayman Chemical | 957054-30-7 |
| MK-2206 | Cayman Chemical | 1032350-13-2 |
| PD 0325901 | Cayman Chemical | 391210-10-9 |
| Rapamycin | MedChemExpress | HY-10219 |
| MG132 | Cayman Chemical | 13697 |
| SCH772984 | Selleck Chemicals | S7101 |
| Benzamidine | Sigma Aldrich | 12072 |
| E64 | Serva | 21100 |
| AEBSF | Serva | 12745 |
| Aprotinin | Serva | 13718 |
| Leupeptin | Serva | 51867 |
| Pepstatin | Serva | 52682 |
| Halt Protease and Phosphatase Inhibitor Cocktail | VWR International | 78444 |
| Sodium orthovanadate | MP Biomedicals | 159664 |
| Sodium fluoride | Alfa Aesar | A13019 |
| Sodium pyrophosphate | Alfa Aesar | A17546 |
| Sodium glycerophosphate | Alfa Aesar | A16269 |
| Polyethylenimine (PEI, MW 250000) | Polysciences | 24314 |
| Polybrene | Tocris | 7711 |
| Proteinase K | NEB | P8107S |
| Benzonase | Merck | 70746 |
| Skim milk powder | Gerbu Biotechnik | 1602 |
| Mass Spec Grade water | Thermo Fisher Scientific | 51140 |

| | | |
|---|---|---|
| Tris Base | Sigma Aldrich | 648310 |
| DNAse-free RNAse | Sigma Aldrich | 11119915001 |
| UltraPure™ SDS Solution 10% | Thermo Fisher Scientific | 15553027 |
| AMPure XP Beads | Beckman Coulter | A63881 |
| Phenol | Th. Geyer | 10673955 |
| 2-propanol | Serva | 39559 |
| TEMED | Carl Roth | 2367 |
| APS | Thermo Fisher Scientific | 17874 |
| SDS | Serva | 20765 |
| Triton X-100 | Sigma Aldrich | 93443 |
| Tween 20 | Santa Cruz Biotechnology | sc-29113 |
| Agarose | Sigma Aldrich | A9539 |
| Acrylamide | Carl Roth | A121.1 |
| DTT | Thermo Fisher Scientific | R0861 |
| β-mercaptoethanol | Sigma Aldrich | M3148 |
| Receptor-grade BSA Fraction V | Serva | 11924 |
| Clarity Max Western ECL substrates | Bio-Rad | 1705062 |
| Trizol | Invitrogen | 15596026 |
| Chloroform | Carl Roth | 7331 |
| Isopropanol | Serva | 39559 |
| Ethanol | Th. Geyer | 11832330 |
| Methanol | VWR | 1.06009.2511 |
| EDTA | Sigma Aldrich | E9884 |
| dNTP mix (10 mM each) | Life Technologies | R0194 |
| Tris-HCl | Thermo Fisher Scientific | A18494 |
| Sodium chloride | Fisher Scientific | 10735921 |
| HEPES | Life Technologies | 15630080 |

| | | |
|---|---|---|
| Magnesium chloride | VWR | SIALM2670 |
| Potassium chloride | Carl Roth | 6781.1 |
| Glycerol | VWR | E520 |

### 3.1.6 Plasmids

**Table 7 – List of plasmids and backbone vectors from other sources used in this study.**

| Vector | Source |
|---|---|
| pCMVR8.74 | Addgene 22036 |
| pCMV-VSV-G | Addgene 8454 |
| pRRL-SFFV-rtTA3-IRES-EcoR-PGK-HygroR | (de Almeida *et al*, 2021) |
| pRRL-TRE3G-Cas9-P2A-BFP | (de Almeida *et al.*, 2021) |
| pRRL-TRE3G-Cas9-P2A-GFP-PGK-BlastR | (de Almeida *et al.*, 2021) |
| pLenti-hU6-sgRNA-iT-EF1as-Thy1.1-P2A-NeoR | (de Almeida *et al.*, 2021) |
| Dual-hU6-sgRNA-mU6-sgRNA-Ef1α-Thy1.1-P2A-NeoR | (de Almeida *et al.*, 2021) |
| Dual-hU6-sgRNA-mU6-sgRNA-Ef1α-mCherry-P2A-PuroR | (de Almeida *et al.*, 2021) |
| pLenti-Cas9-BlastR | Addgene 52962 |
| pSpCas9(BB)-2A-GFP (PX458) | Addgene 48138 |
| LentiGuide-Puro | Addgene 52963 |
| pLV-EF1a-IRES-NeoR | Addgene 85139 |
| pLV-EF1a-IRES-BlastR | Addgene 85133 |

**Table 8 – List of plasmids generated in this study.**

| Generated plasmid | Backbone vector |
|---|---|
| PX458 + sgRNA | PX458 |
| Dual-hU6-sgRNA-mU6-sgRNA-Ef1α-Thy1.1-P2A-NeoR + dsgRNAs | Dual-hU6-sgRNA-mU6-sgRNA-Ef1α-Thy1.1-P2A-NeoR |
| Dual-hU6-sgRNA-mU6-sgRNA-Ef1α-mCherry-P2A-PuroR + dsgRNAs | Dual-hU6-sgRNA-mU6-sgRNA-Ef1α-mCherry-P2A-PuroR |
| pLV-Ef1a-N HA-IRES-NeoR | pLV-Ef1a-IRES-NeoR |

| | |
|---|---|
| pLV-500bp upstream+5'UTR-HA-Rpl29(WT)-NeoR | pLV-Ef1a-N HA-IRES-NeoR |
| pLV-500bp upstream+5'UTR-HA-Rpl29(NAG)-NeoR | pLV-Ef1a-N HA-IRES-NeoR |
| pLV-500bp upstream+5'UTR-HA-Rps3(WT)-NeoR | pLV-Ef1a-N HA-IRES-NeoR |
| pLV-500bp upstream+5'UTR-HA-Rps3(NAG)-NeoR | pLV-Ef1a-N HA-IRES-NeoR |
| pLV-UbC-IRES-BlastR | pLV-Ef1a-IRES-BlastR |
| pLV-5'UTR-HA-Rps25(WT)-BlastR | pLV-UbC-IRES-BlastR |
| pLV-5'UTR-HA-Rps25(NAG)-BlastR | pLV-UbC-IRES-BlastR |
| pLV-Ef1a-C Flag-IRES-NeoR | pLV-Ef1a-IRES-NeoR |
| pLV-Ef1a-ELP3-Flag-NeoR | pLV-Ef1a-IRES-NeoR |
| pLV-Ef1a-Ctu1-Flag-NeoR | pLV-Ef1a-IRES-NeoR |

### 3.1.7 sgRNA sequences

**Table 9 – sgRNA and dual-sgRNA (dsg-RNA) sequences used in this study.**

| Gene | Species | Name | sgRNA sequence 1 | sgRNA sequence 2 |
|---|---|---|---|---|
| Cd9 | mouse | Cd9_sgRNA1 | GAAACCAACCAGCATCATGA | |
| Rosa26 | mouse | Rosa26_sgRNA1 | GAAGATGGGCGGGAGTCTTC | |
| Rosa26 | mouse | Rosa26_sgRNA2 | GCTGGAGTTGCAGATCACGA | |
| Chr1.1 | mouse | Chr1.1_dsgRNA1 | GACAATGAACATAAGCACAT | GTTTGGCCTGAAATCCCACC |
| Chr1.3 | mouse | Chr1.3_dsgRNA1 | GAGCAGCAAACACTTGAAGT | GTTTGGCCTGAAATCCCACC |
| Ctu1 | mouse | Ctu1_dsgRNA1 | GCACGTGTGCCAGCACTG | GTAGGCCACGATGGTGAG |
| Ctu1 | mouse | Ctu1_dsgRNA2 | GTGGAGTCCTTGCCACCAG | GTGGCCTACGAAGATCTCTT |
| Pigt | mouse | Pigt_dsgRNA1 | GATTCGGATCTGCAGCGGGA | GACAGGTGGAGCTCCCGCA |
| Pigt | mouse | Pigt_dsgRNA2 | GCACAGAAGATCCCCGAG | GGGCAAGAGCTTCTTCCA |
| Ilf2 | mouse | Ilf2_dsgRNA1 | GCTCAGCAGAATTAGGGGCA | GTGATTGACAACTTGATTG |
| Ilf2 | mouse | Ilf2_dsgRNA2 | GGAAGCTGTTGCTGCCCTG | GGGCACAGGATCCCTCAGA |
| Kif18b | mouse | Kif18b_dsgRNA1 | GGACCCCTCACCATCCGTG | GGCAGCAATCATCACTGTG |
| Dnajc9 | mouse | Dnajc9_dsgRNA1 | GCACTTGGTAGAGGTCGG | GCAGTGTACGATGAACAG |

| | | | | |
|---|---|---|---|---|
| Gsk3b | mouse | Gsk3b_dsgRNA1 | GTATCAGGATCCAACAAG | GATTCCAAAGGAATGGATAT |
| Hnrnpc | mouse | Hnrnpc_dsgRNA1 | GGTGGTCAAGAAGTCTGATG | GAAACAAACTCACCTAAAACC |
| Mknk2 | mouse | Mknk2_dsgRNA1 | GAGTTTGATACCACTGCCA | GGAGGAGGACCGTTTCTACC |
| Elp3 | mouse | Elp3_dsgRNA1 | GAAAAGGGTCATATCTAGCA | GCTGATGTGTGGACATCTGTG |
| Elp3 | mouse | Elp3_dsgRNA2 | GCTGATGTGTGGACATCTGTG | GAATCGGAGTCAGGTCCTCCG |
| Raptor | mouse | Raptor_dsgRNA1 | GACATTGTGAGAAAATCGA | GAGCTGGAGAATGAAGGATC |
| Rictor | mouse | Rictor_dsgRNA1 | GAACCTTCTGATAACTTGA | GTATCAAATATGAGAAAGCT |
| Rheb | mouse | Rheb_dsgRNA1 | GTTCAGCTTGTAGACACAGCG | GAGCGTTCACCAAGTTGATCA |
| Chr1.1 | human | Chr1.1_dsgRNA1 | GACAATGAACATAAGCACAT | GTTTGGCCTGAAATCCCACC |
| Chr1.3 | human | Chr1.3_dsgRNA1 | GAGCAGCAAACACTTGAAGT | GTTTGGCCTGAAATCCCACC |
| Ctu1 | human | hCtu1_dsgRNA1 | GTGCTCATGAACTTCCTACG | GGACGAGGAGGCGACGCCG |
| Ctu1 | human | hCtu1_dsgRNA2 | GCCTCGGAGAAGTAGTCGAGG | GGTCACAACGCCGACGACA |

### 3.1.8 Commercial kits

**Table 10 – Commercial kits used in this study.**

| Kit | Company | Catalogue number |
|---|---|---|
| Pierce BCA Protein Assay Kit | Thermo Fisher Scientific | 23227 |
| Precision Plus Protein Dual Color Standards | BioRad | 1610374EDU |
| DNA 1Kb ladder | NEB | N3200L |
| DNA 100bp ladder | NEB | N3231L |
| HiFi DNA Assembly Master Mix | NEB | E2621X |
| QIAprep Spin Miniprep Kit | QIAGEN | 27106 |
| QIAquick Gel Extraction Kit | QIAGEN | 28706X4 |
| DNeasy Blood & Tissue Kit | QIAGEN | 69504 |
| NEBuilder® HiFi DNA Assembly Cloning Kit | NEB | E2621L |
| AmpliTaq Gold DNA Polymerase | Thermo Fisher Scientific | 4311820 |
| MycoAlert Mycoplasma Detection | Lonza | LT07 |

| | | |
|---|---|---|
| NextSeq 1000/2000 P2 Reagents | Illumina | 20046811 |

### 3.1.9 Enzymes

**Table 11 – List of enzymes used in this study.**

| Enzyme | Company | Catalogue number |
|---|---|---|
| T4 Polynucleotide Kinase | NEB | M0201 |
| BbsI-HF | NEB | R3539 |
| FastDigest Esp3I | Thermo Fisher Scientific | FD0454 |
| EcoRI-HF | NEB | R3101 |
| BamHI-HF | NEB | R3136 |
| BspDI | NEB | R0557 |
| AfeI | NEB | R0652 |
| Q5 High-Fidelity DNA Polymerase | NEB | M0491L |
| Taq DNA polymerase | Thermo Fisher Scientific | EP0401 |

### 3.1.10 Buffers

**Table 12 – List of buffers used in this study.**

| Buffer | Recipe |
|---|---|
| **PBS 1X** | 137 mM NaCl |
| | 10 mM Na2HPO4 |
| | 1.8 mM KH2PO4 |
| | 2.7 mM KCl |
| | pH to 7.4 |
| **Standard protein lysis buffer** | 50 mM HEPES pH 7.4 |
| | 40 mM NaCl |
| | 2 mM EDTA |

| | |
|---|---|
| | 1 mM Na orthovanadate |
| | 50 mM NaF |
| | 10 mM Na pyrophosphate |
| | 10 mM Na glycerophosphate |
| | 1% Triton X-100 |
| **RIPA buffer** | 50 mM Tris-HCl pH 8 |
| | 150 mM NaCl |
| | 1 % NP-40 |
| | 0.5 % sodium deoxycholate |
| | 0.1 % SDS |
| | 1 mM EDTA |
| | 5 mM MgCl2 |
| **Nascent proteomics lysis buffer** | 300 mM HEPES pH 8 |
| | 1 % SDS |
| **Laemmli Sample Buffer (4X)** | 250 mM Tris pH 6.8 |
| | 50 % Glycerol |
| | 5 % SDS |
| | 0.05 % Bromophenol Blue |
| | 10 % β-Mercaptoethanol |
| **SDS-PAGE Running & Transfer Buffer 1X** | 25 mM Tris base |
| | 192 mM Glycine |
| **SDS-PAGE Running Buffer** | 1x SDS-PAGE Running & Transfer Buffer |
| | 0.1 % SDS |
| **Transfer Buffer** | 1x SDS-PAGE Running & Transfer Buffer |
| | 0.02 % SDS |
| | 20 % methanol |
| **Tris-buffered saline (TBST)** | 20 mM Tris base |

| | |
|---|---|
| | 150 mM NaCl |
| | 0.1 % Tween-20 |
| | Adjust pH to 7.5 |
| **Western Blot Stripping Buffer** | 200 mM Glycine |
| | 0.1 % SDS |
| | Adjust pH to 2.2 |
| **Ponceau S Staining Solution** | 0.2 % Ponceau S |
| | 5 % Glacial Acetic Acid |
| **BSA solution for Antibodies** | 5 % BSA |
| | 0.2125 % NaCl |
| | 0.025 % NaAzide |
| **Genomic DNA extraction lysis buffer** | 10 mM Tris-HCl pH 8 |
| | 50 mM KCl |
| | 2.5 mM MgCl2 |
| | 0.45 % Tween 20 |
| | 0.45 % Triton X-100 |
| | 100 ug/ mL Proteinase K (freshly added) |
| **1.5 M Tris pH 8.8 (1 L)** | 181.71 g Tris base |
| | Adjust pH to 8.8 with concentrated HCl |
| **1.0 M Tris pH 6.8 (1 L)** | 121.14 g Tris base |
| | Adjust pH to 6.8 with concentrated HCl |
| **Tris-borate-EDTA Buffer (TBE)** | 89 mM Tris base |
| | 89 mM Boric acid |
| | 2 mM EDTA pH 8 |
| **Flow cytometry buffer** | 5 % FBS in PBS |

### 3.1.11 Acrylamide gels

**Table 13 – Acrylamide gel recipes for SDS-PAGE used in this study.**

| **Resolving Gel %** | **Solutions** | **For 5 mL** |
|---|---|---|
| **X** % | 1.5 M Tris pH 8.8 | 1.24 mL |
| | Rotiphorese (30 %) | (0.16 x **X**) mL |
| | TEMED | 5 µL |
| | APS (10 % w/v) | 50 µL |
| | SDS (10 % w/v) | 50 µL |
| | H2O | Up to 5 mL |
| **Stacking Gel %** | **Solutions** | **For 5 mL** |
| 5 % | 1.0 M Tris pH 6.8 | 634 µL |
| | Rotiphorese (30 %) | 836 µL |
| | TEMED | 5 µL |
| | APS (10 % w/v) | 50 µL |
| | SDS (10 % w/v) | 50 µL |
| | H2O | Up to 5 mL |

### 3.1.12 Instruments

**Table 14 – Instruments used in this study.**

| **Instrument** | **Company** |
|---|---|
| ChemiDoc Imaging system | Bio-Rad |
| GelDoc Go Imaging System | Bio-Rad |
| CASY Cell Counter and Analyzer | OMNI Life Sciences |
| Guava easyCyte flow cytometer | Merck |
| Infinite 200 Pro plate reader | Tecan |
| Synergy H1 plate reader | BioTek |
| BD FACS Canto II Flow Cytometry System | Becton Dickinson (BD) Biosciences |

| | |
|---|---|
| FACSAria III cell sorter | Becton Dickinson (BD) Biosciences |
| Qubit 4 Fluorometer | Thermo Fisher Scientific |
| AssayMAP Bravo liquid handling system | Agilent technologies |
| Ultimate 3000 UPLC system | Thermo Fisher Scientific |
| Orbitrap Exploris 480 mass spectrometer | Thermo Fisher Scientific |
| EASY-nLC 1200 system | Thermo Fischer Scientific |
| QExactive HF mass spectrometer | Thermo Fischer Scientific |
| NovaSeq6000 platform | Illumina |

### 3.1.13 Software and tools

**Table 15 – Software and tools used in this study.**

| Software | Source |
|---|---|
| Image Lab (v6.0.0.25) | BioRad |
| GraphPad Prism (v10.1.0) | Prism |
| FACSDiva software (v8.0) | Becton Dickinson (BD) Biosciences |
| FlowJo™ Software (v10.6.1) | BD Life Sciences |
| NEBbuilder Assembly Tool | nebuilder.neb.com |
| Spectronaut (v17.1.221229.55965) | Biognosys |
| MaxQuant (version 1.6.14.0) | (Tyanova *et al*, 2016) |
| DIA-NN (version 1.8.1) | (Demichev *et al*, 2020) |
| Limma (version 3.46.0) | (Ritchie *et al*, 2015) |
| DEqMS (version 1.8.0) | (Zhu *et al*, 2020) |

### 3.1.14 Miscellaneous reagents

**Table 16 – List of miscellaneous reagents used in this study.**

| Other | Company |
|---|---|
| Nitrocellulose membranes | Biorad 1620112 |
| Falcon Round Bottom Polystyrene 5mL Tube | Corning 352235 |
| Acclaim PepMap C18 | Thermo Fischer Scientific |
| nanoEase MZ Peptide analytical column | Waters |
| PhaseLock Gel – LIGHT | QuantaBio 733-2477 |
| AMPure XP Bead-Based Reagent | Beckman Coulter A63881 |

## 3.2 Methods

### 3.2.1 Cell culture

Cells (Table 1) were cultured in DMEM/F-12 supplemented with 10 % FBS and 2 mM glutamine. HEK293T cells were cultured for viral production in DMEM supplemented with 10 % FBS and 2 mM glutamine. All cell lines were maintained at 37 °C and 5 % $CO_2$ and routinely tested for mycoplasma (MycoAlert Mycoplasma Detection). Human cells were authenticated by Single Nucleotide Polymorphism (SNP) typing by Multiplexion.

For experiments with amino acid-deficient or SILAC media, amino acid-free, glucose-free DMEM/F-12 was used. Glucose and sodium bicarbonate were re-added to standard DMEM/F-12 concentrations (glucose: 17.5 mM; sodium bicarbonate: 2.4 g/ L) and the pH adjusted to 7.3 (Table 3). For the full media conditions in the CRISPR screen and competitive proliferation assays, all amino acids were re-added to standard DMEM/F-12 concentrations, supplemented with 5 % FBS and physiological albumin levels (2 % BSA). For the leucine starvation CRISPR screen conditions, all amino acids except leucine were re-added to standard DMEM/F-12 concentrations (5 % FBS, 2 % BSA). For nascent proteomics experiments, amino acid starvation medium was prepared by re-adding all amino acids except for methionine, arginine and lysine, supplemented with 5 % dFBS and 200 mg/ L proline. For SILAC medium with L-AHA, intermediate stable isotope-containing lysine and arginine (13C6-Arg, Lys-D4) or heavy stable isotope-containing lysine and arginine (13C6, 15N4-Arg, Lys-D9) were re-added to the amino acid starvation medium, respectively (Table 3).

### 3.2.2 Lentivirus production and transduction

For lentivirus production, the lentiviral plasmid was co-transfected with pCMVR8.74 and pCMV-VSV-G into HEK293T using polyethylenimine (PEI, MW 250,000). Media were changed after 6-8 h and after 24 h. Two days after transfection, viral supernatants were filtered through a 0.45 µM PES filter. Target cells were infected at a transduction efficiency of < 50 % by diluting viral supernatant with media (1:10) in the presence of 10 µg/ mL polybrene.

### 3.2.3 Generation of iCas9 cells

Cell lines with a doxycycline-inducible Cas9 cassette were generated as previously described (Michlits *et al*, 2020). EPP2, KRPC, KPC, and MEFs were transduced with pRRL-SFFV-rtTA3-IRES-EcoR-PGK-HygroR, selected with 50-100 µg/ mL hygromycin and transduced with pRRL-TRE3G-Cas9-P2A-BFP (EPP2, KRPC, MEF) or pRRL-TRE3G-Cas9-P2A-GFP-PGK-BlastR (KPC) by Catarina Pechincha or Melanie de Almeida. After antibiotic selection, cells were sorted as single cells into 96-well plates using a FACSAria III cell sorter by Catarina Pechincha or Melanie de Almeida. For the induction of Cas9, 0.3-1 µg/ mL doxycycline was used. For the final clones, Cas9 induction, gene editing, and tightness of the TRE3G promoter were evaluated by flow cytometry and immunoblotting.

### 3.2.4 Proliferation-based CRISPR-Cas9 screen

The CRISPR-Cas9 screen was performed using an EPP2 iCas9 clone transduced with the Vienna genome-wide sgRNA library (six sgRNAs per gene: total 123,000 sgRNAs), as previously described (Michlits *et al.*, 2020). The EPP2 clone was transduced at a multiplicity of infection (MOI) < 0.11 with a library representation of 1,000-fold (1.23 x $10^9$ cells on the day of transduction). Cells were selected with 0.2 mg/ mL geneticin, and the selection process was followed by immunostaining and flow cytometry detection of Thy1 expression. Throughout the selection process, a library representation of 500- to 1,000-fold was kept. Two days before the start of the CRISPR screen, Cas9 expression was induced by 300 ng/ mL doxycycline in selected EPP2 cells (> 94 % Thy1-positive). At the onset of the screen (day 0), cells were plated under four different conditions. On the one hand, cells were plated in full medium (2 % BSA, 5 % FBS) with 300 nM torin 1 or DMSO. On the other hand, cells were plated under leucine starvation with 300 nM torin 1 or DMSO (4 % BSA for the first 4 days, then 2 % BSA; 5 % FBS), keeping doxycycline for two more days. Throughout the screen, a library representation of at least 600-fold was kept (> 73.8 x $10^6$ cells). Cells in full medium with DMSO (2 x $10^6$ cells per 15 cm plate; 37 plates in total) were replated every second day, with a media change after one day. The torin 1-treated full medium cell population (2.5 x $10^6$ cells per 15 cm plate; 30 plates in total) was replated every

three days with an additional media change after 1.5 days. The DMSO-treated leucine starvation condition (3 x $10^6$ cells per 15 cm plate; 41 plates in total) was replated every four days (starting from day 6) with additional media change after two days (and day 4). The torin 1-treated leucine starvation condition (1.5 x $10^6$ cells per 15 cm plate; 49 plates in total) was replated every four days, with media changes every second day. At day 0, an initial cell population was harvested in two replicates (T0), and final cell populations were harvested after more than 12 population doublings or after 26 days for the leucine starvation condition (each replicate at a library representation of 500-fold in one tube: ≈ 60 x $10^6$ cells). Cellular pellets were stored at – 80 °C until further processing. For immunoblotting, cell samples of all conditions were harvested throughout the screen.

### 3.2.5 Preparation of next-generation sequencing libraries

To prepare samples of the CRISPR-Cas9 screen for sequencing, genomic DNA was isolated, and next-generation sequencing (NGS) libraries were prepared as described previously (de Almeida *et al.*, 2021; Pechincha *et al.*, 2022). Cells were lysed in 10 mM Tris-HCl, 150 mM NaCl, 10 mM EDTA, 0.1 % SDS, and proteinase K for 24-48 h at 55 °C shaking at 1,200 rpm and digested with DNAse-free RNAse for 1-2 h at 37 °C shaking at 1,200 rpm. Afterwards, two rounds of phenol extraction were performed, and DNA was precipitated with 2-propanol using Phase-Lock-Gel Light tubes. After two washes with 70 % EtOH, ten freeze-thaw cycles were performed to enhance polymerase chain reaction (PCR) efficacy. The sgRNA cassettes were amplified by nested PCR. A two-step PCR protocol was used to generate barcoded NGS libraries for each sample. First, 1 µg DNA was amplified in 50 µL reactions using 0.2 µL AmpliTaq Gold. For each sample, the PCR products were pooled and purified using AMPure XP magnetic PCR purification beads. Second, 10 ng of the purified products were used to introduce Illumina adapters using 0.2 µL AmpliTaq Gold. Finally, the libraries were pooled and sequenced on a NovaSeq6000 platform. Primers used to produce the libraries are listed in Table 17.

**Table 17 – List of primers for CRISPR Screen library preparation.**

| Primer ID | Sequence 5' to 3' |
|---|---|
| **First PCR** | |
| Fwd1 | GCATACGAGATAGCTAGCCACC |
| Rev1 | CTCTTTCCCTACACGACGCTCTTCCGATCTNNNNNNXXXXTTCCAGCATAG CTCTTAAAC<br>(NNNNNN: random nucleotides, XXXX: sample specific barcode) |
| **Second PCR** | |
| Fwd2 | CAAGCAGAAGACGGCATACGAGATAGCTAGCCACC |
| Rev2 | AATGATACGGCGACCACCGAGATCTACACTCTTTCCCTACACGACGCT |

### 3.2.6 Analysis of pooled CRISPR-Cas9 screens

Initial steps of the raw sequencing read analysis were performed by Robert Kalis using the crispr-process-nf Nextflow workflow (https://github.com/ZuberLab/crispr-process-nf). As previously described (de Almeida *et al.*, 2021; Pechincha *et al.*, 2022), guides in the sgRNA library were padded with Cs to equal length before generating an index for Bowtie 2 (v2.3.0). The fastx_trimmer from the fastx-toolkit (v0.0.14) (http://hannonlab.cshl.edu/fastx_toolkit/) was used to trim random hexamer nucleotides, followed by demultiplexing via 4mer sample barcodes with fastx_barcode_splitter (--mismatches 1 --bol). Afterwards, Robert Kalis trimmed barcodes and 20mer spacer using fastx_trimmer. Reads were aligned using Bowtie 2 (-L 18 --score-min 'C,0,−1' -N 0 --seed 42) and quantified using featureCounts (v1.6.1).

MAGeCK (v0.5.9) was used to calculate gene-level enrichment or depletion (Li *et al*, 2014b) following the pr-mageck-nf Nextflow workflow (https://github.com/ZuberLab/crispr-mageck-nf). First, sgRNAs with less than 50 counts at day 0 were removed from count tables. The read counts were median normalized and average $\log_2$ fold changes ($\log_2$FC), p values, and false discovery rates (FDRs) calculated. Depletion or enrichment of sgRNAs was calculated for each condition by comparison to day 0, or by comparison between the endpoint conditions (torin 1 versus DMSO).

### 3.2.7 Generation of gene knockout cells

Inducible Cas9 knockout (iKO) cell lines were generated by lentiviral transduction of Dual-hU6-sgRNA-mU6-sgRNA-Ef1α-Thy1.1-P2A-NeoR or Dual-hU6-sgRNA-mU6-sgRNA-Ef1α-mCherry-P2A-PuroR carrying dual-sgRNAs (dsgRNAs) against a target gene (Table 9). Cells with the plasmid were selected with 0.5 mg/ mL geneticin or 2 µg/ mL puromycin. For the generation of inducible double knockout (iDKO) cell lines, both dsgRNA plasmids were transduced and selected with antibiotics one after the other. The expression of Cas9 was triggered by treating the cells with 300 ng/ mL doxycycline for 3-4 days. Knockout efficiency was confirmed by immunoblotting or PCR of genomic DNA. To generate constitutive T24 knockout cells, cells were sequentially transduced with pLenti-Cas9-BlastR and Dual-hU6-sgRNA-mU6-sgRNA-Ef1a-Thy1.1-P2A-NeoR harbouring dsgRNA against Ctu1 and selected with antibiotics (Table 9). For CRISPR/Cas9 experiments, controls were dsgRNAs targeting non-coding chromosome regions (Chr1.1 or Chr1.3; Table 9).

For the generation of clonal Ctu1 knockout (KO) cells, iCas9 EPP2 or iCas9 KRPC clones were co-transfected with a mixture of two pSpCas9(BB)-2A-GFP plasmids carrying either of the two Ctu1 dsgRNA2 sequences or, as control, carrying either of the two sgRNAs targeting the Rosa26 locus (Table 9). For clonal growth, single GFP-positive cells were sorted into 96-well plates using a FACSAria III cell sorter. Knockout specificity was confirmed by PCR of the *Ctu1* locus.

### 3.2.8 Generation of Ctu1 and Elp3 expression constructs

A human Elp3 ORF was obtained from the genomics core facility at the DKFZ, a mouse Ctu1 ORF was obtained from Horizon Discovery. Elp3 and Ctu1 were cloned into pLV-Ef1a-C Flag-NeoR using primers designed with NEBuilder Assembly tool (Table 18). For Elp3 a two fragment Gibson assembly was performed, for Ctu1 a three fragment Gibson assembly was performed using manufacturer´s instructions. The restriction enzymes BamHI and EcoRI and the HiFi DNA Assembly Master Mix were used for cloning.

**Table 18 – List of primers used for cDNA cloning.**

| Primer ID | Sequence 5' to 3' |
|---|---|
| mCtu1_first_fwd | tccatttcaggtgtcgtgaggatccATGCCCGCCCCGACGTGC |
| mCtu1_first_rev | CGGTGCTGCGGGCCACGG |
| mCtu1_second_fwd | cgccgtggcccgcagcaccgCAGGCTCCGGCCGCAGTC |
| mCtu1_second_rev | catcgtcatccttgtaatcgaattcCTCCGCCACGGGGCTCAG |
| hELP3_fwd | tccatttcaggtgtcgtgaggatccATGAGGCAGAAGCGGAAAG |
| hELP3_rev | catcgtcatccttgtaatcgaattcTTTCAGCATCTTCACCATGTAC |

### 3.2.9 Generation of tagged ribosomal protein constructs

For the generation of ribosomal protein constructs with an N-terminal HA-tag, Rpl29 and Rps3 were amplified from an EPP2 cDNA library (wildtype: WT). VAG mutants, in which all VAA codons in the respective WT transcript sequence were exchanged to the corresponding VAG codons, were synthesized by Genewiz. The WT and VAG mutant sequences were cloned into pLV-Ef1a-N HA-NeoR using primers designed with the NEBuilder Assembly tool (Table 19). The restriction enzymes BamHI and EcoRI and the HiFi DNA Assembly Master Mix were used for cloning. To exchange the Ef1a promoter by the endogenous 5'UTR and 500 bp upstream genomic DNA sequence of the respective gene, Ef1a was removed by digestion with BamHI and BspDI; the endogenous promoter sequences were amplified from the genomic DNA of EPP2 cells using primers designed with the NEBuilder Assembly tool (Table 19). The HiFi DNA Assembly Master Mix was used for cloning.

**Table 19 – List of primers used for Rpl29 and Rps3 ribosomal protein tagging.**

| Primer ID | Sequence 5' to 3' |
|---|---|
| Rpl29_fwd | cgacgtcccagactacgctggatccGCCAAGTCCAAGAACCAC |
| Rpl29_rev | tagagcggccgccctcgaggaattcCTATGGGGCCTTCACAGG |
| Rps3_fwd | cgacgtcccagactacgctggatccGCGGTGCAGATTTCCAAG |
| Rps3_rev | tagagcggccgccctcgaggaattcTTATGCTGTAGGCACTGG |
| Rpl29_promoter_fwd | acagcagagatccagtttatGCTCTTCTCCTCTCCTCTGCC |

| | |
|---|---|
| Rpl29_promoter_rev | tgtggttcttggacttggcggatccagcgtagtctgggacgtcgtatgggtacatGTCTGCACCTC GCGACCC |
| Rps3_promoter_fwd | acagcagagatccagtttatTAATATTAAATCTGTGTGCATGTGCGCACGCATG TGTTTTATGCTTGC |
| Rps3_promoter_rev | tcttggaaatctgcaccgcggatccagcgtagtctgggacgtcgtatgggtacatCTTGCAGCC GCGCGCCGC |

For the generation of Rps25 with an N-terminal HA-tag, the pLV-UbC-IRES-BlastR vector was digested using the restriction enzymes BamHI and EcoRI. The WT and VAG mutant sequences were synthesized by Genewiz and introduced into the digested vector. To exchange the UbC promoter by the endogenous 5'UTR sequence of Rps25, UbC was removed by digestion with BamHI and AfeI; the endogenous promoter sequences were amplified from the genomic DNA of EPP2 cells using primers designed with the NEBuilder Assembly tool (Table 20). The HiFi DNA Assembly Master Mix was used for cloning.

**Table 20 – List of primers used for Rps25 ribosomal protein tagging.**

| Primer ID | Sequence 5' to 3' |
|---|---|
| Rps25_promoter_fwd | ccccccctcctcacggcgagcCGCGCTGGCCGAAAGCGA |
| Rps25 WT _promoter_rev | tcttgtcgtccttgggaggggatccagcgtagtctgggacgtcgtatgggtacatGGCGAAGCTCA GAGAGTCGTG |
| Rps25 VAG _promoter_rev | tcttgtcgtctttgggaggggatccagcgtagtctgggacgtcgtatgggtacatGGCGAAGCTCA GAGAGTCGTG |

### 3.2.10 PCR of genomic DNA

To confirm successful editing of *Ctu1*, genomic DNA was isolated using the DNeasy Blood & Tissue Kit according to manufacturer instructions or by the following protocol: Cell pellets were lysed in 10 mM Tris-HCl pH8, 0.45 % Tween 20, 0.45 % Triton X-100, 2.5 mM MgCl2, 50 mM KCl and 100 µg/ mL proteinase K for 1 hour at 56 °C, followed by 10 min at 95 °C and stored at -20 °C. PCR was performed using primers that generate a PCR product from the genomic *Ctu1* locus spanning the two cutting sites of the dsgRNA sequences. The PCR primers are listed in Table 21. Taq Polymerase was used for PCRs according to standard protocols. For WT cells, a PCR product of 660 bp was expected; for Ctu1 KO cells, a PCR product of only 520 bp was expected.

**Table 21 – PCR primers for validation of *Ctu1* editing.**

| Primer ID | Sequence 5' to 3' |
|---|---|
| gDNA_Ctu1_Fwd | AGACTCCCCAGATGACTCCC |
| gDNA_Ctu1_Rev | CAGCCCACCCCACTATCTTG |

### 3.2.11 Cell proliferation assays

For the validation of screen hits, competitive proliferation assays were performed. Cells were treated with doxycycline (300 ng/ mL) for two days before the start of the experiment. At day 0 of the competitive proliferation assay, EPP2 iCas9 cells that carried a dsgRNA-mCherry construct against a target gene were co-cultured with non-sgRNA control cells in 24-well plates in medium with 300 nM torin 1 or DMSO and 2 % albumin (5 % FBS). Cells were passaged as indicated, and doxycycline was added for the first two days of the experiments. The percentage of sgRNA-mCherry+ cells was quantified by Guava easyCyte flow cytometry on day 0, when passaged, and at the end of the experiment.

For proliferation assays, Cas9 expression was induced by 300 ng/ mL doxycycline for three to four days before the start of the experiment. On day 0, cells were plated in 12-well plates, and after 6 h, the medium was changed to the corresponding experimental medium. Cells were counted on day 0 and day 3 in triplicates using a CASY Cell Counter and Analyzer. The cell number as a fold change on day 3 compared to day 0 was plotted.

### 3.2.12 Immunoblotting

Cells were washed with ice-cold PBS and lysed in ice-cold lysis buffer (50 mM HEPES pH 7.4, 40 mM NaCl, 2 mM EDTA, 1 mM Na orthovanadate, 50 mM NaF, 10 mM Na pyrophosphate, 10 mM Na glycerophosphate, 1 % Triton X-100, 1x Halt protease and phosphatase inhibitor cocktail) for 15 min on ice. Lysates were centrifuged at 18,000 g for 5 min at 4 °C. The supernatant with solubilized protein was collected, and protein concentrations were measured with the Pierce BCA Protein Assay. Equal protein

amounts were run in SDS gel electrophoresis and immunoblotted on nitrocellulose membranes following standard Tris-glycine-SDS protocols. To analyze various antibodies on different membranes, sample preparation, electrophoresis and immunoblotting were performed in parallel under the same conditions. Immunoblots were developed on a ChemiDoc Touch imaging system using ECL substrates Clarity Max Western. For stripping, membranes were incubated in stripping buffer (200 mM glycine, 0.1 % SDS, pH 2.2) for 20 min, washed three times with TBST (10 min each), and re-blocked in 5 % milk TBST for 30 min. Individual band intensities were quantified using the Image Lab software (lane statistics: adjusted total lane volume intensity). For each sample, band intensities were normalized to the corresponding β-actin intensity.

### 3.2.13 Puromycin incorporation assay

For puromycin incorporation assays, cells were plated in 6-well plates 24 h before the start of the experiment. Prior to harvesting, puromycin [83 µM] was added to the cell culture medium for 10 min. Cell lysates were collected, and immunoblotting was performed as described. An anti-puromycin antibody was used to detect puromycin incorporation. As a normalization control, immunoblotting of β-actin was performed in parallel under identical conditions. The total lane intensity was quantified for puromycin and normalized to β-actin as described above. An unspecific band at ~ 40 kDa was observed upon incubation with a secondary antibody and excluded from quantifications.

### 3.2.14 mTORC1 re-activation assay

Cells were plated in 6-well plates and, after attachment, treated with torin 1 for 40 h. For the acute re-activation of mTORC1, torin 1 was removed by washing the cells once with media containing 5 mg/ mL fatty-acid poor BSA. Cells were incubated with fresh BSA-supplemented medium for 1 h. To minimize BSA background during immunoblotting, cells were washed three times with ice-cold PBS before lysis.

### 3.2.15 Flow cytometry

For the EPP2 iCas9 clone used in the screen, Cas9 induction and gene editing were evaluated by flow cytometry. Cells were transduced with LentiGuide-Puro carrying an sgRNA against the surface marker Cd9 (Table 9). Upon selection, cells were treated with doxycycline (300 ng/ mL) for the indicated period of time. Cell pellets (200 g, 4 °C for 5 min) were resuspended in Blocking Buffer (3 % BSA in PBS with 5 % FBS) for 30 min on ice. Upon centrifugation at 100 g, 4 °C for 5 min, the supernatant was aspirated, and cells were resuspended in 100 µL antibody solution (5 ug/ mL in Blocking Buffer) for 30 min on ice protected from light. Cells were pelleted again (200 g, 4 °C for 5 min) and resuspended in 500 µL Washing Buffer (PBS with 5 % FBS). Samples were filtered using a 5 mL tube with a cell strainer lid (Corning Falcon round bottom tube) before analysis on a Canto II Flow Cytometry System.

### 3.2.16 Sample preparation for ribosome profiling

For ribosome profiling experiments, two biological independent replicates per condition were performed on consecutive days. Cells were plated on 15 cm plates and treated with 300 nM torin 1 or DMSO for 2 h the next day. Samples were processed by Alexander Kowar as described previously (Loayza-Puch *et al*, 2016). Briefly, cells were rinsed with ice-cold PBS in the presence of 100 µg/ mL cycloheximide, scraped, and pelleted. Cell pellets were lysed in 20 mM Tris-HCl pH 7.5, 10 mM MgCl, 100 mM KCl, 1 % Triton-X 100, 2 mM DTT, 100 ug/ mL CHX and 1x protease inhibitor cocktail for 10 min on ice and centrifuged at 6,400 rpm (4 °C) for 5 min. For RNA sequencing experiments, 10 µL of the supernatant was added to 1 mL Trizol and stored at – 80°C until further processing. For ribosome profiling libraries, the supernatant was digested (2 U/ µL RNase I) at room temperature for 45 min and separated on a linear sucrose gradient (7 % to 47 %) using an SW-41 Ti rotor at 36,000 rpm (4 °C) for 2 h. Monosome-containing fractions were pooled and treated with proteinase K, 1 % SDS at 45 °C for 1 h. RNA fragments were purified with Trizol and precipitated in the presence of glycogen (45 µg).

### 3.2.17 Preparation of ribosome profiling libraries

The preparation of ribosome profiling libraries was performed by Alexander Kowar as described previously (Ingolia *et al*, 2012; Loayza-Puch *et al.*, 2016). Ribosome-protected fragments (RPFs) were size selected (17-34 nucleotides) and dephosphorylated at their 3' ends using T4 PNK at 37 °C for 1 h. Pre-adenylated adaptors were ligated to the 3' ends of the RPFs using T4 RNA Ligase 2 truncated KQ at 22 °C for 3 h. To remove unbound adaptors, samples were incubated with yeast 5'deadenylase (10 U/ µL) and RecJ exonuclease (10 U/ µL) at 30 °C for 45 min. After an incubation with rRNA homologous, biotinylated RNA oligos at 95 °C for 1 min, followed by 37 °C for 15 min, MyOne streptavidin magnetic beads were added for 30 min at 37 °C. Upon magnetic separation, RNA was precipitated and reverse transcribed using the SuperScript III First-Strand Synthesis Kit (50 °C for 50 min), then treated with 5 M NaOH at 95 °C for 3 min to degrade RNA. The cDNA was circularized using the CircLigase II Kit and amplified via PCR to introduce Illumina i7 indices using the Q5 HF 2x MasterMix. The DNA was size-selected on an 8 % non-denaturing PAGE gel, precipitated, and resuspended in nuclease-free water. DNA samples were quantified by Qubit and pooled. Library concentrations of 2 nM were adjusted and sequenced on a NextSeq2000 platform (Illumina) at the DKFZ Sequencing Open Lab.

### 3.2.18 Ribosome profiling data analysis

The DKFZ Genomics Core Facility provided the FASTQ raw files. Further analysis was performed by Alexander Kowar as described previously (Loayza-Puch *et al.*, 2016). First, adapters were trimmed using cutadapt (v3.4). Demultiplexing was performed with barcode_splitter from FASTX-toolkit (v0.0.6). For fragments bigger than 27 nt, unique molecular identifiers were extracted with umi_tools (v1.1.1). Afterwards, rRNA reads were determined and dropped from the processing using BLAST-Like Alignment Tool (BLAT; v36x2). NCBI RefSeq annotation was used to manually design the rRNA index for RNA18S5, RNA28S5 and RNA5-8S5. To align filtered reads to GRCh37/hg19, Spliced Transcripts Alignment to a Reference (STAR; v2.5.3a) was applied with '--readFilesCommand zcat --quantMode TranscriptomeSAM GeneCounts --outSAMmapqUnique 0'.

To determine ribosomal occupancy among different amino acids from filtered RPF reads, differential ribosome codon reading (diricore) analysis was performed (Loayza-Puch *et al.*, 2016). First, reads were normalized to gene-levels to exclude codon frequency biases. Reads with an unambiguous gene ID were quantified for reading frame counts in positions 12 and 15 downstream of the 5' end, representing the P- and A-site of ribosomes, respectively. The P-site did not show any obvious changes in our datasets and thus was not considered for further analysis.

### 3.2.19 RNA isolation and RNA sequencing

For RNA isolation of cell lysates that had been treated with Trizol and stored at – 80 °C during sample preparation of ribosome profiling experiments were thawed on ice. Upon treatment with 200 µL chloroform, vigorous shaking and incubation at room temperature for 2-3 min, samples were centrifuged at 14,000 rpm for 15 min at 4 °C. The aqueous phase was added to 600 µL isopropanol, mixed and incubated at room temperature for 10 min. RNA was precipitated at – 20 °C overnight, then pelleted by centrifugation at 14,000 rpm for 20 min at 4 °C. The pellet was washed twice in 800 µL 70 % EtOH. The RNA pellet was air-dried and resuspended with water by incubation for 10 min at 55 °C shaking at 400 rpm. RNA was quantified by Qubit.

Library preparation and RNA sequencing were performed at the NGS Core Facility at the DKFZ. The TrueSeq mRNA stranded Kit was used to prepare sequencing libraries according to manufacturer instructions. Briefly, oligo(dT) beads were used to purify mRNA from 500 ng total RNA. After fragmentation of poly(A)+ RNA to 150 bp, RNA was reverse transcribed. The cDNA fragments were end-repaired, adenylated, adapterligated, and amplified by PCR. Libraries were validated using Qubit. Sequencing was performed on a NovaSeq6000 platform (100 bp paired-end) according to manufacturer instructions.

### 3.2.20 RNA sequencing data analysis

The DKFZ Genomics & Proteomics Core Facility provided the FASTQ raw files. Differential gene expression analysis was performed by Toman Borteçen using DESeq2 (version 1.30.1) with default settings (raw read counts ≥10 per gene).

### 3.2.21 Sample preparation for steady-state proteomics

Five independent biological replicates per condition were performed on successive days for steady-state proteomics experiments. Cells were plated in 6-well plates and treated after attachment for 40 h with rapamycin (50 nM) or DMSO, with additional media change after 24 h. For protein extraction, cells were rinsed with ice-cold PBS twice and lysed in RIPA buffer (50 mM Tris-HCl pH 8, 150 mM NaCl, 1 % NP-40, 0.5 % sodium deoxycholate, 0.1 % SDS, 1 mM EDTA, 5 mM MgCl2, 1x protease inhibitor cocktail: 5 µM E64, 200 µM AEBSF, 1 µM aprotinin, 20 µM leupeptin, 1 µM pepstatin and 5 mM benzaminidine). Benzonase (250 u/ mL) was added, lysate vortexed and incubated on ice for 15 min. After centrifugation at 18,000 g for 15 min at 4 °C, supernatants with solubilized protein were collected. Protein concentrations were measured with the Pierce BCA Protein Assay. Equal protein amounts (20 µg) were submitted to the DKFZ Proteomics Core Facility for further analysis.

### 3.2.22 LC-MS/MS analysis for steady-state proteomics

At the DKFZ Proteomics Core Facility, protein samples (10 µg) were trypsin digested using an AssayMAP Bravo liquid handling system for the autoSP3 protocol (Müller *et al*, 2020). An Ultimate 3000 UPLC system with an Orbitrap Exploris 480 mass spectrometer was used for analysis. The analysis time was 60 min. Before analytical separation, peptides were desalted on a trapping cartridge (Acclaim PepMap300 C18, 5 µm, 300 Å wide pore) for 3 min using 30 µL/ min flow of 0.1 % (v/v) trifluoroacetic acid in water. A nanoEase MZ Peptide analytical column (300 Å, 1.7 µm, 75 µm x 200 mm) was used for the analytical multistep gradient (300 nL/ min) using solvent A (0.1 % (v/v) formic acid in water) and solvent B (0.1 % (v/v) formic acid in acetonitrile).

After 4 min at 2 % solvent B, the concentration of B was linearly ramped from 5 % to 30 % over 43 min. At the end, washing (78 % B for 2 min) and equilibration (2 % B for 10 min) was performed.

Eluting peptides were analyzed in data independent acquisition (DIA) mode in the mass spectrometer. Fragment spectra were recorded at a full scan at 120k resolution (350-1,400 m/z, 300 % AGC target, 45 ms maxIT. profile mode) and 20 windows of different isolation width (400-1,000 m/z, 1000 % AGC target, 30k resolution, 54 ms maxIT, centroid, 1 Da overlap). Collision energy was set to 28 %.

### 3.2.23 Steady-state proteomics data analysis

Data analysis was carried out by Dominic Helm and Martin Schneider at the DKFZ Proteomics Core Facility. Spectronaut was used in a directDIA+ (deep) library-free mode for analysis of DIA RAW files. Default settings were used with the following adjustments. Within the pulsar search in result filters, the m/z max was set to 300 to 1,800 and relative intensity to 5 %. Within DIA analysis under quantification, the protein LFQ method was set to MaxLFQ. The mouse proteome from Uniprot (mouse reference database with one protein sequence per gene, containing 21,957 unique entries from 03.05.2023) and FASTA from MaxQuant for the contaminants (246 unique entries from 22.12.2022) were used to search data against.

### 3.2.24 Sample preparation for nascent proteomics

For nascent proteomics experiments, three experimental replicates per condition were performed in parallel. Cells were plated in 6-well plates two days before the start of the treatments. Cells were treated with amino acid starvation medium (DMEM-F12 without methionine, arginine and lysine, 5 % dFBS and 200 mg/ L proline) in the presence or absence of 50 nM torin 1, 50 nM rapamycin or DMSO for 45 min. Subsequently, cells were labeled with SILAC medium supplemented with intermediate stable isotope-containing lysine and arginine (13C6-Arg, Lys-D4) or heavy stable isotope-containing lysine and arginine (13C6, 15N4-Arg, Lys-D9), L-AHA (100 µM) and the different drugs

or DMSO for 4 h (Table 3). For the relative quantification of SILAC ratios, the two conditions that were compared were labeled with medium or heavy isotopes, respectively.

For protein extraction, cells were rinsed with ice-cold PBS twice and lysed in 300 mM HEPES pH 8, 1 %SDS and 1x protease inhibitor cocktail (5 µM E64, 200 µM AEBSF, 1 µM aprotinin, 20 µM leupeptin, 1 µM pepstatin and 5 mM benzaminidine). Further sample preparation and enrichment were performed by Toman Borteçen using the QuaNPA workflow (Borteçen *et al*, 2023). First, cell lysates were sonicated in AFA-tube TPX strips using a Covaris LE220R-Plus and protein concentrations were measured with the Pierce BCA Protein Assay. A total of 200 µg protein (100 µg per condition) was used for the enrichment protocol. The lysates of the two conditions that were compared (medium and heavy SILAC isotopes) were pooled and diluted (total of 150 µL in lysis buffer). A Bravo liquid handling system was used for automated enrichment of the newly synthesized proteins. Samples were partially alkylated with 3.4 µL of 600 mM iodoacetamide (IAA) for 20 min at room temperature. To couple AHA-labeled newly synthesized proteins to beads, magnetic alkyne agarose (MAA) beads (20 µl) in a 20 % (v/v) suspension, diluted in lysis buffer, and the Copper(I)-catalyzed Azide Alkyne Cycloaddition (CuAAC) mixture (21.62 mM CuSO4, 216.22 mM pimagedine hydrochloride, 216.22 mM sodium ascorbate, 108.11 mM Tris-hydroxypropyltriazolylmethylamine (THPTA)) were added for 2 h at 40 °C. Afterwards, beads were washed with 150 µL water and bound proteins reduced and alkylated with 150 µL of 10 mM Tris(2-carboxylethyl)phosphine (TCEP) and 40 mM 2-chloroacetaminde (CAA), dissolved (100 mM Tris-HCl pH 8, 200 mM NaCl, 0.8 mM EDTA, 0.8 % SDS) and incubated for 20 min at 70 °C, followed by 15 min at 20 °C. Beads were washed as described previously (Borteçen *et al.*, 2023) and resuspended in 100 mM ammonium bicarbonate (pH 8, 50 µL). Proteins were enzymatically digested off beads (0.5 µg trypsin) and peptides purified using a modified version of the autoSP3 protocol (Müller et al., 2020). Peptides were frozen at – 80 °C and lyophilized (UNIVAPO-150H vacuum concentrator with UNICRYO MC2 cooling trap and UNITHERM 4/14 D closed circuit cooler). To each sample, 5 µL of magnetic carboxylate Sera-Mag Speed Beads (100 µg/ µL in 10 % formic acid) were added. Peptides were aggregated onto beads by the addition of 195 µL acetonitrile and incubated for 18 min shaking at 100 rpm. The beads were washed twice (180 µL

acetonitrile) and dried. Afterward, the beads were resuspended (20 µL 0.1 % formic acid) and sonicated for 10 min using an Ultrasonic Cleaner USC-T. The enriched peptides were dissolved (0.1 % formic acid) and stored for further analysis.

To avoid median normalization, non-enriched pulsed SILAC-AHA-labeled protein lysates were measured. By pooling equal parts of the cell lysates of the two conditions that were compared before the enrichment, 50 µg of lysate was collected. Proteomics samples were prepared using the manual SP3 protein protocol (Hughes *et al*, 2014). Proteins were aggregated on magnetic beads by addition of acetonitrile (50 % (v/v)) for 18 min at room temperature. After washing the beads twice with 80 % (v/v) ethanol and acetonitrile, proteins were digested (trypsin) on beads in 100 mM ammonium bicarbonate (pH 8) for 16 h at 37 °C. After digestion, a magnetic rack was used to remove the supernatant, and trifluoroacetic acid (TFA) was added (final 1 % (v/v)).

### 3.2.25 LC-MS/MS analysis for nascent proteomics

LC-MS/MS analysis was carried out on an EASY-nLC 1200 system connected to a QExactive HF mass spectrometer by Toman Borteçen (Borteçen *et al.*, 2023). Before analytical separation, peptides were desalted on a trapping column (Acclaim PepMap C18, 20 mm × 100 µm, 5 µm C18 particles, 100 Å wide pore) using constant flow of solvent A (0.1 % formic acid) at a pressure of 800 bar. A nanoEase M/Z peptide BEH C18 analytical column (250 mm × 75 µm 1/PK, 130 Å, 1.7 µm) was used for the analytical multistep gradient (300 nL/ min) using solvent A (0.1 % formic acid) and solvent B (80 % acetonitrile). Equilibration of the column was performed with 2 µL solvent A (600 bar maximal pressure). After heating the column to 55 °C, solvent B was gradually increased during elution of peptides. For analyzing the nascent proteome, inputs started with 4 % solvent B, followed by an increase to 6 % within the first minute, increased to 27 % at 51 min, and then increased to 44 % at 70 min. Solvent B was raised to 95 % after 70 min. At the end of the analysis (after 80 min), the system was re-equilibrated using 5 % solvent B for 10 min.

Eluting peptides were analyzed in data independent acquisition (DIA) mode in the mass spectrometer. A full scan at 60,000 FWHM resolution (400-1,000 m/z, 3e6 AGC

target, 20 ms maxIT) was performed followed by 26 windows of equal size (30,000 FWHM, 1e6 AGC target, 40 ms maxIT, 1 Th overlap, 23.3 m/z width), covering a range from 402-982.8 m/z. The first mass was fixed to 200 m/z and collision energy was set to 27 %.

### 3.2.26 Nascent proteomics data analysis

Data analysis was carried out by Toman Borteçen using DIA-NN to analyze raw files (Demichev *et al.*, 2020). A predicted spectral library was generated using the mouse proteome FASTA file from the SwissProt database (version from 12.02.21 with 17056 entries) together with a FASTA file for common contaminants. For the spectral library prediction, default settings were applied with the adjustment of methionine oxidation as variable modification. Raw files were processed using default settings of DIA-NN (functions from plexDIA enabled). Three SILAC channels were registered with mass shifts corresponding to Arg, Arg6 (+6.020129 Da), Arg10 (+10.008269 Da), Lys, Lys4 (+4.025107 Da), Lys9 (+9.056356 Da), and an additional decoy channel with Arginine (+13.9964 Da) and Lysine (+12.0033 Da). The translation of retention times between peptides within the same elution group was allowed. For quantification, the first monoisotopic peak and 13C-isotopic peak were included and the MS1 deconvolution level set to 2. The precursor charge rate was set from 1-4, m/z range of the precursors from 300-1,800, peptide length from 7-30 and fragment ion m/z range from 200-1800. The FDR of precursors was set to 1 %. The precursor output tables were filtered (FDR < 0.01, channel q-value < 0.01, translated q-value < 0.01), and the MBR function in DIA-NN was enabled. The R software environment was used to process the output tables “report.pr_matrix_channels_translated.tsv” and “report.pr_matrix_channels_ms1_translated.tsv” using common scripts. Contaminants were removed. Protein abundance was calculated with the MaxLFQ algorithm, by application to SILAC channels individually, with the function “process_long_format()” of the iq R package (v1.9.6). The “Ms1.translated” and “precursor.translated” quantity was used for MaxLFQ calculations for MS1- and MS2-based quantification, respectively. For each sample, SILAC ratios per protein group were calculated with use of LFQ values. Unique protein groups, defined by single Uniprot identifier, with a

minimum of two SILAC ratios in three replicates were used for differential expression analysis.

For commonly identified newly synthesized proteins, average SILAC ratios were determined in the pooled non-enriched samples using MS1-based quantification. The ratios were used to determine the average protein synthesis rate in the respective condition. Based on these protein synthesis rates, the average ratio was calculated between the two conditions that were compared to center the distribution of SILAC ratios in the newly synthesized proteome data.

### 3.2.27 Statistical analysis of proteomics

Statistical analysis of proteomics data was carried out by Toman Borteçen using the R/Bioconductor packages Limma (Ritchie *et al.*, 2015) and DEqMS (Zhu *et al.*, 2020) for differential expression tests. Data was fitted onto a linear model, followed by performing the empirical Bayes moderated t-test. For the variance estimation in DEqMS, the number of identified precursors considering modified peptide sequences and charge but not SILAC channels was included for each protein group in the newly synthesized proteome data sets. The “GSEA” and “gseGO” function of the clusterProfiler (v3.18.0) R/Bioconductor package was used for gene set enrichment analysis using the log2 fold change values of proteins quantified (Wu *et al*, 2021). The msigdbr (v7.5.1) R package of the CRAN software repository was used to analyze gene lists of the Molecular Signatures Database.

Protein coding mRNA sequences were derived from the mm10 reference transcript coding sequences with canonical annotation of the Ensembl database. For ribosomal protein sequences that were not annotated in these packages, Ensembl transcripts were added manually. For each transcript, codon frequencies were calculated and averaged across the genome to serve as a reference for subsets of differentially expressed proteins. The “codon usage % deviation from transcriptome average” was calculated by subtracting the reference codon frequency from the codon frequency of an individual transcript (with canonical annotation of the Ensembl database). All transcript-coding sequences detected in the newly synthesized or steady-state

proteome data set, respectively, represent “all proteins”. Codon frequencies were calculated for AAA, CAA, GAA, and the sum of all three codons (VAA). As a control, all codons except the VAA codons were used (non-VAA).

### 3.2.28 Mice experiments

Tumor growth experiments using an orthotopic transplantation model of pancreatic cancer were performed by Robert Kalis and Vivien Vogt using 16 and 24 week-old (mixed between groups) female and male (mixed between groups) C57BL/6J Rag2-/- mice. The mice were bred in-house and kept under standard pathogen-free conditions (temperature 22 ± 1 °C, humidity 55 ± 5 %) and a 14 h light : 10 h dark photoperiod with food and water *ad libitum*. All animal experiments were performed in accordance with a protocol approved by the local Ministry. For orthotopic tumor experiments, edited Ctu1 iKO and control EPP2 cells were injected into the pancreas of mice. Surgeries were conducted under isoflurane anesthesia on a heated plate. A small incision was made in the upper left quadrant of the shaved abdomen to expose the spleen, followed by the externalization of the pancreas. A Hamilton syringe was used to inject $5x10^5$ cells suspended in 10 µl PBS into the pancreas. Afterward, organs were carefully repositioned, and the peritoneum was closed with a resorbable 6-0 Vicryl suture, with the skin closed using sterile wound clips. Animals received intraperitoneal injections of carprofen (5 mg/ kg) preemptively and every 12 hours for 48 hours post-surgery. The health status of the mice was checked daily. At day 4 post-injection, the mice were randomly assigned to either the treatment or vehicle cohorts. The treatment cohort received 5 mg/ kg/ day Rapamycin in 50 µl intraperitoneally for 9 days, while the vehicle cohort received 50 µl of vehicle (10 % DMSO, 40 % PEG300, 5 % Tween-80 in PBS). The mice were sacrificed 14 days after the orthotopic injection, and the tumor weight was measured.

### 3.2.29 Statistical analysis

For proteomics data, statistical analysis was performed using the R software environment with software packages described in the respective method section.

Samples were acquired in a randomized manner. Statistical analysis in other experiments was performed by calculating a two-tailed unpaired *t*-test with Welch correction, a one-sample *t*-test with a hypothetical mean of 1, or a Wilcoxon rank test (two-tailed). The figure legends specify the number of experimental and biologically independent replicates, and the statistical parameters used. Western blots were quantified with BioRad Image Lab. Flow cytometry experiments were analyzed using BD FACSDiva software and FlowJo. Statistical analyses were conducted using the R software environment or GraphPad Prism.

# 4 Results

## 4.1 Genome-wide CRISPR-Cas9 screen to identify genes that become essential during mTOR inhibition

### 4.1.1 Rationale for a CRISPR-Cas9 screen to study mTORC1 signaling under different nutrient environments

mTORC1 is a central kinase integrating growth signals and nutrient supply to promote cell proliferation under favorable conditions (Saxton & Sabatini, 2017). Interestingly, the Palm laboratory could show that mTORC1 can also suppress cancer cell proliferation when cells rely on proteins as an amino acid source (Palm *et al.*, 2015). Under amino acid-deprived conditions, mammalian cells can upregulate macropinocytosis, a process by which cells can acquire the amino acid source of extracellular proteins (Bloomfield & Kay, 2016; Palm & Thompson, 2017). Mechanistically, Edoardo Ratto, a former PhD student in the Palm laboratory, showed that mTORC1 suppresses the V-ATPase assembly at lysosomal membranes to regulate lysosome pH and catabolic activity (Ratto *et al.*, 2022). Thus, whether mTORC1 promotes or antagonizes cell proliferation depends on a cell´s amino acid source: free amino acids or proteins. In turn, the inhibition of mTORC1 has opposing effects on cancer cell proliferation depending on the nutrient availability. In my PhD project, I aimed to systematically identify critical regulators of mTOR-mediated cancer cell proliferation depending on the nutrient environment. To this end, I performed a genome-wide CRISPR-Cas9 screen under protein-rich conditions that were either amino acid-rich or -deprived in the presence or absence of the mTOR inhibitor torin 1.

For my screen, I used the murine pancreatic cancer cell line EPP2. To generate the EPP2 cell line, fetal pancreas progenitor cells with an oncogenic $KRas^{G12D}$ mutation and $P53^{loxP/loxP}$ were isolated and engineered to express c-Myc, CreERT2, and Luciferase. The EPP2 cell line was then derived from tumors that were established upon orthotopic injection of the engineered progenitor cells into the pancreas of recipient mice. The tumors showed the histological characteristics of human pancreatic cancer (Rathert *et al*, 2015). Human pancreatic cancer tumors (PDAC) are poorly vascularized and KRas-driven malignancies (Orth *et al*, 2019). The Palm laboratory and others showed that the increased growth factor signaling in pancreatic cancer cells

allows them to sustain their proliferation by actively scavenging extracellular proteins to survive within the vascularly compromised tumor environment (Commisso *et al.*, 2013; Kamphorst *et al.*, 2015; Palm *et al.*, 2015). Thus, the system allowed me to study mTORC1 signaling in cells, which can proliferate depending on either free amino acids or extracellular proteins.

### 4.1.2 Selection of an EPP2 clone

For a genome-wide CRISPR screen, using a clonal inducible Cas9 (iCas9) cell line is beneficial as it allows selection for a clone with tight Cas9 expression and efficient gene editing (Michlits *et al.*, 2020). Moreover, CRISPR-Cas9 editing can be induced time-controlled after transduction and antibiotic selection of the genome-wide sgRNA library. The Palm laboratory uses the tetracycline (tet) inducible system (tet-on) to generate iCas9 cell lines (Das *et al*, 2016). In the tet-on system, the gene of interest is expressed under the control of the tet-dependent promoter TRE (tet responsive element), and a second plasmid carries the reverse tetracycline-controlled transactivator (rtTA). In the presence of tetracycline, or its analog doxycycline, tetracycline (or doxycycline) binds to the rtTA. In turn, rtTA binds to the TRE and induces expression of the gene of interest. For the generation of our iCas9 EPP2 cells, Catarina Pechincha, a former PhD student in the Palm laboratory, transduced EPP2 cells with a plasmid constitutively expressing the transactivator rtTA3 (Figure 4 A). Upon antibiotic selection, Catarina transduced the inducible Cas9-BFP cassette (under control of TRE3G) and sorted BFP-positive single cells (Pechincha *et al.*, 2022). In the iCas9 clones, Cas9 expression can now be induced by doxycycline treatment.

For the screen, rapid activation of Cas9 expression upon doxycycline treatment without basal Cas9 activity was desirable. To test the editing efficiency upon doxycycline treatment and the tightness of the Cas9 cassette for different iCas9 EPP2 clones, I transduced several clones with an sgRNA against the cell surface protein Cd9 (Figure 4 A). After four days of treatment with doxycycline, I analyzed the knockout efficiency by immunostaining of Cd9 using flow cytometry analysis. I could observe high Cd9 knockout efficiency in many clones. To test leakiness, I cultured the sgRNA-Cd9-transduced cells for 22 days without doxycycline treatment and assessed Cd9

expression. Indeed, some clones showed reduced Cd9 expression without doxycycline treatment and, thus, were excluded from further analyses. Based on these data, I selected EPP2 clone 2 for the screen and further validation experiments. I tested editing efficiencies for different doxycycline concentrations (100 to 1,000 ng/ mL) and doxycycline treatment times (one to six days). I optimized the doxycycline treatment to 300 ng/ mL for four days, after which the Cd9 protein was lost from the cell surface (Figure 4 B).

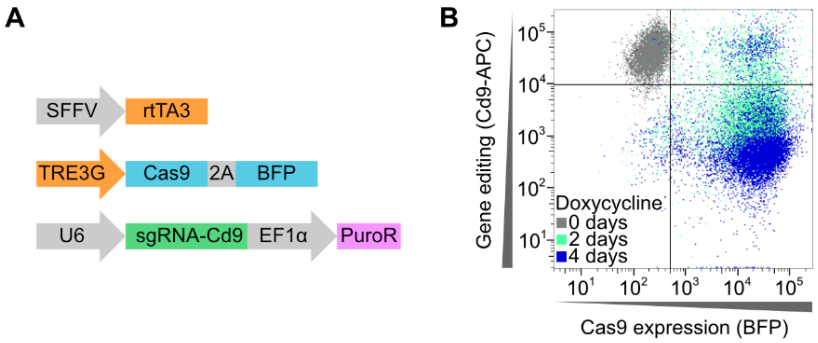


**Figure 4 – Analysis of the editing efficiency and tightness in inducible Cas9 (iCas9) EPP2 cells.** **(A)** Schematic representation of the iCas9 system engineered in EPP2 cells. The transactivator rtTA3 is constitutively expressed under the SFFV promoter and Cas9-BFP is under the control of the tetracycline-responsive element (TRE3G). Catarina Pechincha generated the iCas9 clones. To assess knockout efficiency, cells were transduced with an sgRNA against Cd9, constitutively expressed under the U6 promoter. **(B)** Flow cytometry analysis of Cas9-BFP expression and sgRNA-mediated gene editing of the surface protein Cd9 in iCas9 EPP2 cells after doxycycline treatment [300 ng/ mL] for the indicated time. Cd9 was labeled with anti-Cd9-APC antibody.

### 4.1.3 Optimization of cell culture conditions

Next, I established the cell culture conditions for the screen. I performed proliferation assays with the selected iCas9 EPP2 clone to identify metabolic conditions under which protein-dependent cell proliferation was reproducible and sensitive for the ATP-competitive mTOR inhibitor torin 1. Under amino acid-replete and protein-rich conditions, EPP2 cells proliferated fast, and torin 1 stably suppressed proliferation. In addition to the amino acid-replete conditions, I depleted the essential amino acid leucine while keeping physiological levels of bovine serum albumin (2 % BSA) as an alternative leucine source. Hence, EPP2 cells obtained sufficient amino acids to proliferate slowly without free leucine, and the addition of torin 1 stably enhanced cell proliferation under leucine starvation. To further increase the difference in cell proliferation under leucine starvation in the presence or absence of torin 1, I reduced

FBS concentrations from 10 % to 5 %, limiting the availability of growth factors and proteins. The torin 1 concentration was adjusted to 300 nM to decrease the cell population doubling time under protein- and amino acid-rich conditions by ~ 70 %, allowing for sgRNA enrichment and depletion during the screen. Of note, the torin 1 concentration of 300 nM was set in the presence of 2 % BSA, which partially sequesters the inhibitor from cells and thus reduces its efficiency compared to low-protein conditions (i.e. no BSA and 10 % FBS) as used later in experiments.

After the selection of the iCas9 EPP2 clone and the establishment of the metabolic cell culture conditions, I transduced cells with the Vienna genome-wide sgRNA library (six sgRNAs per gene: total 123,000 sgRNAs) encoding for pLenti-hU6-sgRNA-iT-EF1as-Thy1.1-P2A-NeoR at a low multiplicity of infection (MOI) < 0.11 to ensure that cells receive only one sgRNA. I enriched the population of transduced cells by selecting them with geneticin and followed the selection process by immunostaining and flow cytometry detection of Thy1 expression (> 94 % Thy1-positive). Throughout the infection, I kept a library representation of 500- to 1,000-fold to maintain library complexity.

### 4.1.4 CRISPR-Cas9 screen during mTOR inhibition with either free amino acids or proteins as a nutrient source

Two days before starting the screen, I expanded the iCas9 EPP2 cells carrying the genome-wide CRISPR library and induced Cas9 expression and, thus, CRISPR-Cas9 gene editing with doxycycline. At day 0, I collected an initial cell population in two replicates (T0) and I plated cells under four different conditions: amino acid-rich medium (2 % BSA, 5 % FBS) with 300 nM torin 1 or solvent control (DMSO) or leucine starvation medium (4 % BSA for the first four days, then 2 % BSA; 5 % FBS) with 300 nM torin 1 or DMSO (Figure 5 A). Doxycycline was added for the first two days of the screen. Throughout the screen, I kept a library representation of at least 600-fold for each metabolic condition to prevent the influence of random changes on the sgRNA representation. I replated cells in amino acid-rich medium (DMSO) every second day, with a media change after one day. The torin 1-treated amino acid-rich medium cell population was replated every three days with an additional media change after

1.5 days. I replated both leucine starvation conditions every four days with additional media change after 2 days, starting only at day 6 for the DMSO-treated leucine starvation conditions, as the cells needed more time to adapt to the stressful condition. I harvested the final cell populations after culturing the cells for 12 population doublings in the respective media conditions or 26 days for the DMSO-treated leucine starvation condition.

The growth curves of the screen showed results as expected from the optimized proliferation assays for the different metabolic conditions (Figure 5 A). Under amino acid-replete and protein-rich conditions, EPP2 cells proliferated fast, while treatment with torin 1 suppressed proliferation (Figure 5 A). In contrast, the proliferation rate of the leucine starvation condition was very slow, and the cells mainly stopped proliferation after three splits (Figure 5 A). Under leucine starvation, torin 1 treatment allowed EPP2 cells to proliferate faster (Figure 5 A). Comparing both torin 1 conditions revealed a similar proliferation rate at the beginning of the screen, suggesting that under mTOR inhibition, cell proliferation seems hardly affected by the presence or absence of leucine.

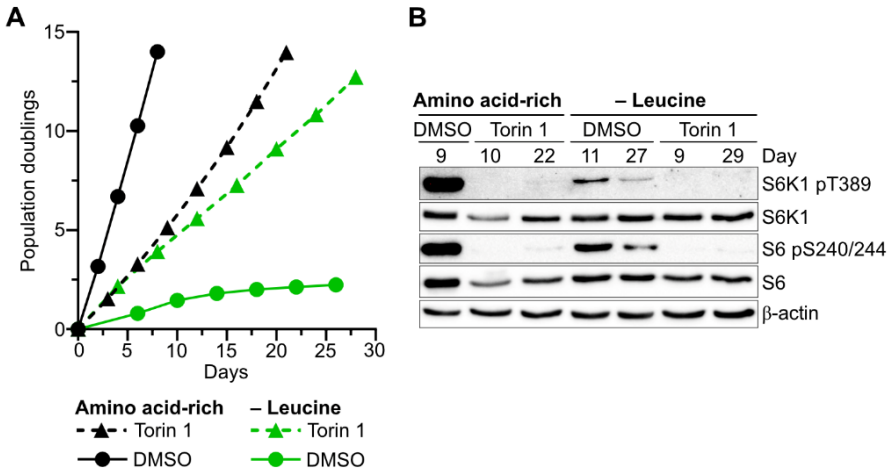


**Figure 5 – CRISPR-Cas9 screen during mTOR inhibition with either free amino acids or proteins as a nutrient source.**
**(A)** Proliferation of iCas9 EPP2 cells during CRISPR screens in the presence of torin 1 [300 nM] or DMSO under amino acid-rich or leucine starvation conditions (2 % BSA in all conditions). Data are shown as population doublings. **(B)** Immunoblotting analysis of mTOR pathway activity in iCas9 EPP2 cells harvested at indicated times throughout the screen among given conditions.

To confirm efficient mTOR pathway inhibition by torin 1 throughout the screening, I harvested protein samples of all conditions and analyzed them by immunoblotting (Figure 5 B). The blots showed a substantial reduction in phosphorylation of the

mTORC1 target S6K1 pT389 and the S6K target S6 pS240/244 upon torin 1 treatment (Figure 5 B), confirming continuous suppression of mTOR signaling throughout the screen. Moreover, I found that mTOR is active even under leucine starvation, although at a reduced level compared to amino acid-rich conditions, indicating that leucine is not essential for mTOR activity.

### 4.1.5 Identification and validation of screen hits

I collected cell pellets at the beginning and after 12 population doublings for each condition or after 26 days for the DMSO-treated leucine starvation condition, as in this condition, the cells almost stopped proliferation. Upon genomic DNA extraction and purification, I performed two PCRs. In the first PCR, I amplified the sgRNAs and added sample-specific barcodes. After the first PCR, the products of all conditions were pooled and purified. In the second PCR, I introduced sequencing primers and adapters. Unfortunately, I repeatedly could not observe any band for the first PCR product for the DMSO-treated leucine starvation condition in which cells were very stressed and almost stopped proliferation. As sequencing of this condition was not possible, I continued processing the samples of the three remaining conditions. I sent those for sequencing at the Sequencing Core Facility at the IMP in Vienna.

The pre-processing of the sequencing results was done by Robert Kalis from the Zuber lab in Vienna. To identify enriched and depleted genes from the CRISPR-Cas9 screens with high sensitivity, I used the pre-processed sequencing data to run MAGeCK (Li *et al.*, 2014b). For each gene in each condition, I used MAGeCK to calculate the $\log_2$ fold-change ($\log_2$FC) and p-value of the sgRNA abundance (average counts of six sgRNAs per gene) either relative to the initial representation (T0) or relative to the endpoint of each of the other conditions. As I lost the DMSO-treated leucine starvation sample during sample preparation, it was challenging to interpret the results of the torin 1-treated leucine starvation condition. Thus, I focused on comparing the amino acid-rich conditions with or without mTOR inhibition. As leucine starvation was no longer relevant for selecting the hits to work with, all following experiments, except the competitive proliferation assays for validation of hits, were performed in amino acid-rich media (no BSA and 10 % FBS).

To identify genes that became selectively essential or detrimental under mTOR inhibition, I quantified changes in sgRNA abundance between torin 1-treated and control amino acid-rich conditions. I found that the loss of most genes did not have any effect on cell proliferation as indicated by $log_2FC$ values close to 0 (Figure 6 A). About 190 genes became selectively essential under torin 1 treatment ($log_2FC < 2$; $p < 0.01$; Figure 6 A), including the mTORC1 signaling pathway and genes related to protein synthesis. In contrast, I identified 80 genes as selectively detrimental under torin 1 treatment ($log_2FC > 2$; $p < 0.01$; Figure 6 A), including negative regulators of the mTORC1 signaling pathway.

To validate selected hits, I performed competitive proliferation assays in a medium with 300 nM torin 1 or solvent control (DMSO) in the presence of 2 % BSA and 5 % FBS to recapitulate the screen conditions. I transduced iCas9 EPP2 cells with a dual-sgRNA (dsgRNA)-mCherry plasmid (Dual-hU6-sgRNA-mU6-sgRNA-Ef1α-mCherry-P2A-PuroR) targeting the gene of interest or a dsgRNA against a non-coding chromosome region (Chr1.1) as a control (Table 9). After antibiotic selection, cells expressing the dsgRNA-mCherrry plasmid and non-transduced cells were treated for two days with doxycycline to induce CRISPR-Cas9 editing of the gene of interest (iKO). At the start of the competitive proliferation assay, iCas9 EPP2 cells carrying a dsgRNA-mCherry plasmid were co-cultured with non-transduced control cells in the presence of doxycycline for two more days. Thus, the percentage of fluorescently-labeled knockout cells ($dsgRNA^+$ cells %), quantified by flow cytometry on day 0 and when passaged, allowed me to follow how the loss of an individual gene affects cell proliferation in competition with non-transduced wildtype cells (Figure 6 B). With this sensitive medium-throughput approach, I found that Pigt-, Kif18b- or Dnajc9-deficient cells were rapidly outcompeted by control cells, specifically under mTOR inhibition (Figure 6 B). In contrast, the genes Ilf2, Gsk3b, Hnrnpc, and Mknk2 were detrimental for cell proliferation under mTOR inhibition as the respective iKO cells outcompeted wildtype cells under torin 1 treatment (Figure 6 B), confirming the results from the CRISPR-Cas9 screens.

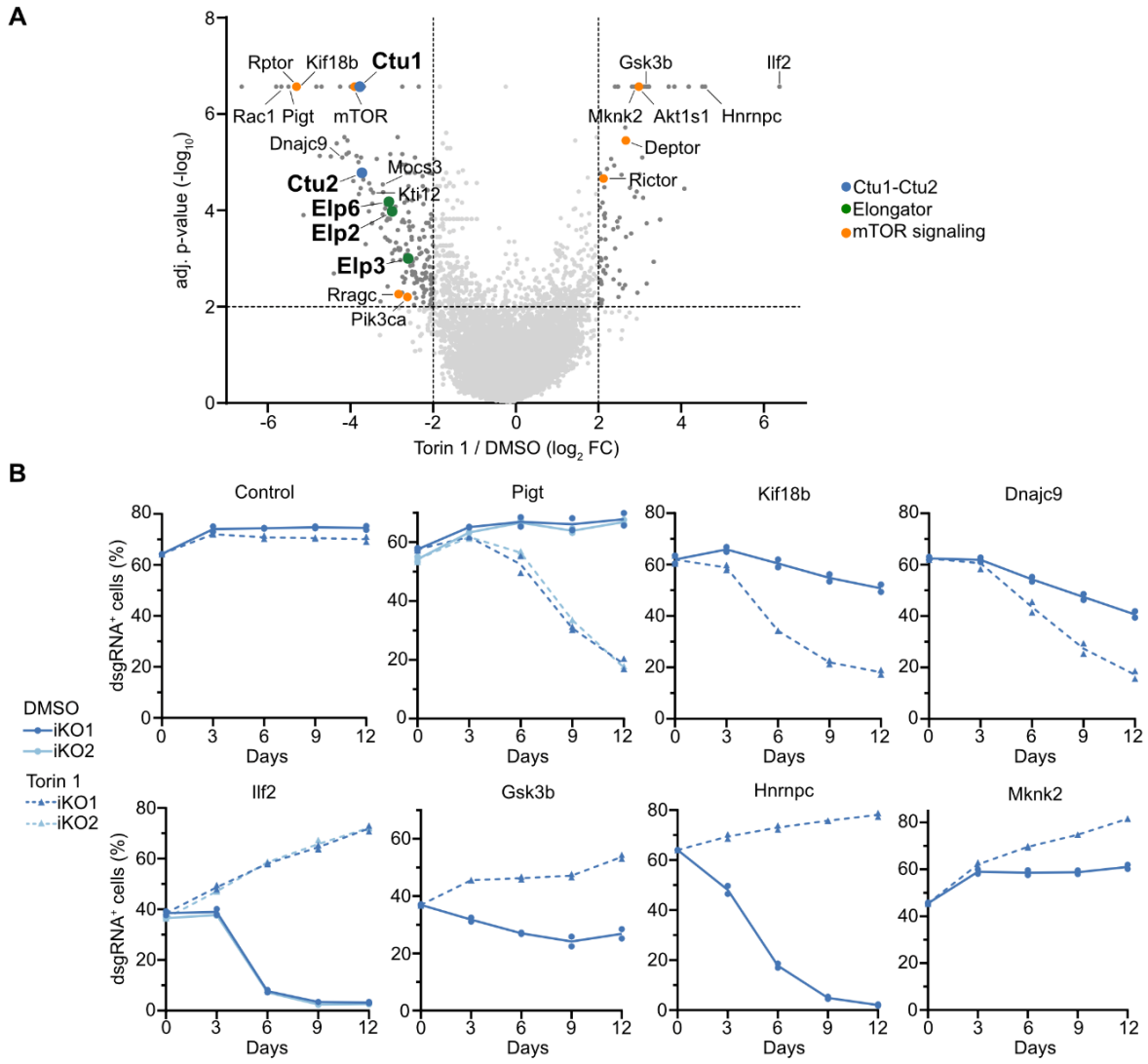


**Figure 6 – CRISPR-Cas9 screen hits and validation.**
**(A)** Gene-level enrichment or depletion of sgRNAs upon torin 1 treatment versus solvent control (DMSO). Dashed lines indicate significantly enriched or depleted genes ($p < 0.01$; $\log_2$ fold change (FC) > |2|). Selected hits are highlighted. **(B)** Competitive proliferation assays of iCas9 EPP2 cells carrying dsgRNAs targeting the gene of interest (dsgRNA$^+$) against non-transduced control cells ± torin 1 [300 nM] in the presence of 2 % BSA and 5 % FBS. Data are shown as mean and individual replicates (n=2).

## 4.2 $U_{34}$-enzymes are essential for cell proliferation during mTORC1 inhibition *in vitro* and in tumors

### 4.2.1 $U_{34}$-enzymes are required for cell proliferation under mTOR inhibition

In the screen, I identified several components of the Elongator complex (Elp2, Elp3, Elp6) and the Cytosolic Thiouridylase Subunits 1/2 (Ctu1/2) as being more essential during mTOR inhibition (Figure 6 A). These genes encode for components of tRNA-

modifying enzymes that form $mcm^5s^2$ modifications at uridine position 34 (wobble position) of a tRNA anticodon ($U_{34}$-enzymes; Figure 7 A). Codons that require tRNA wobble modifications for efficient translation are AAA (lysine), CAA (glutamine), and GAA (glutamate) (Dewez *et al.*, 2008; Huang *et al.*, 2005; Karlsborn *et al.*, 2014; Schaffrath & Leidel, 2017), hereafter referred to as VAA codons. Thus, in my screen, I genetically found many components of the pathway that are crucial for the formation of a tRNA wobble modification, making $U_{34}$-enzymes a high-confidence hit. As the connection between tRNA wobble modification and mTORC1 signaling in mammalian cells was not clear, it was interesting to investigate the link between both translational regulators during my PhD project.

For validation and further characterization experiments, I generated Ctu1 and Elp3 inducible knockout (iKO) cell lines by transduction of iCas9-expressing cells with Dual-hU6-sgRNA-mU6-sgRNA-Ef1α-Thy1.1-P2A-NeoR or Dual-hU6-sgRNA-mU6-sgRNA-Ef1α-mCherry-P2A-PuroR carrying dual-sgRNAs (dsgRNAs) against Ctu1 or Elp3. Knockouts were induced by doxycycline treatment. The loss of Ctu1 or Elp3 was validated by either PCR for Ctu1 using primers that generate a PCR product from the genomic Ctu1 locus spanning the two cutting sites of the dsgRNA sequences or by immunoblotting for Elp3 (Figure 7 B, C). Additionally, I generated single-cell derived Ctu1 knockout (KO) clones. To this end, I co-transfected iCas9 EPP2 or iCas9 KRPC cells with a mixture of two pSpCas9(BB)-2A-GFP plasmids carrying either of the two distinct Ctu1 dsgRNAs or, as control, carrying either of the two sgRNAs targeting the Rosa26 locus (Table 9) followed by single-cell sorting of GFP-positive cells. Again, I validated the loss of Ctu1 by PCR in the single-cell-derived clonal cell lines (Figure 7 D).

To validate the screen results of Ctu1, I performed competitive proliferation assays. Under control conditions (DMSO), Ctu1-deficient cells were slowly outcompeted by non-transduced control cells (Figure 7 E). In contrast, upon mTOR inhibition with torin 1, Ctu1 KO cells were rapidly outcompeted (Figure 7 E), confirming that the loss of Ctu1 strongly reduces cell proliferation selectively under mTOR inhibition.

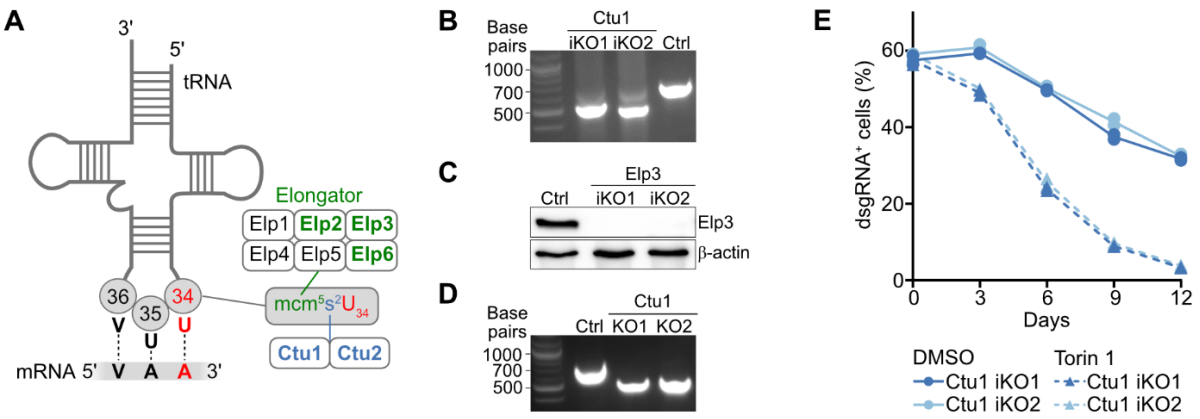


**Figure 7 – CRISPR-Cas9 screen identifies $U_{34}$-enzymes as essential for cell proliferation during mTOR inhibition.**
**(A)** Schematic representation of $mcm^5s^2$ modifications at the wobble anticodon uridine ($U_{34}$) catalyzed by the Elongator complex (Elp1-Elp6) and Cytosolic Thiouridylase (Ctu1/2). Subunits identified as selectively essential during mTOR inhibition in the screen are highlighted. **(B)** Editing of *Ctu1* upon 4 days doxycycline treatment [300 ng/ mL] in Ctu1 iKO EPP2 cells was confirmed by PCR. **(C)** Editing of *Elp3* upon 4 days doxycycline treatment [300 ng/ mL] in Elp3 iKO EPP2 cells was confirmed by immunoblotting. **(D)** Editing of *Ctu1* in single-cell derived clonal Ctu1 KO EPP2 cells was confirmed by PCR. **(E)** Competitive proliferation assay of Ctu1 iKO EPP2 cells ($dsgRNA^+$) against non-transduced control cells ± torin 1 [300 nM] in the presence of 2 % BSA and 5 % FBS. Data are shown as mean and individual replicates (n=2).

### 4.2.2 mTORC1 is essential for $U_{34}$-enzyme-deficient proliferation in various cell models

The serine/ threonine kinase mTOR is the catalytic subunit in two distinct protein complexes, mTORC1 and mTORC2, both suppressed by the ATP-competitive mTOR inhibitor torin 1 (Thoreen *et al*, 2009). To distinguish the relevance of mTORC1 and mTORC2, I used rapamycin, a highly selective, partial mTORC1 inhibitor (Li *et al*, 2014a), to specifically block mTORC1 and then monitor the proliferation of $U_{34}$-enzyme-deficient cells. I performed proliferation assays in Ctu1- and Elp3-deficient cells in the presence or absence of torin 1 or rapamycin. Since proliferation assays show inevitable variability among different experiments, often due to differences in the starting cell numbers, I plotted proliferation data as replicate means of technical triplicates obtained from biologically independent experiments. For the screen, I used physiological levels of BSA to provide an alternative leucine source for the leucine starvation conditions. As protein-rich conditions were no longer relevant to our phenotype of interest, all the following experiments were performed in an amino acid-rich medium (10 % FBS) without additional BSA. First, I titrated both inhibitors to find a minimal concentration that potently suppressed mTORC1 signaling while selectively

suppressing the proliferation of $U_{34}$-enzyme-deficient cells. Torin 1 is a potent mTOR inhibitor that strongly reduces cell proliferation at higher concentrations. I established a concentration of 25 nM for torin 1, which suppressed mTORC1 signaling and only slightly reduced cell proliferation in EPP2 cells (Figure 8 A-C, E). Rapamycin showed maximal mTOR inhibition effects at low nanomolar ranges, and using 12.5 nM rarely affected EPP2 cell proliferation (Figure 8 C, E). Using these conditions, I found that the loss of Ctu1 itself slightly reduced cell proliferation of EPP2 cells by about 20 %, to a similar extent as inhibitor treatments in control cells (Figure 8 D). The loss of Elp3 moderately reduced cell proliferation by about 35 - 40 % (Figure 8 F). In contrast to Ctu1/2, whose only known function is the thiolation of $U_{34}$ at tRNA anticodons, Elongator also modifies other anticodons (Karlsborn et al., 2014). This could explain the more pronounced cell proliferation defect of Elp3 KO cells. Importantly, cell proliferation of Ctu1- and Elp3-deficient cells were strongly and highly significantly suppressed in combination with a low torin 1 concentration, validating our screen results (Figure 8 C-F). Similarly, Ctu1- and Elp3-deficient EPP2 cells showed strongly reduced proliferation in the presence of rapamycin, to a similar extent as in the presence of torin 1 (Figure 8 C-F). Interestingly, $U_{34}$-enzyme-deficient EPP2 cells retained weak mTORC1 signaling when treated with a low concentration of torin 1, indicating that decreased mTORC1 activity is not the reason for their sensitivity to mTOR inhibitors (Figure 8 A, B).

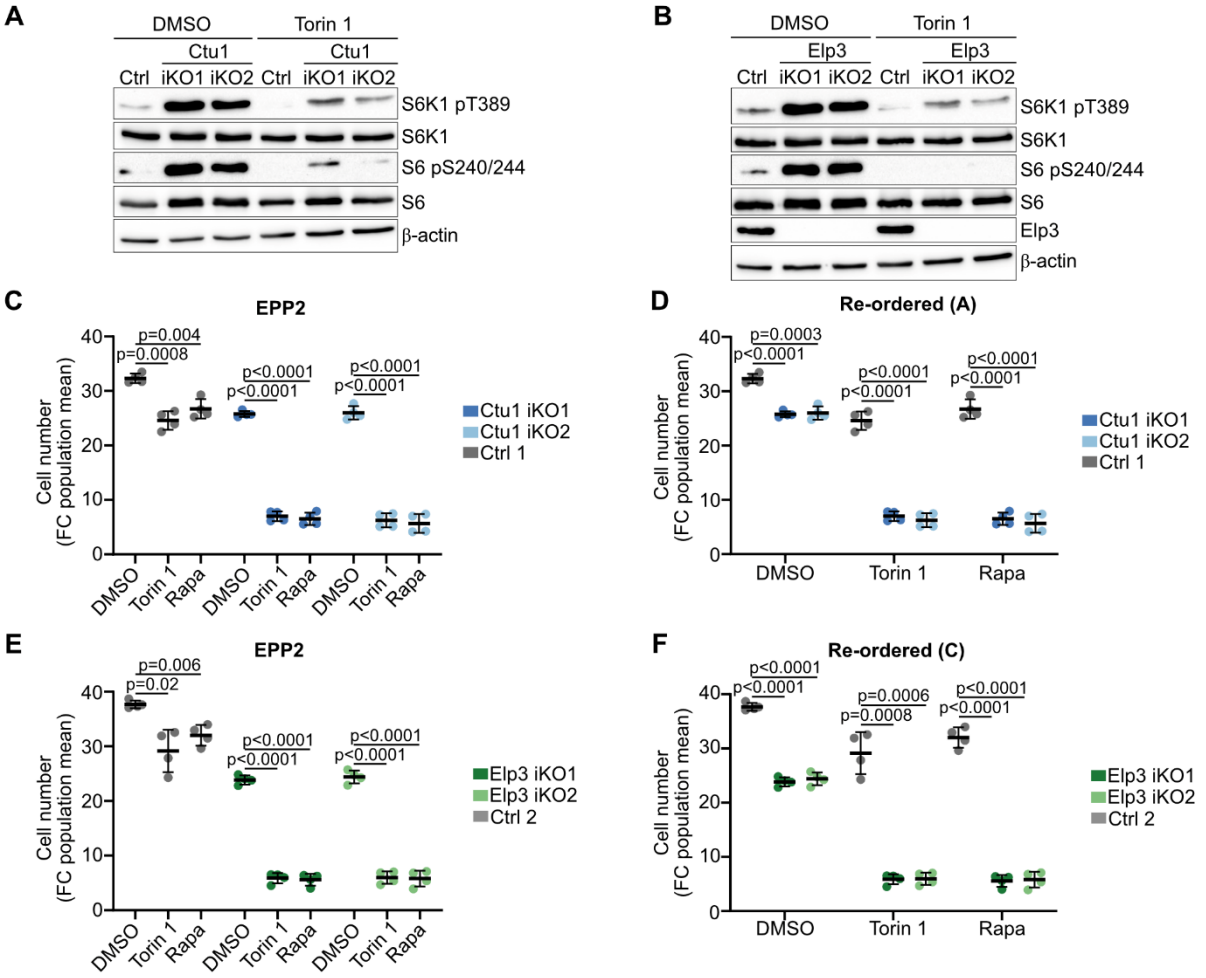


**Figure 8 – $U_{34}$-enzymes are essential for cell proliferation during mTORC1 inhibition *in vitro*.** **(A)**, **(B)** Immunoblotting analysis of mTOR pathway activity in (A) Ctu1 iKO and (B) Elp3 iKO EPP2 cells after 16 h ± torin 1 [25 nM]. **(C) - (F)** Cell number in fold change (FC) of (C), (D) Ctu1 iKO and (E), (F) Elp3 iKO EPP2 cells after 3 days ± torin 1 [25 nM] or rapamycin [12.5 nM]. Data are represented as population means ± SD (n = 4 independent experiments, replicate means of technical triplicates are shown). Note that (D) and (F) represent the same experiments as in (C) and (E), respectively, which were re-ordered for visual clarity of p values. p values were calculated by two-sided unpaired *t*-test with Welch correction.

To validate the proliferation phenotype in additional cell lines, I tested clonal Ctu1 KO EPP2 and KRPC cells. KRPC cells are murine pancreatic cancer cells with genetics similar to EPP2 cells, but they were generated independently (Lito et al, 2014). To take clonal variability into account, I performed proliferation assays for five different Ctu1 KO clones and three different control clones in EPP2 or KRPC, respectively (Figure 9 A, B). In clonal EPP2 cells, the loss of Ctu1 slightly reduced cell proliferation (Figure 9 A). In KRPC cells, the loss of Ctu1 reduced cell proliferation slightly, although not significantly, indicating that the loss of Ctu1 has only weak defects in cell proliferation (Figure 9 B). Rapamycin did not significantly perturb cell proliferation of control clones

(Figure 9 A, B). However, cell proliferation of all clonal Ctu1 KO cells was significantly suppressed in combination with mTORC1 inhibition using rapamycin (Figure 9 A, B), consistent with the results using pooled iCas9 Ctu1 KO cells. Next, I stably re-expressed Ctu1 in the clonal Ctu1 KO EPP2 and KRPC cells to rescue the phenotype (Figure 9 C, D). The proliferation defects of Ctu1 KO cells both in DMSO and rapamycin were rescued upon Ctu1 re-expression (Figure 9 C, D). Similarly, the stable expression of Elp3 in Elp3 iKO EPP2 cells restored cell proliferation to a similar level as in control cells (Figure 9 E). Finally, I generated Ctu1 iKO in KRPC cells, KPC cells, and $KRas^{G12D}$ murine embryonic fibroblasts (MEFs). KPC is a widely used murine pancreatic cancer cell model carrying an oncogenic $Kras^{G12D}$ mutation and a gain-of-function mutation (R272H) or KO of P53 (Hingorani et al, 2005). $KRas^{G12D}$ MEFs were SV40-immortalized (Palm et al., 2015). The sensitivity of the different cell lines to torin 1 and rapamycin was variable; however, cell proliferation was strongly reduced by the loss of Ctu1 in combination with mTORC1 inhibition (Figure 9 F-H). I also tested human carcinoma cell lines, but there was no apparent additive reduction in cell proliferation by the combination of Ctu1 KO with mTORC1 inhibitors (data not shown). However, as discussed later in this thesis, the molecular mechanism by which co-suppression of $U_{34}$-enzymes and mTORC1 reduces cell proliferation is conserved in human cells, suggesting that the precise genetic background affects cell proliferation and might mask the proliferation defects in the investigated human cell lines. Taken together, mTORC1 inhibition strongly reduces cell proliferation of Ctu1- and Elp3-deficient cells, while the loss of $U_{34}$-enzymes by itself only moderately reduces cell proliferation.

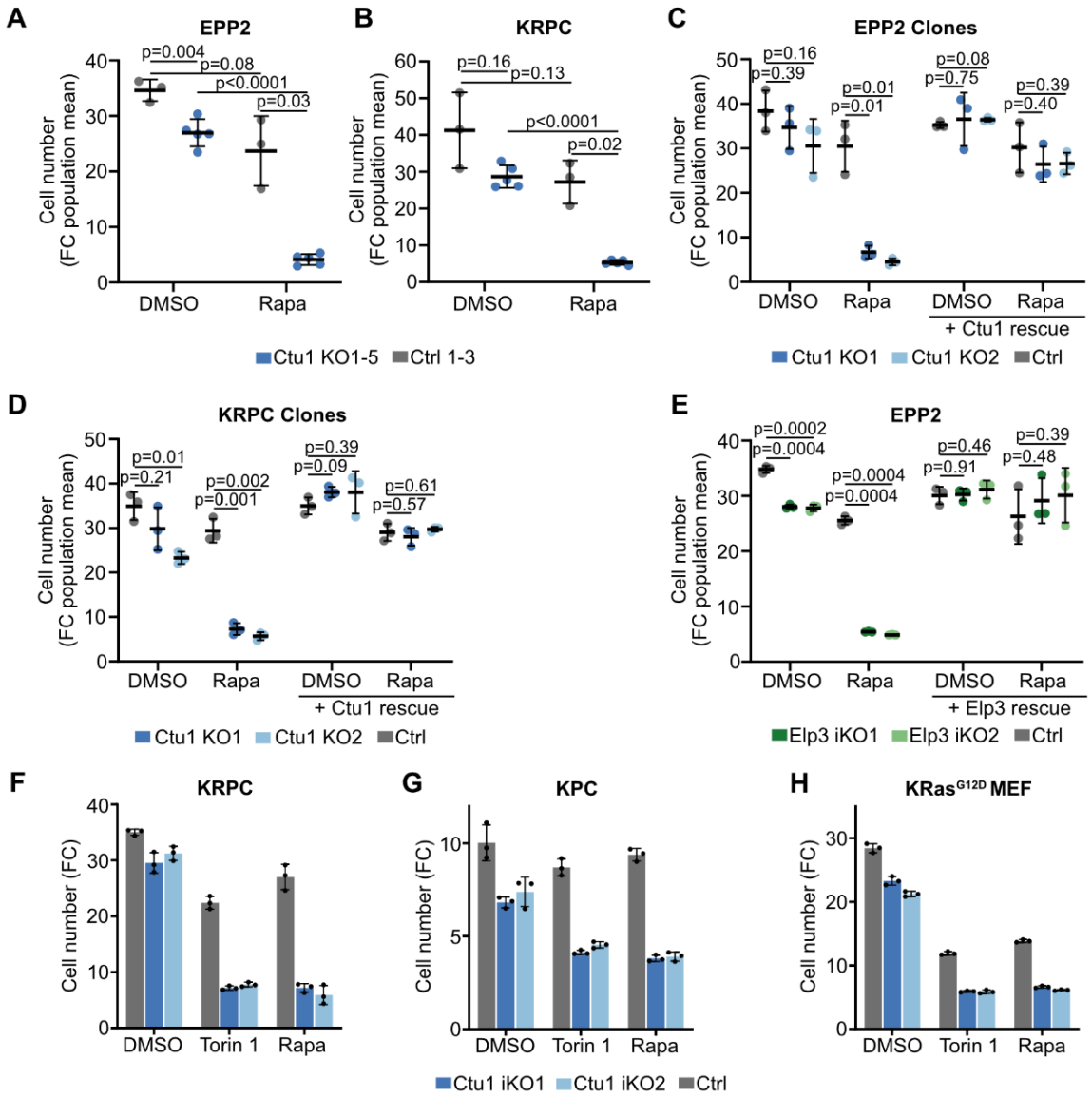


**Figure 9 – tRNA wobble modification is essential for cell proliferation during mTORC1 inhibition in different mouse cell lines.**
**(A), (B)** Cell number in fold change (FC) of different single-cell derived clonal Ctu1 KO (A) EPP2 and (B) KRPC cells after 3 days ± rapamycin [50 nM] or DMSO. Data are represented as population means ± SD (n = 3-5 independent clones, replicate means of technical triplicates are shown). **(C), (D)** Cell number in fold change (FC) of clonal Ctu1 KO (C) EPP2 and (D) KRPC cells with or without stably expressing Ctu1 after 3 days ± rapamycin [12.5 nM]. Data are represented as population means ± SD (n = 3 independent experiments, replicate means of technical triplicates are shown). **(E)** Cell number in fold change (FC) of Elp3 iKO EPP2 cells with or without stably expressing Elp3 after 3 days ± rapamycin [12.5 nM]. Data are represented as population means ± SD (n = 3 independent experiments, replicate means of technical triplicates are shown). **(F) – (H)** Cell number in fold change (FC) of Ctu1 iKO (F) KRPC cells, (G) KPC cells, and (H) KRas$^{G12D}$ MEFs after 3 days ± torin 1 [25 nM], rapamycin [12.5 nM] or DMSO. Data are shown as cell number fold change of day 3 to day 0 with mean ± SD (n=3). In (A)-(E), p values were calculated by two-sided unpaired *t*-test with Welch correction.

### 4.2.3 Ctu1 deficiency sensitives proliferating cells to inhibition of the PI3K-Akt-mTORC1 signaling pathway

Rapamycin sensitivity indicates that mTORC1 is the critical protein complex essential for cell proliferation upon loss of $U_{34}$-enzymes. To further distinguish between mTORC1 and mTORC2, I genetically disrupted a component of each complex. In the background of the clonal Ctu1 KO iCas9 EPP2 cells, I introduced dsgRNAs targeting Raptor, a component of mTORC1, or Rictor, a component of mTORC2 (Figure 10 A, B). The loss of Raptor itself only slightly reduced cell proliferation of control cells but strongly suppressed the proliferation of Ctu1 KO cells (Figure 10 A). In contrast, the loss of Rictor did not affect both control and Ctu1-deficient cells (Figure 10 B). The data confirms that mTORC1, not mTORC2, is the critical mTOR complex becoming essential for cell proliferation upon loss of Ctu1.

To examine the relevance of signaling pathways upstream of mTORC1, I knocked out Rheb, a small GTPase activating mTORC1 in response to growth factor availability, in Ctu1 KO EPP2 cells (Figure 10 C). The loss of Rheb did not affect the proliferation of control cells but strongly suppressed the proliferation of Ctu1 KO cells (Figure 10 C). This indicates that the growth factor signaling pathway is critical. Next, I inhibited upstream kinases using pharmacological inhibitors. Inhibition of the MAPK pathway kinases MEK and ERK decreased cell proliferation of Ctu1-deficient and control EPP2 cells similarly (Figure 10 D, E). I then inhibited the upstream kinases PI3-kinase (PI3K) and Akt. By immunoblotting, I confirmed that these pharmacological inhibitors efficiently suppress kinase activities (Figure 10 F). Rapamycin abolished the phosphorylation of the mTORC1 targets S6K1 pT389 and 4E-BP1, while phosphorylation of the Akt mTORC2 site S473 slightly increased (Figure 10 F). The increased Akt S473 phosphorylation upon mTORC1 inhibition can be explained by increased PI3K-mTORC2-Akt signaling activity due to a decline in negative feedback, as described previously (Wan et al, 2007; Yu et al, 2011). Inhibitors against the kinases PI3-kinase or Akt suppressed cell proliferation of specifically Ctu1-deficient cells (Figure 10 G). Thus, the data indicate that the PI3K-Akt-mTORC1 signaling pathway is required for the proliferation of $U_{34}$-enzyme-deficient cells.

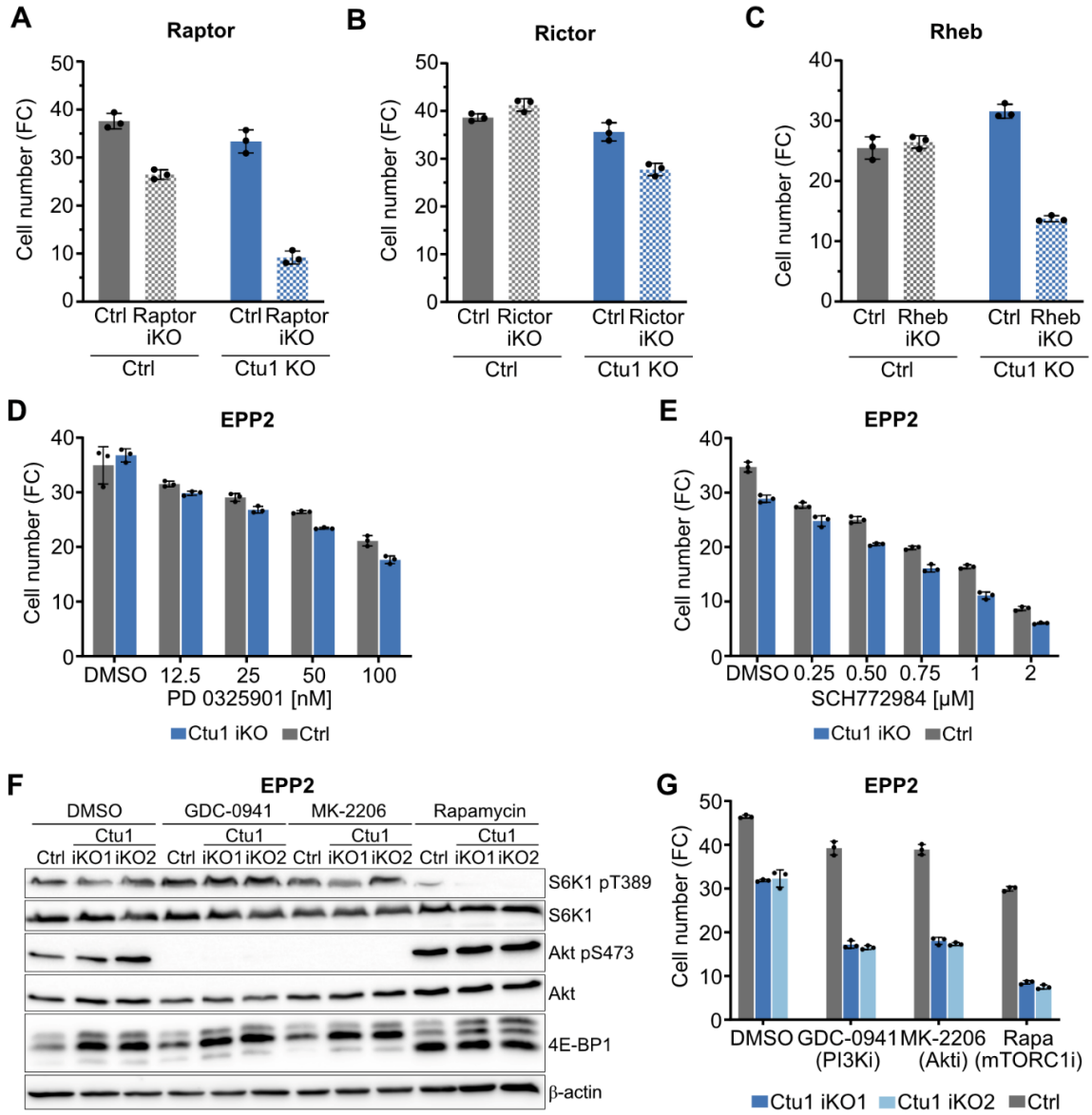


**Figure 10 – The loss of Ctu1 sensitives proliferating cells to inhibition of the PI3K-Akt-mTORC1 signaling pathway.**
**(A) – (C)** Cell number in fold change (FC) of clonal Ctu1 KO or control iCas9 EPP2 cells expressing dsgRNAs targeting non-coding chromosome regions (Ctrl), (A) Raptor, (B) Rictor or (C) Rheb after 3 days in culture. **(D), (E)** Cell number in fold change (FC) of Ctu1 iKO EPP2 cells after 3 days ± (D) PD0325901 [12.5 – 100 nM] or (E) SCH772984 [0.25 – 2 µM] or DMSO. **(F)** Immunoblotting analysis of mTOR pathway activity in Ctu1 iKO EPP2 cells after 16 h ± GDC-0941 [1 µM], MK-2206 [2 µM], rapamycin [12.5 nM] or DMSO. **(G)** Cell number in fold change (FC) of Ctu1 iKO EPP2 cells after 3 days ± GDC-0941 [1 µM], MK-2206 [2 µM], rapamycin [12.5 nM] or DMSO. In (A) – (E) and (G), data are shown as cell number fold change of day 3 to day 0 with mean ± SD (n=3).

### 4.2.4 Ctu1 is essential for cell proliferation during mTORC1 inhibition in tumors

To understand the relevance of mTORC1 inhibitors for $U_{34}$-enzyme-deficient tumor growth *in vivo*, I evaluated an orthotopic transplantation model of pancreatic cancer. I generated Ctu1 iKO EPP2 and control cells and sent them to our collaborators in the

Zuber lab at IMP in Vienna. Robert Kalis and Vivien Vogt induced the loss of Ctu1 upon doxycycline treatment and injected edited Ctu1 iKO and control EPP2 cells into the pancreas of Rag2 -/- mice. After the establishment of tumors (four days post-injection), Robert Kalis and Vivien Vogt treated the mice with rapamycin [5 mg/ kg/ day] or vehicle control for nine days, and tumor weight was measured at the end of the experiment. The loss of Ctu1 did not affect tumor growth, and rapamycin treatment in control tumors only slightly reduced tumor weights (Figure 11 A, B). However, the tumor weight derived from Ctu1-deficient cells was strongly reduced when mice were treated with rapamycin (Figure 11 A, B). Thus, co-suppression of $U_{34}$-enzymes and mTORC1 potently inhibits cancer cell proliferation in tumors *in vivo*.

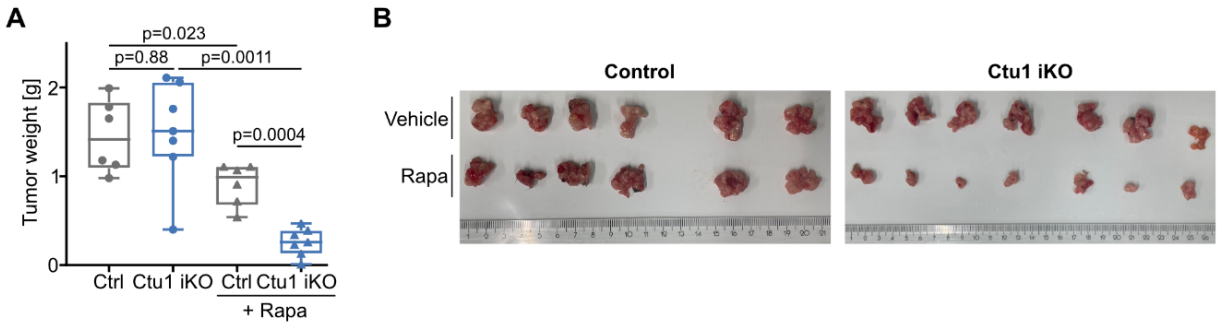


**Figure 11 – Ctu1 is essential for cancer cell proliferation during mTORC1 inhibition in tumors.** **(A), (B)** Tumor (A) weight and (B) images of orthotopic pancreatic tumors from Ctu1 iKO or control EPP2 cells in C57BL/6J Rag2-/- mice upon treatment with rapamycin [5 mg/ kg/ day] or vehicle for 9 days. Data was produced jointly with Robert Kalis and Vivien Vogt. In (A), box plots are represented as min to max. p values were calculated by two-sided unpaired *t*-test with Welch correction.

Taken together, I investigated the impact of mTORC1 and $U_{34}$-enzyme activity on cell proliferation using different CRISPR-Cas9 editing approaches (iKOs in a pooled population, single-cell derived KO clones), genetic and pharmacological manipulation of the relevant signaling pathway in different mouse cell lines, as well as rescue experiments for different $U_{34}$-enzyme knockouts (Ctu1 and Elp3). I showed that the loss of $U_{34}$-enzymes strongly suppresses cell proliferation in combination with mTORC1 inhibition, while the loss of tRNA wobble modifications alone only moderately reduces proliferation. Thus, $U_{34}$-enzymes are essential for cell proliferation during mTORC1 inhibition *in vitro* and in tumor *in vivo*.

## 4.3 The role of tRNA wobble enzymes in protein synthesis

### 4.3.1 The loss of $U_{34}$-enzymes reduces the synthesis of most proteins

To address whether tRNA wobble enzymes functionally interact with mTORC1 to produce a specific subset of proteins, we directly measured the translation output of $U_{34}$-enzyme-deficient cells using quantitative analysis of the newly synthesized proteome (QuaNPA) (Borteçen et al., 2023). I labeled newly synthesized proteins in Ctu1- or Elp3-deficient and control EPP2 cells with azidohomoalanine (AHA), a methionine analog, and with SILAC isotopes. After collecting protein lysates, Toman Borteçen enriched the AHA-labeled newly synthesized proteins via click chemistry from whole-cell lysates. Toman Borteçen further quantified protein abundance in those samples using liquid chromatography-mass spectrometry coupled with SILAC analysis.

As tRNA wobble modifications are required to efficiently translate specific codons, a global defect in protein synthesis of $U_{34}$-enzyme-deficient cells was conceivable. However, conventional quantitative proteomic analyses, which assume that most proteins are not changed, apply median normalization that masks global shifts in protein synthesis. Using median normalization, identifying a newly synthesized protein as up-/ downregulated could be true or a normalization artifact, respectively. Thus, Toman Borteçen developed a novel normalization approach for the QuaNPA workflow capable of detecting global up- or downregulation in protein synthesis (method not yet published). To this aim, he pooled equal parts of the AHA-SILAC labeled cell lysates of the two conditions that were compared before enrichment and measured protein abundance with SILAC analysis. For each sample, average SILAC ratios were determined for newly synthesized proteins commonly identified in the non-enriched samples. These ratios allowed us to calculate an average rate of protein synthesis within each condition. The rate of protein synthesis of both conditions was used to determine an average ratio by which newly synthesized proteins are up- or downregulated (normalization factor). Finally, individual SILAC ratios were normalized by shifting their median to the calculated normalization factor. This normalization approach assumes that most previously synthesized proteins are similar between the compared conditions. Toman Borteçen could show in his PhD thesis that even high concentrations of the translation inhibitor cycloheximide (4 h) did not change the

protein abundance of previously synthesized proteins while reducing new protein synthesis to a non-detectable level. Thus, this novel normalization approach accurately quantifies newly synthesized proteins between two conditions.

Using this powerful method, I observed that the loss of Ctu1 reduced the synthesis of most proteins (Figure 12 A). This global decrease in protein synthesis was also observed in Elp3-deficient EPP2 cells, suggesting that tRNA wobble enzymes regulate the synthesis of most proteins (Figure 12 B).

To further confirm that $U_{34}$-enzymes are required for decoding specific codons, I performed ribosomal profiling with differential ribosome codon reading (diricore) analysis in collaboration with Alexander Kowar and Fabricio Loayza-Puch (Loayza-Puch et al., 2016). I prepared Ctu1-deficient and control EPP2 cells for these experiments, and Alexander Kowar performed the library preparation and diricore analysis. The loss of Ctu1 increased ribosome occupancy at the A site of VAA codons but not VAG codons (Figure 12 C). Similar observations were made in $U_{34}$-enzyme-deficient yeast and worms (Nedialkova & Leidel, 2015; Zinshteyn & Gilbert, 2013). I found increased ribosome density, particularly at AAA codons, and less prominently at CAA and GAA codons (Figure 12 C). Moreover, ribosome occupancy was increased at the arginine codon AGA, as described previously (Laguesse *et al.*, 2015; Nedialkova & Leidel, 2015). All other codons showed no bias in ribosomal occupancy upon loss of Ctu1 (Figure 12 C). Thus, I can show that $U_{34}$-enzymes are required to efficiently decode VAA codons, especially AAA ones.

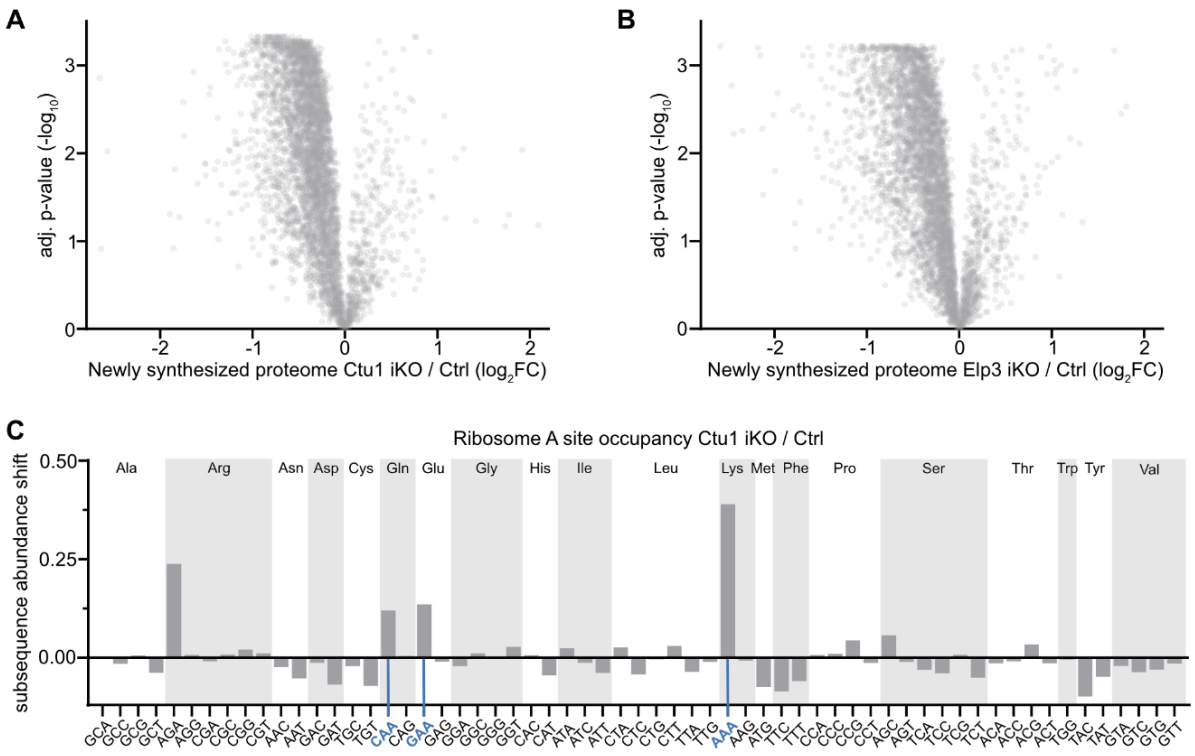


**Figure 12 – tRNA wobble enzymes regulate protein synthesis globally.**
**(A), (B)** Changes in the newly synthesized proteome of (A) Ctu1 iKO and (B) Elp3 iKO EPP2 cells. Newly synthesized proteins were labeled using AHA and SILAC isotopes and enriched via click chemistry. Data was acquired using mass spectrometry (MS) followed by quantitative analysis of the newly synthesized proteome (QuaNPA) workflow (n = 3 experimental replicates). Data was produced jointly with Toman Borteçen. **(C)** Codon changes in the ribosome A site occupancy in Ctu1 iKO EPP2 cells. Data was analyzed by diricore. VAA codons, which $U_{34}$-enzymes modify, are highlighted. Data are shown as mean (n = 2 independent experiments). Data was produced jointly with Alexander Kowar.

### 4.3.2 $U_{34}$-enzymes are required for efficient synthesis of proteins with AAA and GAA-rich mRNAs

The above data raises the question of whether the mRNA codon content determines how efficiently a particular protein is synthesized upon loss of $U_{34}$-enzymes. To address this, Toman Borteçen and I analyzed the protein-coding mRNA codon content for each newly synthesized protein detected in the nascent proteome of Ctu1 iKO EPP2 cells. First, we calculated codon frequencies for all canonical protein-coding transcripts and averaged them across the genome, which was used as reference codon frequency. Next, the “codon usage % deviation from transcriptome average” was determined by subtracting the reference codon frequency from the codon frequency of an individual transcript detected in the nascent proteome. We analyzed codon frequencies for all proteins detected in the nascent proteome of Ctu1- or Elp3-

deficient EPP2 cells. By separating the datasets into decile ranks of the $log_2FC$, I could determine whether newly synthesized proteins whose abundance was most up- / or downregulated after loss of $U_{34}$-enzymes showed a bias in VAA codons (Figure 13 A, B). Interestingly, transcripts encoding for proteins whose synthesis was strongest decreased upon loss of Ctu1 or Elp3, represented by the lowest deciles, were significantly and progressively enriched in VAA codons compared to the codon usage of all proteins (Figure 13 A, B). All other codons (non-VAA) were significantly depleted in those proteins (Figure 13 A, B). In contrast, mRNAs of proteins whose abundance was increased upon loss of Ctu1 or Elp3, represented by the last decile, were significantly depleted in VAA and enriched in non-VAA codons (Figure 13 A, B). We further analyzed the impact of the individual AAA, GAA, and CAA codons on protein synthesis in $U_{34}$-enzyme-deficient cells. Among the three different VAA codons, AAA and GAA were significantly enriched in transcripts whose synthesis was most decreased upon loss of Ctu1 or Elp3 (Figure 13 C, D). The CAA codon did not show any apparent bias (Figure 13 C, D). Thus, mRNAs enriched in AAA and GAA codons require tRNA wobble modifications for efficient synthesis.

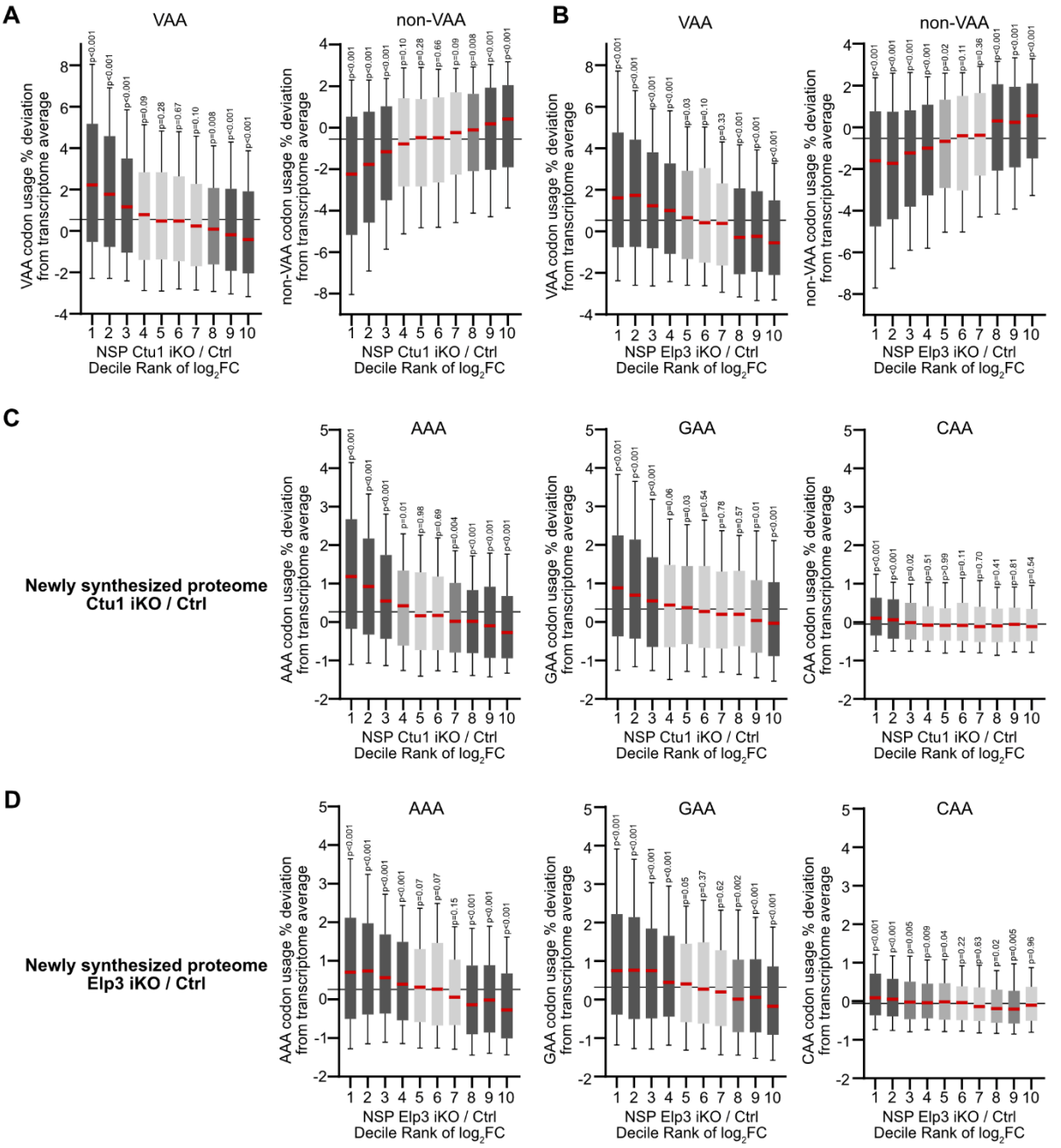


**Figure 13 – $U_{34}$-enzymes are required to efficiently synthesize proteins with AAA and GAA-rich mRNAs.**

**(A) – (D)** Correlation of codon deviation and protein changes in the newly synthesized proteome (NSP) of (A), (C) Ctu1 iKO and (B), (D) Elp3 iKO EPP2 cells, as in Figure 12 A, B. Protein changes are depicted as decile rank of the $log_2FC$ (i.e. 1 = 10 % lowest $log_2FC$; 10 = 10 % highest $log_2FC$). Box plots represent $10^{th}$ to $90^{th}$ percentiles and median (red). Grey line highlights the median codon usage of all quantified proteins. p values were calculated by Wilcoxon rank test, grey color of the box represents significance: $p < 0.001$: dark grey, $p < 0.01$: grey, $p < 0.05$: light grey, $p \geq 0.05$: bright grey. Data was produced jointly with Toman Borteçen.

## 4.4 The role of tRNA wobble modification in sustaining levels of ribosomal protein synthesis

### 4.4.1 Efficient synthesis of ribosomal proteins requires tRNA wobble modification

Based on the above finding that $U_{34}$-enzymes are required to synthesize proteins with AAA and GAA-rich mRNAs, I reasoned that some proteins or protein families might depend more on tRNA wobble modifications than others. To address this, Toman Borteçen performed gene set enrichment analysis (GSEA) using the newly synthesized proteome data. Interestingly, proteins whose synthesis was most substantially depleted upon loss of Ctu1 were ribosomal proteins (Figure 14 A). The loss of Ctu1 or Elp3 decreased the synthesis of most ribosomal proteins (Figure 14 B, C). This was not caused by a reduction in mRNA levels, as shown by RNA sequencing (Figure 14 B, C). To investigate why the synthesis of ribosomal proteins was particularly affected by the loss of tRNA wobble modifications, I analyzed the codon usage of ribosomal proteins. Unexpectedly, ribosomal protein-coding mRNAs were not enriched in VAA codons (Figure 14 D). Instead, the AAA codon was highly enriched in ribosomal protein mRNAs, whereas the codons GAA and CAA were actually depleted (Figure 14 D). AAA encodes for the amino acid lysine, a positively charged amino acid that mediates interactions between ribosomal proteins and negatively charged ribosomal RNAs within the ribosome. Consistent with the codon usage of ribosomal protein mRNAs, the decreased synthesis of ribosomal proteins upon loss of $U_{34}$-enzymes correlated with their AAA codon content but not their VAA codon content (Figure 14 E, F). As described above, ribosomes mainly accumulated at AAA codons in Ctu1-deficient cells (Figure 12 C), which may help explain why the synthesis of the AAA codon-rich ribosomal proteins depends on tRNA wobble modification. Of note is that ribosomal protein mRNAs are generally rich in the amino acid lysine (An & Harper, 2020; Wyant *et al*, 2018); thus, the AAG codon is also enriched in ribosomal proteins. The AAG codon, however, does not require tRNA wobble modification for efficient translation, suggesting that the $U_{34}$-enzyme-dependent synthesis of AAA-rich ribosomal protein mRNAs might not be a specific regulation.

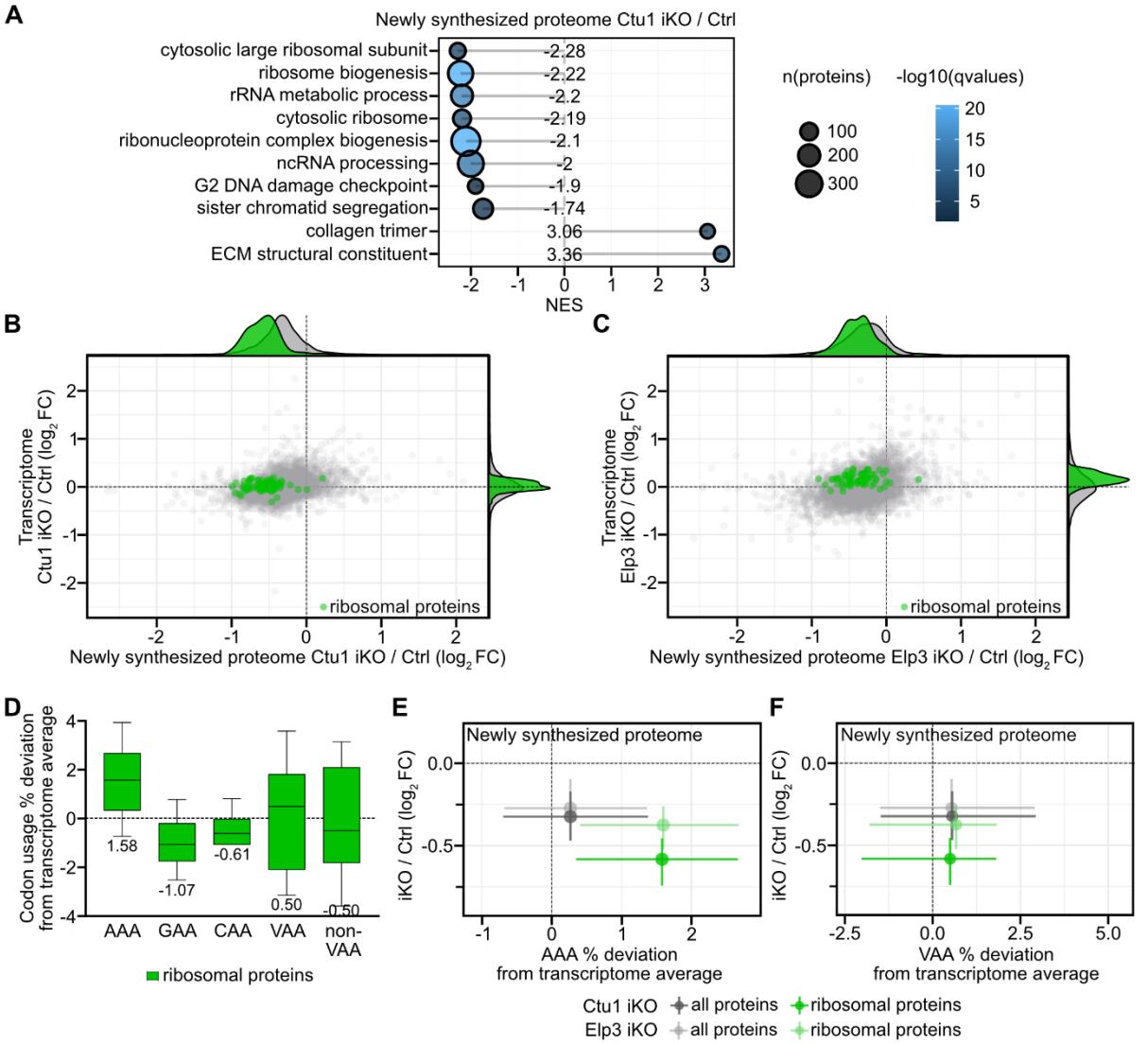


**Figure 14 – The loss of $U_{34}$-enzymes reduces the synthesis of ribosomal proteins.**
**(A)** Gene set enrichment analysis (GSEA) in the nascent proteome of Ctu1 iKO EPP2 cells. The most strongly depleted and enriched protein groups are shown. **(B), (C)** Scatter plot comparing changes in the nascent proteome versus transcriptome of (B) Ctu1 iKO and (C) Elp3 iKO EPP2 cells. The nascent proteome was quantified as in Figure 12 A, B, the transcriptome was quantified by RNA sequencing (n = 2 independent experiments). **(D)** Codon usage deviation from transcriptome average of mRNAs encoding for ribosomal proteins quantified in the nascent proteome of Ctu1 iKO EPP2 cells. Box plots represent 10$^{th}$ to 90$^{th}$ percentiles and median. **(E), (F)** Correlation between mRNA codon deviation for (E) AAA codons and (F) VAA codons versus changes in the nascent proteome of Ctu1 or Elp3 iKO EPP2 cells. Data are shown as interquartile range and median. Data in (A)-(C) and (E)-(F) was produced jointly with Toman Borteçen.

Based on GSEA, I identified further protein groups whose synthesis was reduced in cells lacking tRNA wobble modifications. These included proteins involved in ribosome biogenesis, ribonucleoprotein complexes, non-coding RNA processing, G2 DNA damage checkpoint, and sister chromatid segregation (Figure 14 A). The reduced synthesis of these protein groups correlated with their AAA and GAA codon usage (Figure 15 A-D). Their mRNAs, however, were not enriched in CAA codons (Figure 15 E, F). Previous studies identified kinesins as a protein family enriched in VAA codons,

thus depending on tRNA wobble modifications for efficient synthesis (Rapino et al, 2021). Consistently, in my nascent proteome data, the decreased synthesis of kinesins correlated with enrichment in VAA codons, particularly in AAA and GAA codons (Figure 15 A-H). Although the synthesis of most proteins decreased upon loss of U34-enzymes, the synthesis of collagens and extracellular matrix proteins increased (Figure 14 A). Their mRNA codon content analysis revealed that these protein groups are not enriched in any VAA codon (Figure 15), which conceivably explains their efficient translation in the absence of tRNA wobble enzymes.

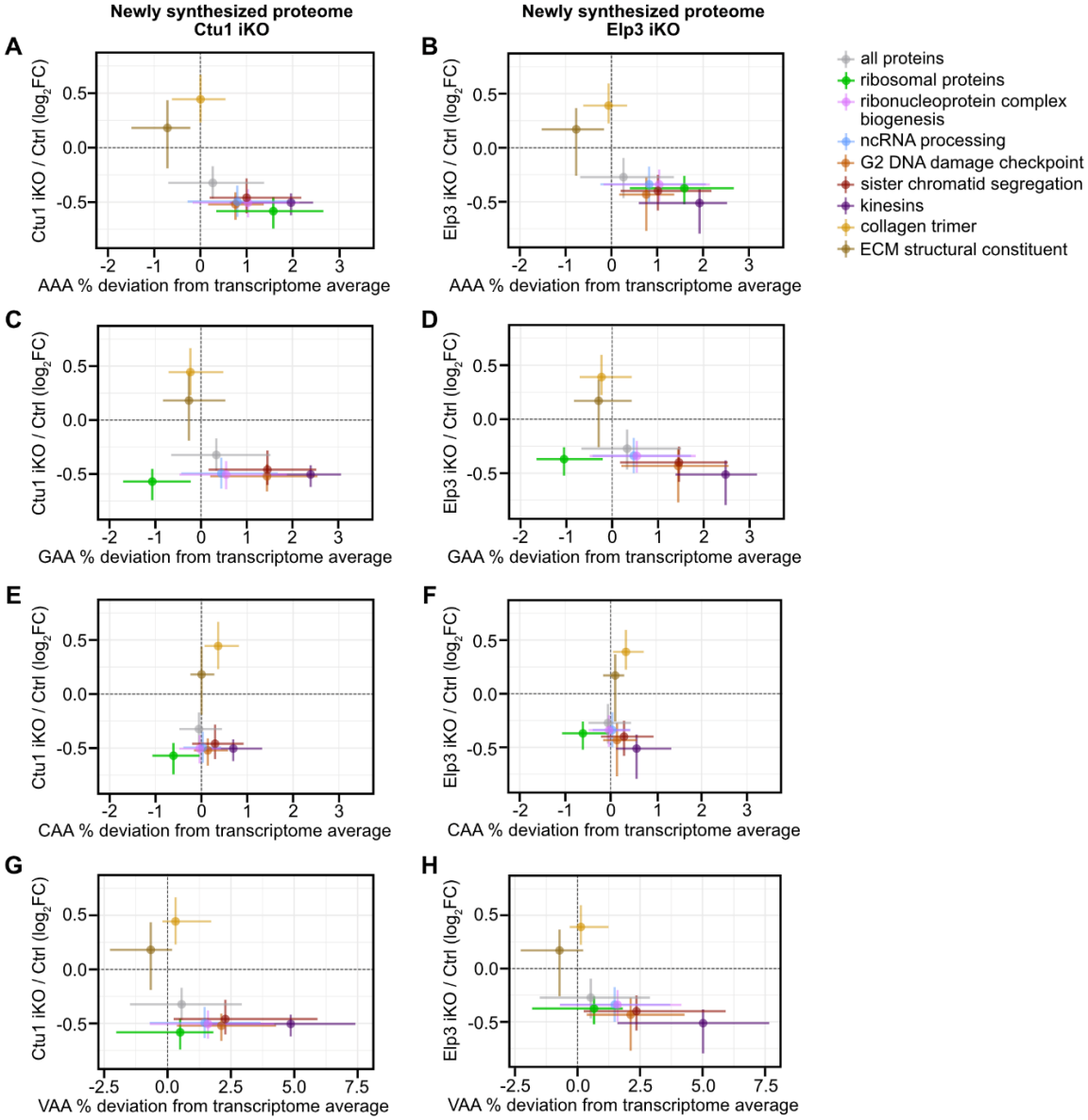


**Figure 15 – The loss of $U_{34}$-enzymes reduces the synthesis of proteins whose mRNAs are enriched in AAA and GAA codons.**
**(A) – (H)** Correlation between mRNA codon deviations vs. changes in the nascent proteome of EPP2 cells, quantified as in Figure 12 A, B. (A) AAA Ctu1 iKO; (B) AAA Elp3 iKO; (C) GAA Ctu1 iKO; (D) GAA Elp3 iKO; (E) CAA Ctu1 iKO; (F) CAA Elp3 iKO; (G) VAA Ctu1 iKO; (H) VAA Elp3 iKO. Protein groups whose synthesis is strongly altered upon loss of Ctu1 are indicated. Data are shown as interquartile range and median. Data was produced jointly with Toman Borteçen.

My data suggests that AAA- and GAA-rich mRNAs, but not mRNAs enriched in CAA codons, require tRNA wobble modifications for efficient synthesis. Moreover, my correlation analyses of the nascent proteome data allowed a systematic identification of protein groups whose synthesis depends on tRNA wobble modifications, particularly ribosomal proteins and other proteins functioning in RNA-related processes.

### 4.4.2 $U_{34}$-enzymes maintain steady-state levels of ribosomal proteins

The substantial reduction in the synthesis of ribosomal proteins upon loss of $U_{34}$-enzymes raised the question of whether steady-state protein levels might also be affected. To investigate the extent to which defects in protein synthesis materialize in the steady-state proteome of $U_{34}$-enzyme-deficient cells, I extracted proteins of Ctu1- and Elp3-deficient EPP2 cells and submitted the lysates to the DKFZ Proteomics Core Facility for further processing, liquid chromatography-mass spectrometry measurement, and label-free quantification. Toman Borteçen and I analyzed the codon usage of all proteins detected in the steady-state proteome of Ctu1- and Elp3-deficient cells (Figure 16 A, B). Transcripts encoding for proteins whose protein levels were most decreased upon loss of Ctu1 or Elp3 (20 % most decreased) were significantly enriched in VAA codons (Figure 16 A, B). In contrast, proteins whose synthesis was most enriched upon loss of $U_{34}$-enzymes were significantly reduced in VAA codons (Figure 16 A, B). Moreover, GSEA of the steady-state proteome data identified proteins related to ribosomal RNA processing, RNA metabolism, and biogenesis of ribosomes as well as ribonucleoproteins as the most depleted groups in Ctu1-deficient cells (Figure 16 C). Thus, with GSEA, I identified similar protein groups in the steady-state proteome and the nascent proteome of Ctu1-deficient cells, indicating that the defects in protein synthesis materialize to some extent at the steady-state level.

Next, I systematically compared the protein abundance of affected protein groups in the nascent and steady-state proteome of Ctu1- or Elp3-deficient EPP2 cells. Ribosomal proteins were most strongly decreased at the level of synthesis upon loss of tRNA wobble modifications (Figure 14 A). Their steady-state protein levels were slightly but consistently reduced upon loss of Ctu1 or Elp3 (Figure 16 D, E).

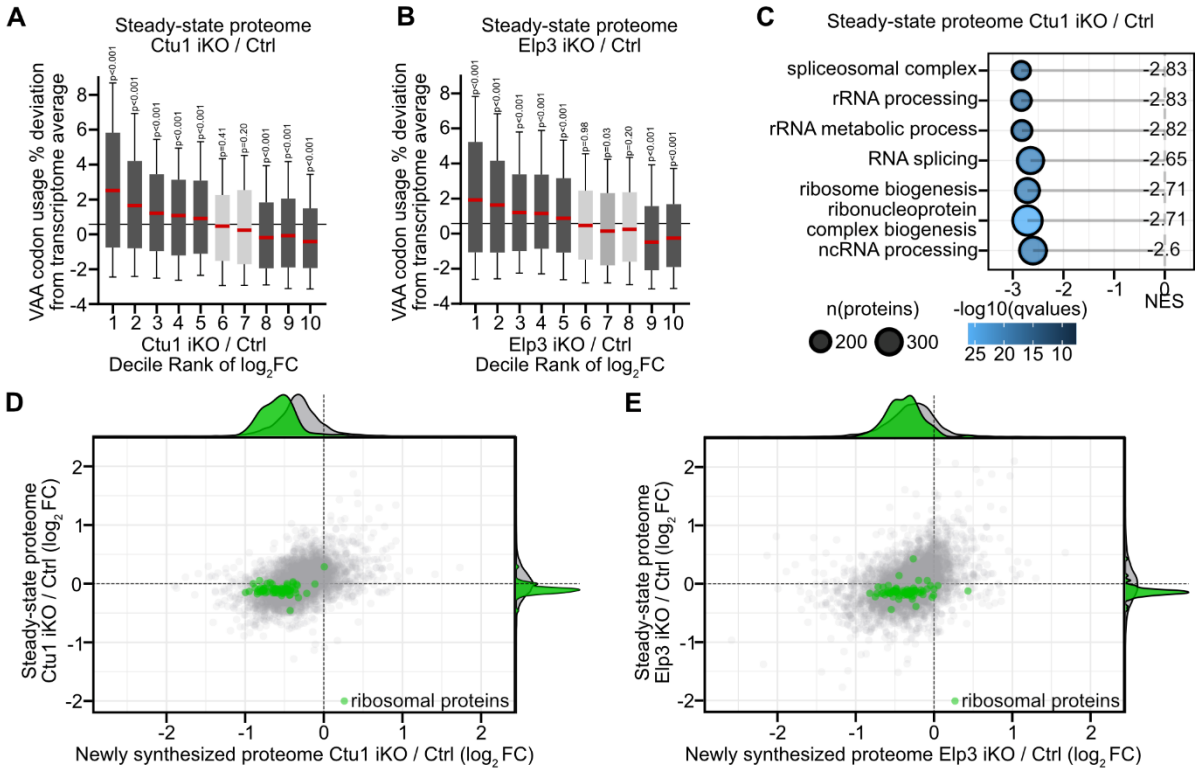


**Figure 16 – The loss of $U_{34}$-enzymes slightly reduces steady-state levels of ribosomal proteins.** **(A), (B)** Correlation of codon deviation and protein changes in the steady-state proteome of (A) Ctu1 iKO and (B) Elp3 iKO EPP2 cells. Steady-state proteins were acquired using label-free mass spectrometry (n = 5 independent experiments). Protein changes are depicted as decile rank of the $log_2$FC (i.e. 1 = 10 % lowest $log_2$FC; 10 = 10 % highest $log_2$FC). Box plots represent $10^{th}$ to $90^{th}$ percentiles and median (red). Grey line highlights the median codon usage of all quantified proteins. p values were calculated by Wilcoxon rank test, grey color of the box represents significance: $p < 0.001$: dark grey, $p < 0.01$: grey, $p < 0.05$: light grey, $p \geq 0.05$: bright grey. **(C)** Gene set enrichment analysis (GSEA) in the steady-state proteome of Ctu1 iKO EPP2 cells. The most strongly depleted protein groups are shown. **(D), (E)** Scatter plot comparing changes in the nascent proteome versus steady-state proteome of (D) Ctu1 iKO and (E) Elp3 iKO EPP2 cells. The nascent proteome was quantified as in Figure 12 A, B; the steady-state proteome as in A, B. Data in (A)-(E) was produced jointly with Toman Borteçen.

Other protein groups whose synthesis decreased upon loss of tRNA wobble modifications also showed a slight but consistent decrease in their steady-state protein levels (Figure 17). Taken together, the defects in protein synthesis upon loss of tRNA wobble modifications correlate to some extent with a decrease in steady-state protein levels. However, the nascent proteome's effects are generally stronger than steady-state-level changes.

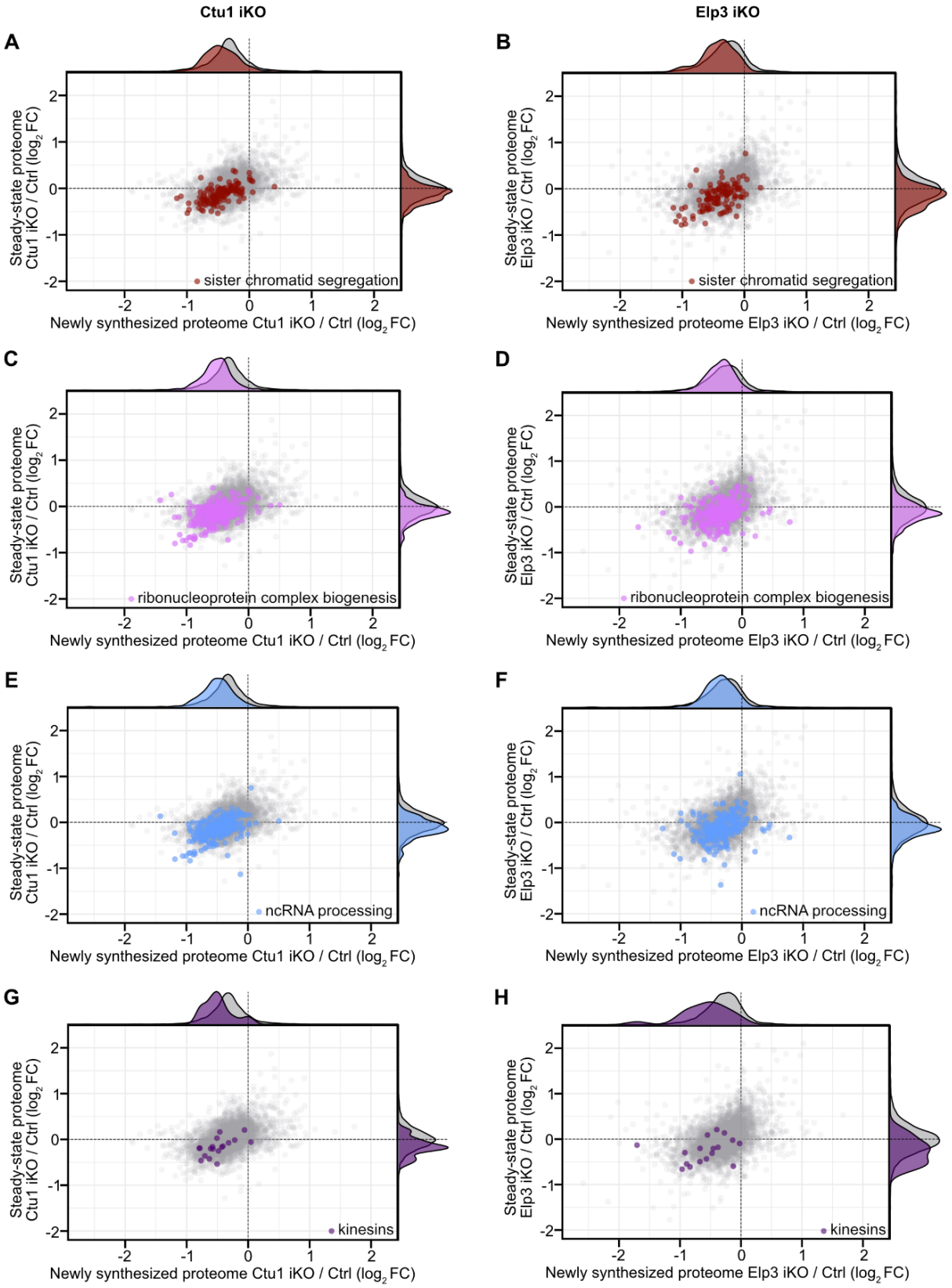


**Figure 17 – Correlation of protein synthesis and protein abundance upon loss of $U_{34}$-enzymes.** **(A) – (H)** Scatter plot comparing changes in the nascent proteome versus steady-state proteome of (A), (C), (E), (G) Ctu1 iKO and (B), (D), (F), (H) Elp3 iKO EPP2 cells. The nascent proteome was quantified as in Figure 12 A, B; the steady-state proteome as in Figure 16 A, B. Data was produced jointly with Toman Borteçen.

## 4.5 mTORC1 signaling and tRNA wobble modification converge on the synthesis of ribosomal proteins

### 4.5.1 mTORC1 is not required for codon-specific mRNA translation

My data highlight a crucial role for tRNA wobble modifications in synthesizing ribosomal proteins. Interestingly, the translation regulator mTORC1 controls the production of ribosomal proteins, as their mRNAs contain 5′ terminal oligopyrimidine (TOP) motifs (Hsieh et al., 2012; Thoreen et al., 2012). Thus, I reasoned that mTORC1 and $U_{34}$-enzymes might converge on the synthesis of ribosomal proteins. First, I investigated how mTORC1 affects the translation of specific codons using ribosomal profiling with differential ribosome codon reading (diricore) analysis (Loayza-Puch et al., 2016). I treated Ctu1-deficient or control EPP2 cells with torin 1 for two hours, and Alexander Kowar performed the library preparation and diricore analysis. Brief treatment with the mTORC1 inhibitor torin 1 did not induce ribosome accumulation at any specific codon in control cells (Figure 18 A). Moreover, torin 1 did not affect the increased A site ribosome occupancy at VAA codons, particularly at AAA codons, in Ctu1-deficient cells (Figure 18 B). Thus, mTORC1 is not required for codon-specific translation, in contrast to $U_{34}$-enzymes.

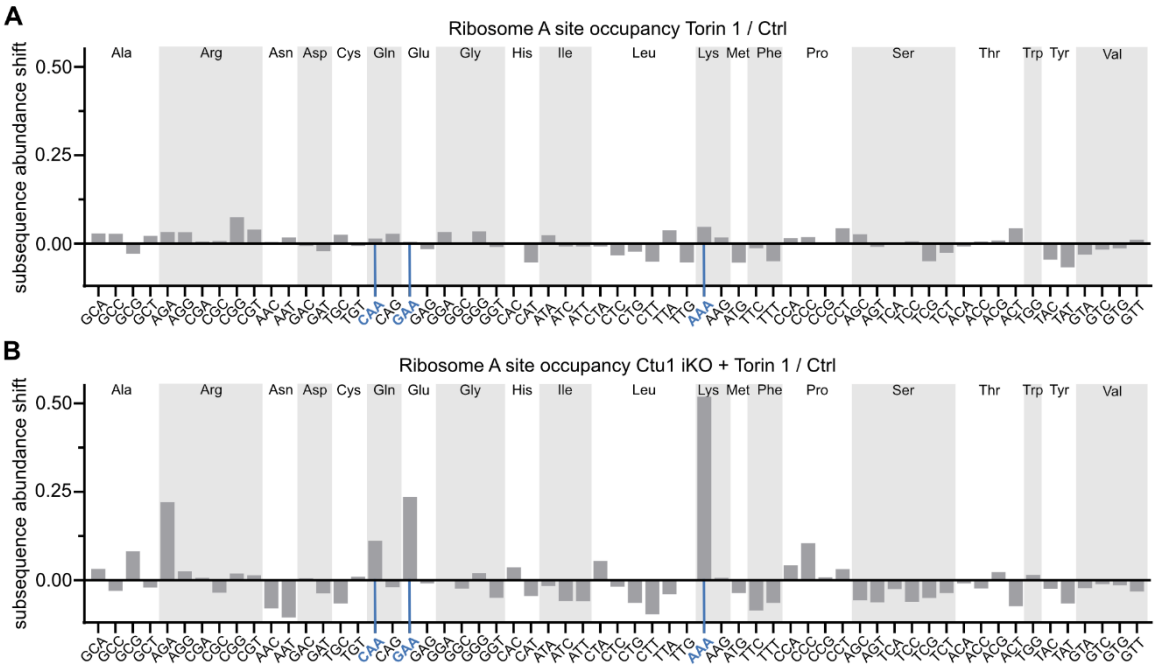


**Figure 18 – mTORC1 inhibition does not affect the codon-specific translation defects of $U_{34}$-deficient cells.**
**(A), (B)** Codon changes in the ribosome A site occupancy in (A) control and (B) Ctu1 iKO EPP2 cells after 2 h ± torin 1 [300 nM]. Data was analyzed by diricore. VAA codons which are modified by $U_{34}$-enzymes are highlighted. Data are shown as mean (n = 2 independent experiments). Data was produced jointly with Alexander Kowar.

### 4.5.2 mTORC1 and $U_{34}$-enzymes promote the synthesis of ribosomal proteins

Next, I investigated the effect of mTORC1 inhibition on the newly synthesized proteome of EPP2 cells. As in previous nascent proteomics experiments, I labeled newly synthesized proteins in Ctu1-deficient or control EPP2 cells with azidohomoalanine (AHA) and SILAC isotopes and added the mTORC1 inhibitors torin 1 or rapamycin for five hours. To dissect the additive effect of mTORC1 inhibition and the loss of Ctu1, I made different comparisons. To address the Ctu1 effect, I compared mTORC1 inhibition in Ctu1-deficient and control EPP2 cells (mTORC1 inhibitor ± Ctu1 iKO). To address the inhibitor effect, I compared mTORC1 inhibitor and DMSO treatment in Ctu1-deficient or control EPP2 cells, respectively (Ctu1 iKO ± mTORC1 inhibitor or control ± mTORC1 inhibitor). I adjusted the mTOR inhibitor concentrations to a level that strongly decreased ribosomal protein synthesis without affecting global protein synthesis, using 50 nM of torin 1 or rapamycin for five hours. The treatments efficiently suppressed mTORC1 activity, as analyzed by immunoblotting of the mTORC1 targets S6K1 pT389 and 4E-BP1 and the Akt mTORC2 site S473 (Figure 19 A). After collecting protein lysates, Toman Borteçen enriched the AHA-labeled proteins and analyzed samples using liquid chromatography-mass spectrometry coupled with SILAC analysis.

My codon usage analysis revealed that mTORC1 inhibition in Ctu1-deficient versus control cells (Ctu1 effect) did not affect the reduced protein synthesis from VAA-rich mRNAs that results from the loss of Ctu1 alone (Figure 19 B, C: Ctu1 effect). Consistently, the mTORC1 inhibitor effects did not show a clear VAA codon bias for protein-coding mRNAs whose synthesis was most decreased (Figure 19 B, C: inhibitor effect). However, I found that brief treatment of control EPP2 cells with mTORC1 inhibitors strongly reduced the synthesis specifically of ribosomal proteins without reducing overall protein synthesis (Figure 19 D, E). The synthesis of other protein groups that I identified as being reduced upon loss of $U_{34}$-enzymes, including ribonucleoprotein complex biogenesis, ncRNA processing, G2 DNA damage checkpoint, sister chromatid segregation, and kinesins, was not affected by mTORC1 inhibition (Figure 19 F, G). Taken together, I showed that mTORC1 regulates the synthesis of ribosomal proteins, but it is not required for efficient decoding of VAA

codons. Thus, ribosomal proteins are the only protein group affected by both pathways: mTORC1 and tRNA wobble enzymes.

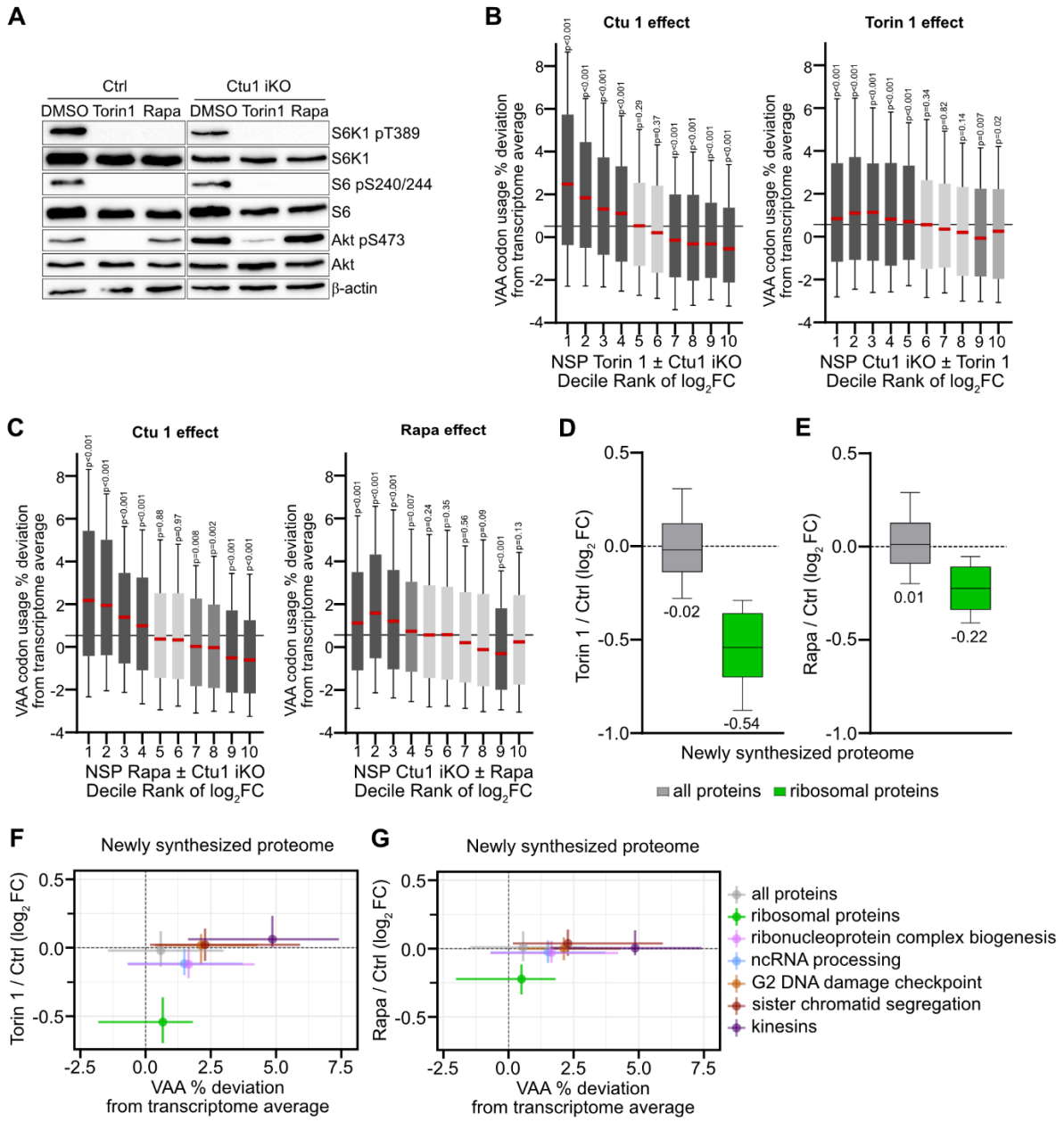


**Figure 19 – mTORC1 and Ctu1 promote the synthesis of ribosomal proteins.**
**(A)** Immunoblotting analysis of mTOR pathway activity in control or Ctu1 iKO EPP2 cells after 5 h ± torin 1 [50 nM] or rapamycin [50 nM]. Cells were treated with AHA-SILAC medium and inhibitors as described for the nascent proteome experiments. **(B), (C)** Correlation of codon deviation and protein changes in the newly synthesized proteome of EPP2 cells after 5 h mTORC1 inhibitor ± Ctu1 iKO (Ctu1 effect) or Ctu1 iKO ± 5 h mTORC1 inhibitor (inhibitor effect). Inhibitors were (B) torin 1 [50 nM] or (C) rapamycin [50 nM]. Data was acquired using mass spectrometry (MS) followed by quantitative analysis of the newly synthesized proteome (QuaNPA) workflow (n = 3 experimental replicates). Protein changes are depicted as decile rank of the $log_2FC$ (i.e. 1 = 10 % lowest $log_2FC$; 10 = 10 % highest $log_2FC$). Box plots represent $10^{th}$ to $90^{th}$ percentiles and median (red). Grey line highlights the median codon usage of all quantified proteins. p values were calculated by Wilcoxon rank test, grey color of the box represents significance: $p < 0.001$: dark grey, $p < 0.01$: grey, $p < 0.05$: light grey, $p \geq 0.05$: bright grey. **(D), (E)** Changes in protein abundance of all proteins and ribosomal proteins in the nascent proteome of EPP2 cells after 5 h ± (D) torin 1 [50 nM] or (E) rapamycin [50 nM]. Data was acquired using mass spectrometry (MS) followed by

quantitative analysis of the newly synthesized proteome (QuaNPA) workflow (n = 3 experimental replicates). Box plots represent $10^{th}$ to $90^{th}$ percentiles and median. **(F), (G)** Correlation between mRNA VAA codon deviation versus changes in the nascent proteome of EPP2 cells after 5 h ± (F) torin 1 [50 nM] or (G) rapamycin [50 nM]. Protein groups whose synthesis was most decreased upon loss of Ctu1 are shown. Data show interquartile range and median. Data was produced with Toman Borteçen.

As mentioned above, I performed different newly synthesized proteome comparisons to understand the functional interaction of mTORC1 and Ctu1 in regulating the synthesis of ribosomal proteins. The combination of mTORC1 inhibition and the genetic loss of Ctu1 globally decreased the synthesis of most proteins (Figure 20 A, B). Interestingly, the synthesis of ribosomal proteins was strongly reduced in the nascent proteome of mTORC1 inhibitor ± Ctu1 iKO (Ctu1 effect) to a similar extent as in the nascent proteome of Ctu1 iKO ± mTORC1 inhibitor (inhibitor effect) (Figure 20 A-F). This effect on ribosomal proteins was more substantial than the individual manipulations alone. Taken together, my data indicate that mTORC1 signaling and tRNA wobble modifications converge on the synthesis of ribosomal proteins.

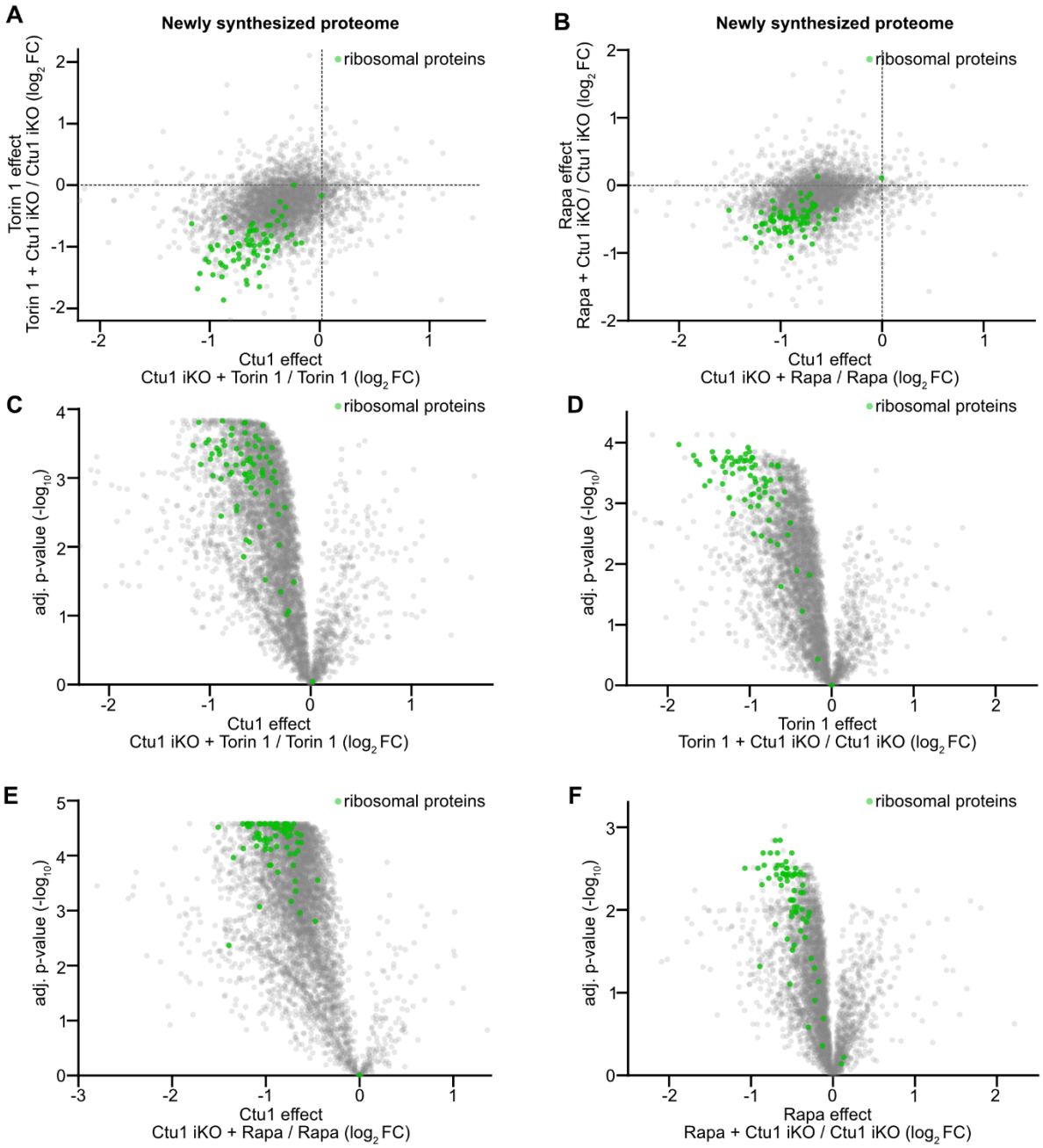


**Figure 20 – mTORC1 and Ctu1 converge on the synthesis of ribosomal proteins**.
**(A), (B)** Scatter plot comparing the nascent proteome of EPP2 cells after 5 h mTORC1 inhibitor ± Ctu1 iKO (Ctu1 effect) versus Ctu1 iKO ± 5 h mTORC1 inhibitor (inhibitor effect). Inhibitors were (A) torin 1 [50 nM] or (B) rapamycin [50 nM]. The nascent proteome was quantified as in Figure 19 B, C. Data was produced jointly with Toman Borteçen. **(C) – (F)** Changes in the nascent proteome of EPP2 cells showing the (C), (E) Ctu1 iKO and (D), (F) mTORC1 inhibitor effect separately. Inhibitors were (C), (D) torin 1 [50 nM] or (E), (F) rapamycin [50 nM], as in (A), (B).

### 4.5.3 mTORC1 and tRNA wobble modification sustain steady-state levels of ribosomal proteins

After establishing the role of ribosomal proteins as a point of convergence for mTORC1 and $U_{34}$-enzymes in shaping the nascent proteome, I investigated their impact on the steady-state protein levels. To this end, I collected protein lysates from Ctu1- or Elp3-deficient EPP2 cells with or without long-term (40 h) mTORC1 inhibition using rapamycin. I submitted the lysates to the DKFZ Proteomics Core Facility for liquid chromatography-mass spectrometry measurement and label-free quantification. The loss of Ctu1 or Elp3, or long-term mTORC1 inhibition by itself, only slightly reduced steady-state levels of ribosomal proteins (Figure 21 A, B). However, ribosomal protein levels decreased upon loss of $U_{34}$-enzymes in combination with mTORC1 inhibition (Figure 21 C). To validate these findings, I performed quantitative immunoblotting to measure levels of the two ribosomal proteins, Rpl29 and Rps3 (Figure 21 D). The loss of Ctu1 or Elp3, or rapamycin treatment alone did not significantly affect protein levels of Rpl29 and Rps3 (Figure 21 E). Torin 1 treatment also only slightly reduced ribosomal protein levels. However, treating Ctu1- or Elp3-deficient cells with rapamycin or torin 1 significantly depleted Rpl29 and Rps3 protein levels (Figure 21 E).

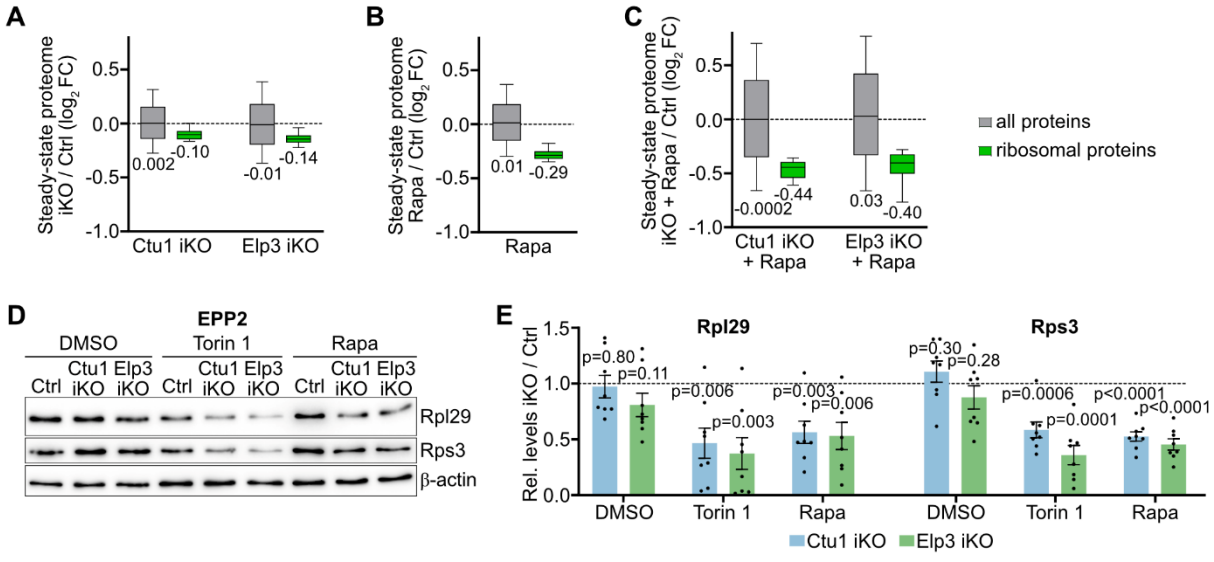


**Figure 21 – Levels of ribosomal proteins strongly decrease upon combined suppression of mTORC1 and $U_{34}$-enzymes.**
**(A) – (C)** Changes in protein abundance of all proteins and ribosomal proteins in the steady-state proteome of EPP2 cells. (A) Ctu1 iKO and Elp3 iKO; (B) control ± 40 h rapamycin [50 nM]; (C) Ctu1 iKO and Elp3 iKO ± 40 h rapamycin [50 nM]. The steady-state proteome of A as in Figure 16 A, B; others were acquired using label-free mass spectrometry (n = 5 independent experiments). Box plots represent $10^{th}$ to $90^{th}$ percentiles and median. Data was produced jointly with Dominic Helm and Martin Schneider.
**(D)** Immunoblotting analysis of ribosomal protein levels Rpl29 or Rps3 in Ctu1 iKO or Elp3 iKO EPP2

cells after 40 h ± torin 1 [300 nM] or rapamycin [50 nM]. **(E)** Changes in ribosomal protein levels Rpl29 or Rps3, quantified by immunoblotting as in (D). Data are represented as normalized replicate mean ± SEM (n = 8 independent experiments). Dashed lines show protein levels in control cells with DMSO. p values were calculated by one sample *t*-test with a hypothetical mean of 1.

To further validate these findings in additional cell lines, I generated inducible Ctu1/ Elp3 double knockouts (iDKO) in EPP2 cells, KPC cells, and $KRas^{G12D}$ MEFs (Figure 22 A-F) as well as Ctu1 iKOs in KPC cells, MEFs and human bladder carcinoma T24 cells (Figure 22 G-L). These cell lines largely maintained Rpl29 and Rps3 levels upon loss of Ctu1, Ctu1/Elp3, or rapamycin treatment alone (Figure 22 A-L). However, the levels of Rpl29 and Rps3 significantly decreased upon loss of $U_{34}$-enzymes in combination with mTORC1 inhibition (Figure 22 A-L). Thus, the concerted effect of suppressing mTORC1 and $U_{34}$-enzymes on ribosomal protein levels is conserved between murine and human cells.

To further corroborate that $U_{34}$-enzymes are critical to maintaining levels of ribosomal proteins under mTORC1 inhibition, I stably expressed Ctu1 in clonal Ctu1 KO EPP2 and KRPC cells as well as Elp3 in Elp3 iKO EPP2 cells to rescue the phenotype on ribosomal protein levels (Figure 22 M-O). The re-expression of $U_{34}$-enzymes restored the levels of ribosomal proteins to control levels upon mTORC1 inhibition (Figure 22 M-O). Taken together, I showed that mTORC1 and $U_{34}$-enzymes cooperate to maintain steady-state levels of ribosomal proteins. The manipulation of each pathway individually, however, only slightly affects steady-state levels of ribosomal proteins.

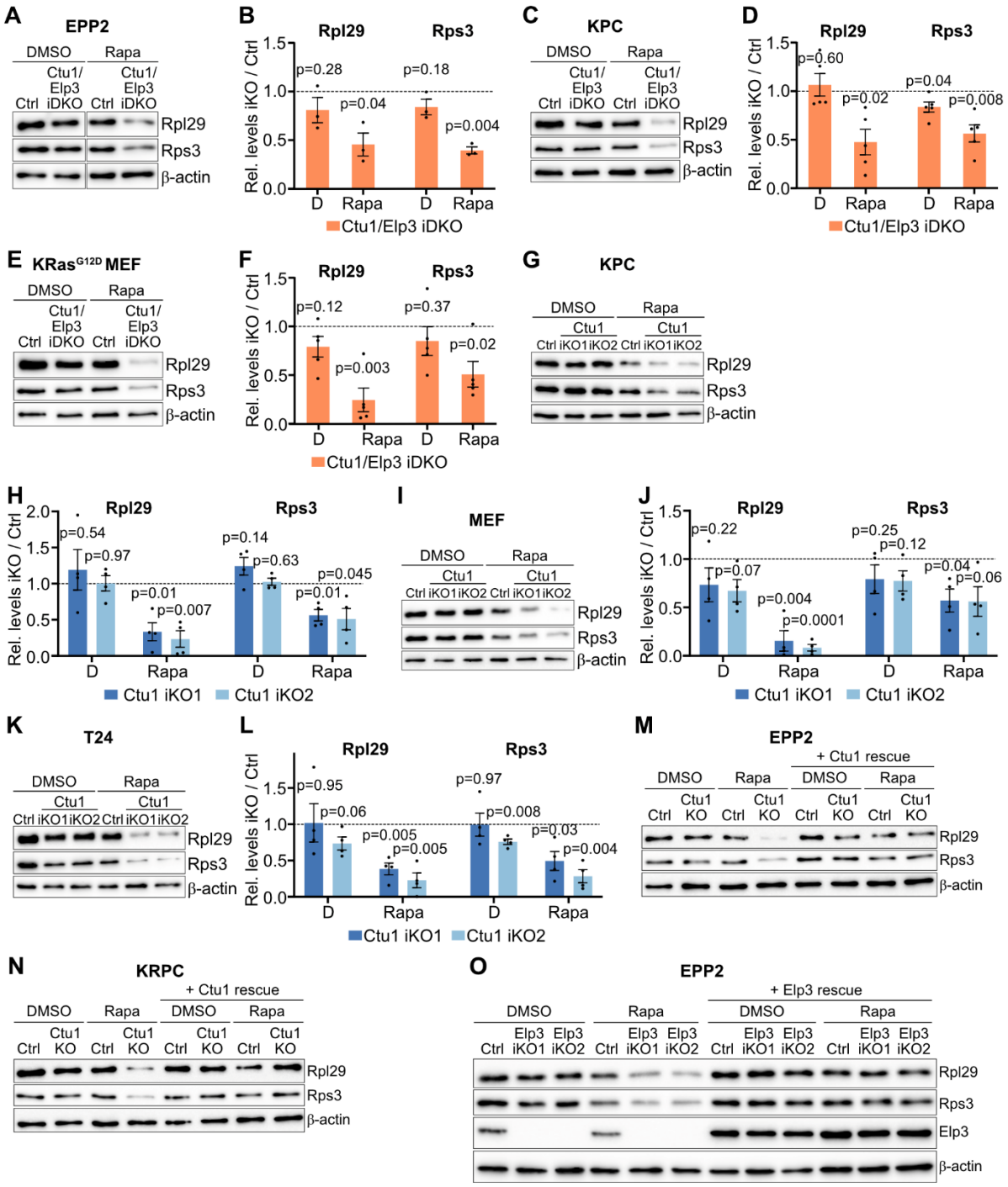


**Figure 22 – mTORC1 and $U_{34}$-enzymes maintain levels of ribosomal proteins.**
**(A) – (L)** Changes in ribosomal protein levels Rpl29 or Rps3 in different $U_{34}$ enzyme-deficient cell lines after 40 h ± rapamycin [50 nM], quantified by immunoblotting. (A), (B) Ctu1/Elp3 iDKO EPP2 cells; (C), (D) Ctu1/Elp3 iDKO KPC cells; (E), (F) Ctu1/Elp3 iDKO $KRas^{G12D}$ MEFs; (G), (H) Ctu1 iKO KPC cells; (I), (J) Ctu1 iKO MEFs; (K), (L) Ctu1 KO T24 cells. Data are represented as normalized replicate mean ± SEM (n = 3 - 5 independent experiments). Dashed lines show protein levels in control cells with DMSO. p values were calculated by one sample *t*-test with a hypothetical mean of 1. **(M), (N)** Immunoblotting analysis of ribosomal protein levels Rpl29 or Rps3 in clonal Ctu1 KO (M) EPP2 and (N) KRPC cells with or without stably expressing Ctu1 after 40 h ± rapamycin [50 nM]. **(O)** Immunoblotting analysis of ribosomal protein levels Rpl29 or Rps3 in Elp3 iKO EPP2 cells with or without stably expressing Elp3 after 40 h ± rapamycin [50 nM].

### 4.5.4 The translation defect of ribosomal proteins upon loss of Ctu1 is codon-dependent

I identified ribosomal proteins as being particularly dependent on tRNA wobble modifications, which correlated with their high AAA codon content. Accordingly, the exchange of AAA codons to their corresponding AAG codons in transcripts of ribosomal proteins should render their mRNA translation insensitive to the loss of tRNA wobble modifications. To confirm this, I tagged the ribosomal proteins Rpl29, Rps25, and Rps3 with HA tags and generated a VAG mutant in which I exchanged each VAA codon in the wildtype (WT) transcript sequence to its synonymous VAG codon (VAG Mut.). I replaced all VAA codons to exclude confounding effects from other codons. All constructs were expressed under the control of the respective endogenous 5'UTR and stably expressed in Ctu1 iKO EPP2 cells. Through doxycycline treatment, I induced the deletion of Ctu1 to directly compare Ctu1-deficient cells to control cells carrying the same construct. I treated the cells with rapamycin for 40 h to maximize the ribosomal protein synthesis defect. As ribosomal proteins that are not incorporated into ribosomes get rapidly degraded (Lam et al, 2007; Sung et al, 2016), I treated cells with a proteasome inhibitor (MG132) to prevent the degradation of newly synthesized proteins, including the HA-tagged constructs. By preventing the degradation of the HA-tagged codon variants, I could capture defects in codon-dependent ribosomal protein translation upon loss of Ctu1. My results show that protein levels of the wildtype Rpl29 and Rps25 transcript sequences were significantly decreased upon loss of Ctu1 (Figure 23 A-D). In contrast, protein levels of the corresponding VAG mutants were similar between control and Ctu1-deficient cells and higher compared to the wildtype sequence (Figure 23 A-D). Interestingly, protein levels of the wildtype Rps3, as well as the VAG mutant Rps3, were similar between Ctu1-deficient and control cells (Figure 23 E, F). When I compared the codon usage of the three ribosomal proteins, I found that only Rpl29 and Rps25 are enriched in VAA, particularly AAA, codons (Figure 23 G). In contrast, Rps3 is among the few ribosomal proteins not enriched in AAA codons (Figure 23 G). Thus, my results suggest that the translation of Rpl29 and Rps25 is reduced in $U_{34}$-enzyme-deficient cells due to their high VAA codon content. The data further indicates that the translation of Rps3, which is not increased in VAA codons, is not dependent on $U_{34}$-enzymes. Interestingly, I observed that levels of Rps3 decreased upon combined suppression of mTORC1 and $U_{34}$-enzymes in the absence of

proteasome inhibitors. This might be explained by increased degradation of Rps3 due to defects in the synthesis of other ribosomal proteins, which prevent the incorporation of Rps3 into ribosomes.

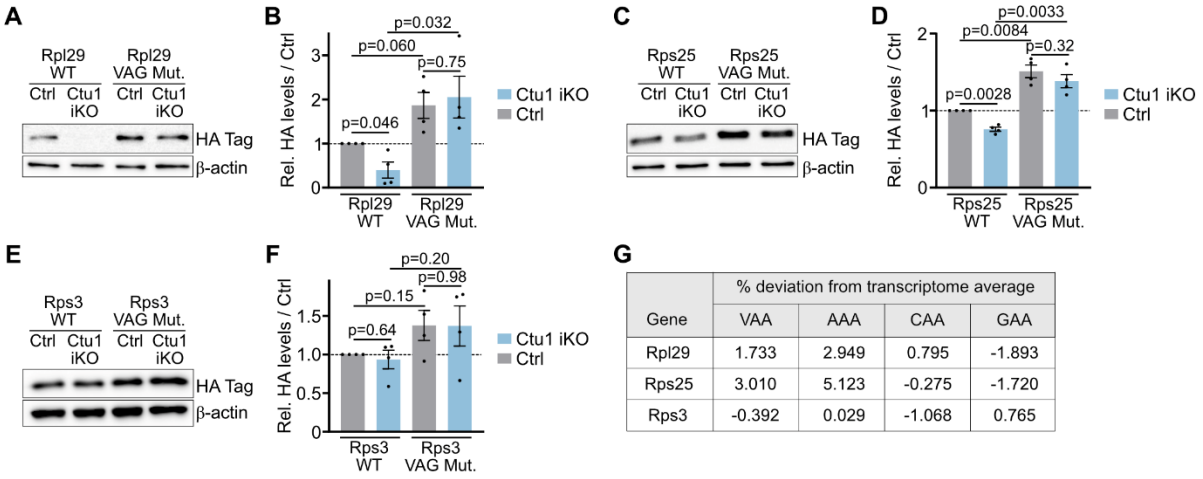


| Gene | % deviation from transcriptome average | | | |
|---|---|---|---|---|
| | VAA | AAA | CAA | GAA |
| Rpl29 | 1.733 | 2.949 | 0.795 | -1.893 |
| Rps25 | 3.010 | 5.123 | -0.275 | -1.720 |
| Rps3 | -0.392 | 0.029 | -1.068 | 0.765 |

**Figure 23 – Reduced translation of ribosomal protein mRNAs in Ctu1-deficient cells is codon-dependent.**
**(A) - (F)** Changes in HA abundance in Ctu1 iKO EPP2 cells stably overexpressing N-terminal HA-tagged (A), (B) Rpl29; (C), (D) Rps25 or (E), (F) Rps3 wild-type (WT) or VAG mutant (VAG Mut.) transcripts after 40 h + rapamycin [50 nM] and MG132 [200 nM], quantified by immunoblotting. For the VAG mutant sequence, all VAA codons were exchanged to the synonymous VAG codon. The loss of Ctu1 was induced upon 4 days doxycycline treatment [300 ng/ mL] after antibiotic selection. (B), (D), (F) Data are represented as normalized replicate mean ± SEM (n = 4 independent experiments). Dashed lines show protein levels in control cells carrying the WT construct. p values were calculated by two-sided unpaired *t*-test with Welch correction. **(G)** Overview of codon usage deviation from transcriptome average of wildtype transcripts of the ribosomal proteins Rpl29, Rps25 and Rps3.

### 4.5.5 mTORC1 and $U_{34}$-enzymes maintain the cellular translation capacity

The previous results established that mTORC1 signaling and $U_{34}$-enzymes converge on the synthesis and, thus, the production of ribosomal proteins. As ribosomal proteins constitute a major component of the translation machinery, I investigated the effects on the cellular translation capacity. I performed puromycin incorporation assays as a proxy for cellular translation capacity. To this end, I treated cells shortly with puromycin, which gets incorporated into nascent polypeptides and terminates translation. Thus, immunoblotting using anti-puromycin antibodies can visualize nascent polypeptides labeled with puromycin. First, I treated $U_{34}$-enzyme-deficient and control EPP2 cells, KRPC cells, and KPC cells with mTORC1 inhibitors (torin 1 and rapamycin) for 16 h to

deplete ribosomal proteins. Then, I performed puromycin incorporation assays. The loss of Ctu1, Elp3, or Ctu1/ Elp3 slightly decreased puromycin incorporation (Figure 24 A, B, D, E, G-L). This is consistent with the reduction in overall protein synthesis, which I observed in the nascent proteome of Ctu1- and Elp3-deficient EPP2 cells (Figure 12 A, B). Similar to the loss of $U_{34}$-enzymes, treatment of control cells with mTORC1 inhibitors only moderately reduced puromycin incorporation (Figure 24 A, D, G, I, K, M). Strikingly, puromycin incorporation was strongly and significantly decreased upon loss of $U_{34}$-enzymes in combination with mTORC1 inhibition (Figure 24 A, B, D, E, G-N). Moreover, I found that puromycin incorporation of Ctu1-deficient cells was also strongly suppressed upon treatment with inhibitors against PI3-kinase or Akt (Figure 24 C, F). Taken together, the loss of tRNA wobble modifications combined with long-term inhibition of PI3K, Akt or mTORC1 reduces cellular protein synthesis.

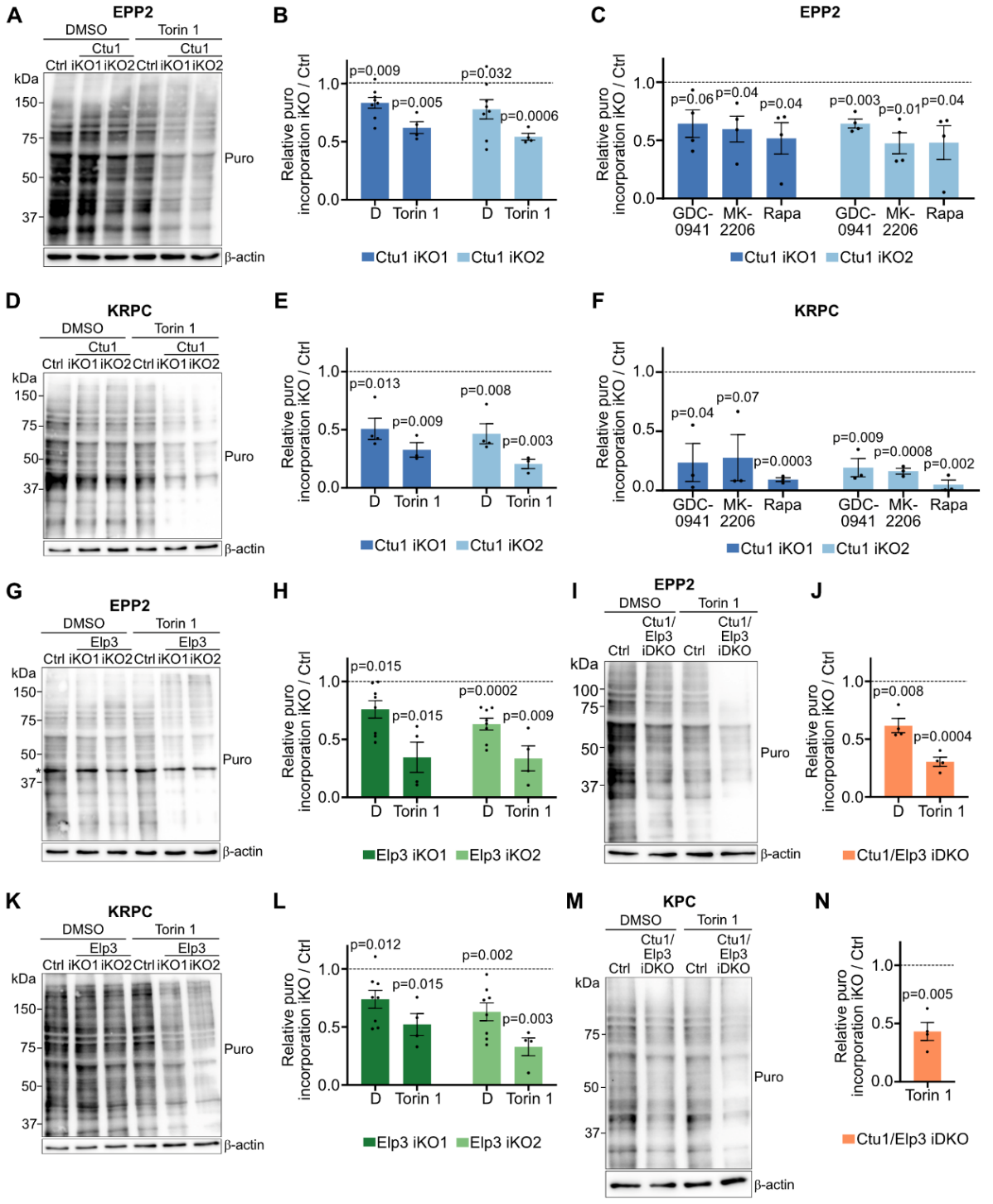


**Figure 24 – mTORC1 and tRNA wobble modifications maintain cellular translation capacity.**
**(A) – (N)** Puromycin (puro) incorporation in $U_{34}$-enzyme-deficient cells after 16 h ± inhibitor treatment, quantified by immunoblotting. (A), (B) Ctu1 iKO EPP2 cells ± torin 1 [300 nM]; (C) Ctu1 iKO EPP2 cells ± GDC-0941 [1 μM], MK-2206 [2 μM], rapamycin [12.5 nM]; (D), (E) Ctu1 iKO KRPC cells ± torin 1 [300 nM]; (F) Ctu1 iKO KRPC cells ± GDC-0941 [1 μM], MK-2206 [2 μM], rapamycin [12.5 nM]; (G), (H) Elp3 iKO EPP2 cells ± torin 1 [300 nM]; (I), (J) Ctu1/Elp3 iDKO EPP2 cells ± torin 1 [300 nM]; (K), (L) Elp3 iKO KRPC cells ± torin 1 [300 nM]; (M); (N) Ctu1/Elp3 iDKO KPC cells ± torin 1 [300 nM]. Asteriks indicate an unspecific band. Data are represented as normalized replicate mean ± SEM (n = 3 - 8 independent experiments). Dashed lines show puro incorporation in control cells with DMSO. p values were calculated by one sample *t*-test with a hypothetical mean of 1.

The kinase mTORC1 promotes protein synthesis globally by increasing initiation and elongation. Moreover, mTORC1 enhances the translation of mRNAs that carry a TOP motif, mainly ribosomal proteins and a few other translation components (Hsieh et al., 2012; Jefferies et al., 1994; Terada et al, 1994; Thoreen et al., 2012). Thus, mTORC1 regulates translation via translation-promoting signaling and via ribosome biogenesis. To understand to what extent each process contributes to maintaining the cellular translation capacity, I first analyzed the timeline over which mTORC1 inhibition affects the translational output. As described above, I performed puromycin incorporation assays in Elp3-deficient EPP2 cells and treated the cells with the mTOR inhibitor torin 1 for 2 h to 40 h. Short-term treatment potently suppressed mTORC1 signaling, but puromycin incorporation was only slightly reduced (Figure 25 A). However, long-term mTORC1 inhibition decreased puromycin incorporation in Elp3-deficient cells drastically, much stronger than in control cells (Figure 25 A). Thus, mTORC1 signaling sustains cellular translation output in Elp3-deficient cells long-term. Finally, I dissected the role of mTORC1 in translation-promoting signaling and ribosome biogenesis. To this end, I treated Elp3-deficient cells with the mTOR inhibitor torin 1 for 40 h to deplete ribosomal proteins and re-activated mTORC1 by washing out torin 1. To wash out the inhibitor, I supplied cell culture medium with fatty acid-poor BSA, which sequesters the inhibitor from cells. Within 1 h of drug washout, mTORC1 signaling was re-activated, leading to a significant increase in puromycin incorporation in control cells (Figure 25 B, C). In contrast, Elp3-deficient cells showed an attenuated increase in puromycin incorporation, although mTORC1 signaling was re-activated to a similar level as in control cells (Figure 25 B, C). These data suggest that $U_{34}$-enzyme-deficient cells are limited in their translation capacity when ribosomal proteins are depleted by long-term mTORC1 inhibition.

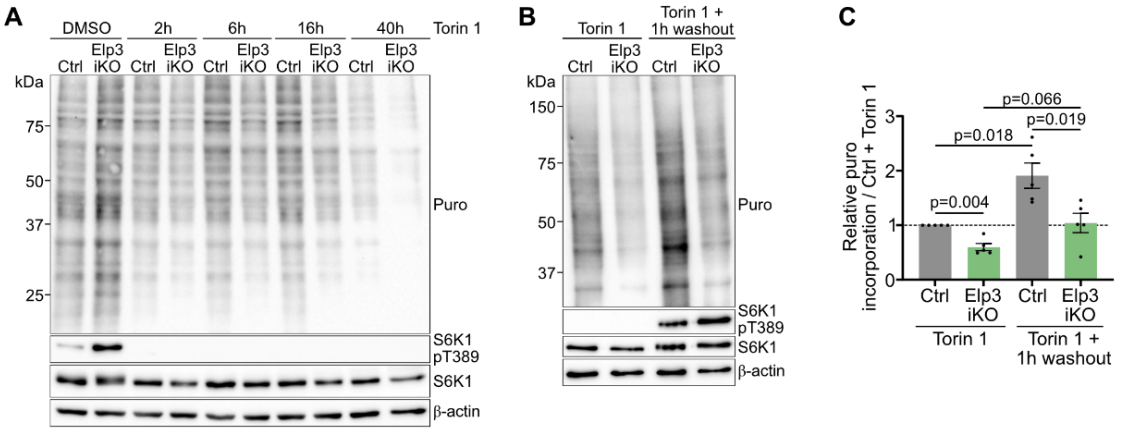


**Figure 25 – $U_{34}$-enzyme-deficient cells are limited in their translation capacity.**
**(A)** Puromycin (puro) incorporation in Elp3 iKO EPP2 cells after ± torin 1 [300 nM] treatment for indicated time points, analyzed by immunoblotting **(B), (C)** Puro incorporation in Elp3 iKO EPP2 cells after 40 h torin 1 [300 nM] followed by washout of torin 1 for 1 h, quantified by immunoblotting. Data are represented as normalized replicate mean ± SEM (n = 5 independent experiments). Dashed lines show puro incorporation in control cells + torin 1. p values were calculated by two-sided unpaired *t*-test with Welch correction.

Taken together, in my PhD thesis, I showed that the loss of $U_{34}$-enzymes sensitizes mammalian cells for mTOR inhibition. I established a molecular mechanism to explain the substantial proliferation defect of $U_{34}$-enzyme-deficient cells under mTORC1 inhibition. I showed that the concerted suppression of mTORC1 and tRNA wobble modifications depletes the pool of ribosomal proteins, which are enriched in $U_{34}$-enzyme-dependent AAA codons. The reduced levels of ribosomal proteins result in a decrease in the protein synthesis machinery, limiting cellular translation capacity and suppressing cell proliferation.

# 5 Conclusion and discussion

In my PhD project, I performed genome-wide proliferation-based CRISPR screens in the presence or absence of the mTOR inhibitor torin 1 to identify genes essential for cell proliferation under mTORC1 suppression. Upon validation of screen hits, I found that tRNA-modifying enzymes that form $mcm^5s^2$ at wobble uridines of tRNAs ($U_{34}$-enzymes), Elongator and Ctu1/2, became selectively essential for cell proliferation under mTORC1 inhibition *in vitro* and in tumors *in vivo*. As the functional role of tRNA wobble modifications in mammalian cells was unclear, I first systematically characterized the role of $U_{34}$-enzymes in shaping the proteome output. Nascent proteomics, steady-state proteomics, and ribosome profiling experiments revealed that tRNA $U_{34}$ wobble modifications globally affect protein synthesis. Interestingly, the synthesis of ribosomal proteins was particularly affected, which correlated with their high content in AAA codons. I further characterized the role of mTORC1 suppression in $U_{34}$-enzyme-deficient cells. mTORC1 regulates the production of ribosomal proteins. Thus, ribosomal protein synthesis represents the point of convergence for both pathways (Figure 26). Consequently, the simultaneous inhibition of mTORC1 and tRNA wobble modifications depleted levels of ribosomal proteins, leading to a breakdown in protein translation and cell proliferation. Taken together, my data established an interplay between mTORC1 and tRNA wobble modification in generating the protein synthesis machinery to maintain high protein translation rates and hence, fast cell proliferation (Figure 26).

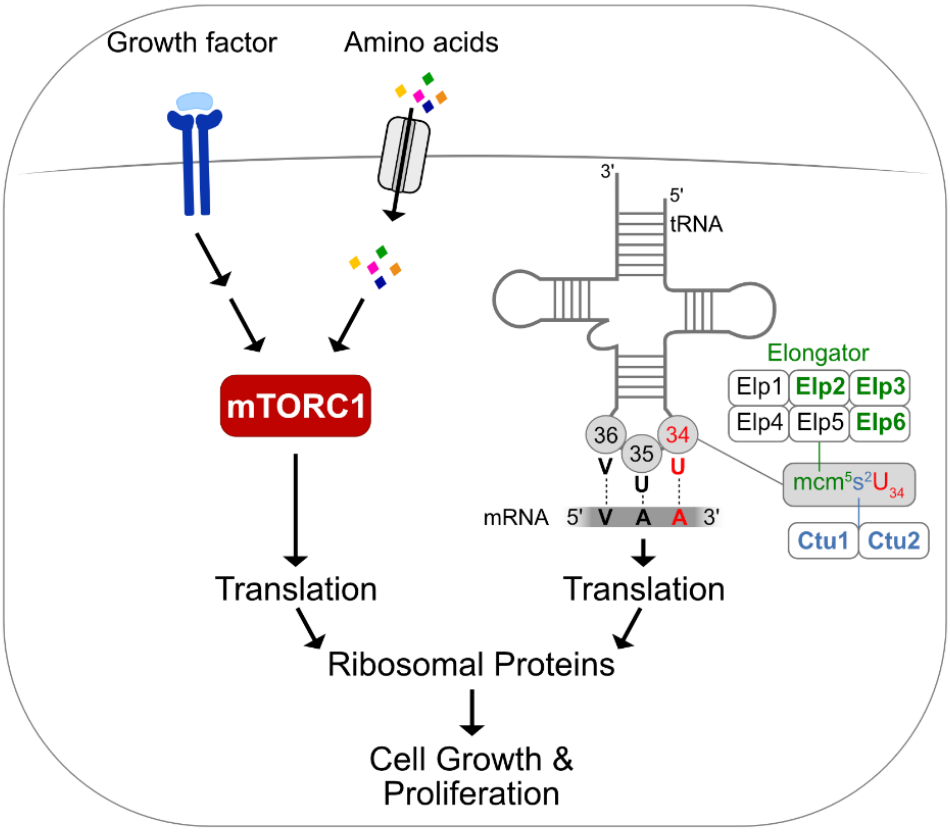


**Figure 26 – Schematic summary of the interplay between mTORC1 and tRNA wobble modification in generating the protein synthesis machinery.**
Under nutrient-rich conditions, mTORC1 is active and induces protein translation, particularly the production of ribosomal proteins that carry a TOP motif. Additionally, tRNA wobble modifications ($mcm^5s^2U_{34}$) catalyzed by Elongator and Ctu1/2 globally affect protein synthesis by efficiently translating AAA-enriched ribosomal protein mRNAs. Thus, mTORC1 and $U_{34}$-enzymes cooperate in generating ribosomal proteins to sustain cellular translation capacities and maintain fast cell proliferation.

## 5.1 Genome-wide CRISPR screens to systematically identify mTORC1 regulators

Loss-of-function genetic screens are a powerful tool for identifying genes and pathways affecting cell proliferation under defined metabolic conditions. In particular, CRISPR screens have been used to systematically characterize essential genes in mammalian cells (Michlits et al., 2020; Sanjana et al, 2014; Wang et al, 2015; Wang et al, 2014). Among others, components of the mTORC1 signaling pathway were identified as core fitness genes (Hart et al, 2015; Rossiter et al, 2021). To more specifically identify positive regulators of mTORC1, fluorescence-activated cell sorting (FACS)-based CRISPR screens were performed that used phosphorylation of ribosomal protein S6 as a readout for mTORC1 activity (Condon *et al*, 2021; Yan *et al*, 2023). Indeed, in response to amino acid starvation conditions, genes related to positive regulation of mTORC1 signaling, such as mTOR, Raptor, or GATOR2 components were identified (Condon *et al.*, 2021). Furthermore, a mechanism by which mitochondrial function signals to mTORC1 was clarified (Condon *et al.*, 2021). Interestingly, in a recently published paper, a FACS-based screen was performed to identify modulators of mTORC1 signaling upon amino acid starvation with re-stimulation (Yan *et al.*, 2023). Again, as a readout for mTORC1 activity, phosphorylation levels of ribosomal protein S6 were monitored by FACS (Yan *et al.*, 2023). Here, the interleukin enhancer binding factor 2/3 (Ilf2/3) was identified as being essential for binding the GATOR complex to lysosomal membranes and, thus, for activating mTORC1 in response to amino acids (Yan *et al.*, 2023). With my screen, I could validate Ilf2 as detrimental to cell proliferation under mTORC1 inhibition. How Ilf2, which forms heterodimers with Ilf3, suppresses cell proliferation under mTORC1 inhibition remains to be investigated. The recent study suggests a critical role of Ilf2 in regulating mTORC1 signaling.

Moreover, CRISPR screens have been used to analyze gene-drug interactions systematically. Drug suppressor screens allow the discovery of synthetic lethality or resistance mechanisms to drugs in human cells (Yu *et al*, 2022). For example, to identify new therapeutic targets that synergize with PI3K inhibitors, CRISPR screens were performed in PDAC cells in the presence of PI3K inhibitors (Milton et al, 2020). The study showed that PDAC cells depend on mTOR signaling for proliferation under

PI3K inhibition, suggesting that combinatorial treatment of PI3K and mTOR inhibitors might overcome PI3K inhibitor resistance (Milton *et al.*, 2020). In another study, a genome-wide CRISPR screen under MEK inhibition was performed in colon cancer cells, identifying PLK1 as an exciting target for overcoming MEK inhibitor resistance (Yu *et al.*, 2022). In my project, I performed CRISPR screens under protein-rich conditions that were either amino acid-rich or deprived in the presence of the mTOR inhibitor torin 1 to systematically identify critical regulators of mTOR-mediated cancer cell proliferation depending on the nutrient environment. With this powerful approach, I identified tRNA $U_{34}$ wobble modification, the absence of which sensitives proliferating cells to mTORC1 inhibitors.

Taken together, CRISPR screens are a powerful approach to identify novel positive and negative signaling pathway regulators and to improve treatment strategies by systematically analyzing gene-drug interactions.

## 5.2 The physiological role of tRNA wobble modifications

During protein synthesis, tRNAs are required to translate the genetic code into amino acids (Alberts *et al.*, 2008). If uridine is present at the anticodon wobble position ($U_{34}$), tRNAs bind to the cognate adenosine (A) but also wobble to guanosine (G) (Crick, 1966a). More recently, the chemical modification $mcm^5s^2U_{34,}$ which increases the efficiency of anticodon-codon interactions, was identified, restricting the wobble base pairing of VAA codons (Dewez *et al.*, 2008; Huang *et al.*, 2005; Karlsborn *et al.*, 2014; Schaffrath & Leidel, 2017). Previously, the loss of tRNA wobble modification was associated with various phenotypes in yeast, worms, and mammalian cells. Two different models were developed to explain these phenotypes (Schaffrath & Leidel, 2017). The first model describes that an individual protein whose mRNA is enriched in VAA codons gets translated inefficiently without tRNA wobble modifications. Consequently, the reduced protein output triggers loss-of-function phenotypes (Schaffrath & Leidel, 2017). A second model describes that codon-specific translation defects upon loss of tRNA wobble modification result in an imbalance between protein synthesis and folding (Schaffrath & Leidel, 2017). As a result, proteotoxic stress

triggers pleiotropic cellular phenotypes by modulating the proteome output or affecting downstream cellular signaling pathways (Schaffrath & Leidel, 2017).

As both models were developed mainly based on observations in yeast, in my PhD project, I aimed to uncover the physiological role of tRNA wobble modification in mammalian cells to understand why $U_{34}$-enzyme-deficient cells become hypersensitive to mTOR inhibition. To systematically characterize the role of $U_{34}$-enzymes in shaping the proteome output, together with Toman Borteçen, we developed a novel normalization method for the QuaNPA workflow that enables the quantification of absolute proteome-wide changes in protein synthesis (method not published yet). By integrating this powerful nascent proteomics approach with steady-state proteomics and ribosome profiling, I could, to my knowledge for the first time, systematically characterize the role of $U_{34}$-enzymes in shaping protein translation and output in mammalian cells. I found that upon loss of $U_{34}$-enzymes, ribosomes accumulated mainly at lysine AAA codons. Consequently, the synthesis of transcripts whose mRNAs were enriched in AAA codons and, to a certain degree, in GAA codons was strongly decreased. I identified protein groups whose synthesis depends on $U_{34}$-enzymes, including ribosomal proteins and other proteins functioning in RNA-related processes. The defect in protein synthesis correlated to some extent with a decrease in steady-state levels. However, effects in the nascent proteome were generally more substantial than changes in the steady-state proteome. This data indicates that AAA and GAA codons, but not CAA codons, are more accurate predictors of $U_{34}$-enzyme-dependent translation. In contrast to the first model, showing that the translation of only an individual VAA codon-rich transcript is affected by the lack of $U_{34}$-enzymes, my work demonstrates that whole classes of proteins enriched in AAA and GAA codons are sensitive to the loss of tRNA wobble modification.

Previous studies in yeast, worms, and mammalian cells described tRNA wobble modifications as critical to translating VAA codons efficiently (Karlsborn *et al.*, 2014; Laguesse *et al.*, 2015; Nedialkova & Leidel, 2015; Rapino *et al.*, 2018; Zinshteyn & Gilbert, 2013). Consequently, several proteins were identified whose levels decreased upon loss of $U_{34}$-enzymes. These proteins were enriched in VAA codons, and thus, their efficient synthesis depends on tRNA wobble modifications (Delaunay *et al.*, 2016; Fernández-Vázquez *et al.*, 2013; Rapino *et al.*, 2018; Rapino *et al.*, 2021; Xu *et al.*,

2019). My data revealed a substantial defect of $U_{34}$-enzyme-deficient cells in synthesizing most proteins. I found that besides the class of ribosomal proteins, the synthesis of other protein groups involved in ribosome biogenesis, ribonucleoprotein complexes, or non-coding RNA processing was also strongly decreased upon loss of $U_{34}$-enzymes. Thus, in contrast to most previous studies, my data suggests that the loss of tRNA wobble modification globally affects translation, partially because of the disrupted production of ribosomal proteins as part of the protein synthesis machinery.

A recent study indicated that in addition to the VAA codon content of the mRNA transcript, an additional hydrophilic motif determines whether translation defects result in protein-level changes (Rapino *et al.*, 2021). I could not find any correlation between this hydrophilic motif and the proteins whose synthesis was most decreased in $U_{34}$-enzyme deficient cells in my nascent proteomics datasets (data not shown). Thus, the hydrophilic motif might be a cell-type-specific phenotype, as the study only used different breast cancer cell lines (Rapino *et al.*, 2021).

Previous studies revealed that the loss of $U_{34}$-enzymes induced pleiotropic phenotypes, including the aggregation of misfolded proteins, and thus led to proteotoxic stress in yeast cells and mammals (Laguesse *et al.*, 2015; Nedialkova & Leidel, 2015; Rapino *et al.*, 2018; Rapino *et al.*, 2021). In my nascent proteomics and steady-state proteomics data, I could not find evidence for the induction of genes belonging to the unfolded protein response or integrated stress response (data not shown). Thus, protein aggregation and proteotoxic stress might not be a conserved phenotype of $U_{34}$-enzyme deficiency in all cell lines, and further studies are needed to clarify this in detail. Moreover, the steady-state proteome in $U_{34}$-enzyme-deficient yeast cells was only mildly disrupted (Rezgui *et al*, 2013; Zinshteyn & Gilbert, 2013). I also observe relatively mild changes in the steady-state proteome upon loss of tRNA wobble modification, indicating that the decreased translation efficiency of VAA codons only partially materializes in the proteome of $U_{34}$-enzyme-deficient cells.

In my data, ribosomal protein production was particularly affected by the loss of $U_{34}$-enzymes, which correlated with their high AAA mRNA codon content. As outlined above, the synthesis of other protein groups also decreased in $U_{34}$-enzyme-deficient cells. Like ribosomal proteins, these nucleic acid-binding protein classes were enriched in lysine, a positively charged amino acid that facilitates interactions with nucleic acids

(Bartas *et al*, 2021; Wyant *et al.*, 2018). Thus, their requirement for lysine codons could explain the disrupted synthesis of nucleic acid-binding proteins. However, the overall reduction in protein synthesis observed upon loss of $U_{34}$-enzymes likely stems, at least partially, from the disrupted ribosome production.

## 5.3 Functional interplay between mTORC1 and tRNA wobble modification

While ribosomal protein synthesis declined with the loss of $U_{34}$-enzymes, their steady-state abundance was only slightly affected. However, as ribosomal proteins make up a large portion of the cellular proteome, comprising 4-6 %, even those modest changes in protein abundance can significantly impact the biomass (Nagaraj *et al.*, 2011; Wisniewski *et al.*, 2014). As I could not find a decrease in cell size or total protein content in $U_{34}$-enzyme-deficient cells (data not shown), their reduced proliferation rate may allow $U_{34}$-enzyme-deficient cells to compensate for the reduced protein synthesis. Notably, the crucial role of $U_{34}$-enzymes in shaping the proteome becomes evident under mTORC1 suppression. The mRNAs of ribosomal proteins carry TOP motifs. Thus, their translation is highly sensitive to mTORC1 activity (Hsieh *et al.*, 2012; Jefferies *et al.*, 1994; Terada *et al.*, 1994; Thoreen *et al.*, 2012). Consequently, the concerted inhibition of mTORC1 and $U_{34}$-enzymes depletes levels of ribosomal proteins, drastically reduces protein synthesis, and restricts cell proliferation substantially.

In budding yeast, the tRNA $U_{34}$ thiolation status was coupled to the availability of the sulfur amino acids cysteine and methionine, linking protein synthesis to nutrient availability (Laxman *et al.*, 2013). Whether tRNA wobble modifications in mammalian cells respond to nutrient availability is still unclear. I starved $U_{34}$-enzyme-deficient EPP2 cells for all amino acids and sulfur amino acids, but I could not find any difference in puromycin incorporation or cell proliferation between Ctu1 KO and control cells (data not shown). Furthermore, a study in fission yeast showed that Elongator promotes translation of TORC2 components and TORC1 repressors (Candiracci *et al.*, 2019). My proteomics datasets did not show any changes in the synthesis or steady-state levels of components of the mTORC1/ mTORC2 signaling pathways (data not shown).

Moreover, a study in mammalian cells showed that the PI3K-mTORC2 axis regulates $U_{34}$-enzymes directly by Elp1 phosphorylation and stabilization (Rapino *et al.*, 2018). In my data, the loss of the mTORC2 component Rictor did not affect the hypersensitivity of Ctu1 KO cells to rapamycin (data not shown), indicating that Ctu1-deficient cells do not depend on mTORC2. Thus, further studies are needed to clarify if a possible co-regulation of mTORC1 and tRNA wobble modification is an additional mechanism to adapt protein translation to environmental changes. Regardless of directly regulating each other, my data suggests that mTORC1 and tRNA wobble modification functionally converge on the downstream process of regulating ribosomal protein synthesis.

## 5.4 The anabolic role of $U_{34}$-enzymes becomes essential upon mTORC1 inhibition

The loss of tRNA wobble modifications rendered yeast cells sensitive to various external stresses such as elevated temperature or nutrient stress. This was interpreted because of defects in VAA codon-rich mRNA translation or proteotoxic stress (Fernández-Vázquez *et al.*, 2013; Laxman *et al.*, 2013; Nedialkova & Leidel, 2015; Zinshteyn & Gilbert, 2013). Moreover, yeast cells became hypersensitive to rapamycin upon loss of $U_{34}$-enzymes, also interpreted as an increased stress sensitivity (Nedialkova & Leidel, 2015; Zinshteyn & Gilbert, 2013). Mechanistically, it was shown in budding yeast that tRNA modifications were required for TOR-dependent regulation of cell growth in response to nitrogen signals (Scheidt *et al.*, 2014). Moreover, a central role of Elongator in regulating levels of TORC1 and TORC2 was shown in fission yeast (Candiracci *et al.*, 2019). Elongator promoted the translation of TORC2 components and TORC1 repressors, which was required for sexual differentiation under nutrient starvation (Candiracci *et al.*, 2019).

In my project, I reported for the first time that mammalian cells also become hypersensitive to mTORC1 inhibition upon loss of tRNA wobble modification. I could not find evidence that $U_{34}$-enzyme-deficient cells show a general stress sensitivity as cell proliferation upon MEK-ERK pathway inhibition or osmotic stress (NaCl; data not shown) was comparable between Ctu1 KO and control EPP2 cells. Moreover,

analyzing my nascent and steady-state proteomics datasets did not reveal any changes in the synthesis or steady-state levels of mTORC1/2 subunits or other mTOR signaling pathway components (data not shown). Thus, my data indicates that the hypersensitivity of $U_{34}$-enzyme-deficient cells to mTORC1 inhibitors is conserved between mammals and yeast. The mechanistic explanation, however, is different.

The previous models contradict many studies that established a critical role of mTORC1 inhibition as an adaptive response to various stresses. Upon mTORC1 suppression, a reduction in protein synthesis allows cells to preserve their resources, and the induction of protein catabolism prevents the accumulation of misfolded proteins (Advani & Ivanov, 2019; Ben-Sahra & Manning, 2017; Saxton & Sabatini, 2017). Additionally, the increased protein catabolism reduces proteotoxic stress through the clearance of aggregated proteins (Heras-Sandoval *et al*, 2014). Consequently, my study provides another explanation for the hypersensitivity of $U_{34}$-enzyme-deficient mammalian cells to mTORC1 suppression. My data revealed a critical role of $U_{34}$-enzymes in generating ribosomal proteins. Under mTORC1 inhibition, this anabolic role becomes essential for mammalian cells. As a result, the concerted suppression of mTORC1 and $U_{34}$-enzymes strongly suppresses cell proliferation as the anabolic capacity of the cell breaks down.

## 5.5 The concerted suppression of mTORC1 and $U_{34}$-enzymes is a potential target to suppress cancer growth

Protein translation is commonly dysregulated in cancer cells to promote aberrant cell proliferation (Bhat *et al.*, 2015). Since many cancer-related mutations affect the translation machinery, it is crucial to understand translation control to target cancers efficiently (Bhat *et al.*, 2015; Truitt & Ruggero, 2016). mTORC1 acts downstream of the PI3K-Akt signaling pathway and induces the translation of components of the protein synthesis machinery and, thus, global protein translation and other anabolic processes (Saxton & Sabatini, 2017). Consequently, activating mutations in PI3K or loss-of-function mutations in PTEN hyperactivate mTORC1 activity in many cancers, which increases cancer growth (Hsieh *et al.*, 2012; Zoncu *et al.*, 2011). Similarly, increased levels of $U_{34}$-enzymes have been identified in several cancers (Suzuki,

2021), and $U_{34}$-enzyme-dependent transcripts with pro-tumorigenic functions in tumor initiation, cancer progression, and therapy resistance were characterized (Delaunay *et al.*, 2016; Ladang *et al.*, 2015; Rapino *et al.*, 2018).

My work suggests that tRNA wobble modifications are required for efficient protein translation by supporting the generation of ribosomal proteins. Targeting upregulated protein translation in cancer is a promising therapeutic target for treatments. However, although the anti-proliferative effects of mTOR inhibitors were promising in cell culture experiments, their efficiency in clinical trials for different cancer types was low (Bhat *et al.*, 2015). In my PhD study, I showed that $U_{34}$-enzyme-deficient cells became hypersensitive to mTORC1 inhibitors and upstream PI3K-Akt signaling pathway inhibitors. Rapamycin, a partial mTORC1 inhibitor that failed in most clinical trials to treat different human cancers (Benjamin *et al.*, 2011), strongly suppressed cell growth of $U_{34}$-enzyme-deficient mouse cell lines *in vitro* and in tumors. Thus, my data suggests that the combined inhibition of mTORC1 and $U_{34}$-enzymes might be a potential cancer therapy.

A conditional Elp3 knockout in the forebrain of mice revealed that the deletion of Elp3 induces the unfolded protein response, resulting in fewer projection neurons in all cortical layers (Laguesse *et al.*, 2015). These defects in neurogenesis led to microcephaly (Laguesse *et al.*, 2015). Thus, directly inhibiting elongator was linked to fatal neurodegeneration. Moreover, the loss of Elp3 is embryonic lethal, indicating an essential role of Elp3 in early development (Yoo *et al*, 2016). In my project, I investigated the relevance of mTORC1 inhibitors for Ctu1-deficient tumor growth *in vivo*. In contrast to Elongator, the only known function of Ctu1/2 is the thiolation of $U_{34}$ at tRNA anticodons (Karlsborn *et al.*, 2014). Thus, whether the inhibition of Ctu1/2 also leads to neurodegeneration, defects in embryonic development, or other toxic effects, as well as the selectivity of potential $U_{34}$-enzyme inhibitors, needs to be clarified in future studies.

The mTORC1 inhibitor rapamycin was initially described as an antifungal agent (Vézina *et al*, 1975). Further studies have shown immunosuppressive and anti-proliferative properties (Laplante & Sabatini, 2012; Saxton & Sabatini, 2017). Consequently, rapamycin was successfully used in animal models of organ transplantation and approved as an immunosuppressive agent (Sehgal, 2003). As the

molecular mechanism of action is well established, many rapamycin analogs (rapalogues) were developed and tested in the clinics (Laplante & Sabatini, 2012). Although the drugs were generally well tolerated, most showed weak therapeutic efficacy in treating cancers (Bhat *et al.*, 2015; Laplante & Sabatini, 2012). As rapamycin strongly suppressed $U_{34}$-enzyme-deficient pancreatic tumor growth in my project, more studies are needed to clarify the efficacy and selectivity of rapamycin treatment combined with $U_{34}$-enzyme inhibitors to suppress cancer growth among various cell types. Differences in the mTORC1 signaling pathway activity among different cancer cell lines may limit the potential of rapamycin in suppressing $U_{34}$-enzyme-deficient tumor growth.

Finally, in my project, I could only observe substantial proliferation defects upon mTOR inhibition in $U_{34}$-enzyme-deficient mouse cell lines carrying an oncogenic KRas mutation. Whether non-transformed cells, primary cells, or non-proliferative cells (mouse and human) also show a substantial reduction in cell proliferation by concerted suppression of $U_{34}$-enzymes and mTORC1 remains to be investigated. I found that in human cells, levels of ribosomal proteins were also depleted upon combined inhibition of tRNA wobble modification and mTORC1; thus, the underlying molecular mechanism is conserved between mouse and human cells. Further studies are needed to clarify the relevance of the combined treatment approach in various mouse and human cell lines with different genetic backgrounds.

## 5.6 Open questions and future perspective

My PhD project established the interplay between mTORC1 and $U_{34}$-enzymes in generating the protein synthesis machinery, thus highlighting the anabolic role of tRNA wobble modifications in mammalian cells. However, further studies are needed to clarify the following questions.

A key question remains whether there is a direct cross-talk between mTORC1 and tRNA wobble modifications. As the $U_{34}$ thiolation status in yeast was coupled to the availability of sulfur amino acids (Laxman *et al.*, 2013), it seems possible that mTORC1 could communicate the nutrient status to $U_{34}$-enzymes to adapt the formation of tRNA

wobble modifications to environmental inputs. Furthermore, in fission yeast, Elongator regulates the translation of TORC1/2 components (Candiracci *et al.*, 2019). As described above, I could not find evidence for a direct cross-talk between mTORC1 and tRNA wobble modification. To understand if mTORC1 directly controls the formation of tRNA wobble modifications, the modifications could be directly measured by mass spectrometry in the presence or absence of mTORC1 inhibitors of $U_{34}$-enzyme-deficient cells. My data suggests that both pathways do not directly regulate each other; their synergy arises from their concerted effect on controlling the production of ribosomal proteins.

Moreover, my data indicates that the synthesis of nucleic acid-binding proteins was particularly affected by the loss of $U_{34}$-enzymes, which correlated with their high AAA mRNA codon content. To understand more in detail how codon biases and the codon distribution along a transcript affect the translation of individual mRNAs, ribosome profiling in combination with RNA sequencing could be performed. These experiments could reveal where exactly ribosomes accumulate along the transcript and help to understand whether defects in translation initiation or elongation are crucial.

As the functional role of tRNA wobble modifications has been mainly studied in yeast so far, it would be interesting to know if my molecular mechanism is conserved in yeast and other organisms. Thus, the relevance of my findings could be further extended.

# 6 References


Advani VM, Ivanov P (2019) Translational Control under Stress: Reshaping the Translatome. *Bioessays* 41: e1900009

Agris PF (2004) Decoding the genome: a modified view. *Nucleic Acids Res* 32: 223-238

Alberts B, Johnson A, Lewis J, Raff M, Roberts K, Walter P (2008) *Molecularbiology of the Cell*. Garland Science, Taylor & Francis Group

An H, Harper JW (2020) Ribosome Abundance Control Via the Ubiquitin–Proteasome System and Autophagy. *J Mol Biol* 432: 170-184

Avcilar-Kucukgoze I, Kashina A (2020) Hijacking tRNAs From Translation: Regulatory Functions of tRNAs in Mammalian Cell Physiology. *Front Mol Biosci* 7: 610617

Bar-Peled L, Chantranupong L, Cherniack AD, Chen WW, Ottina KA, Grabiner BC, Spear ED, Carter SL, Meyerson M, Sabatini DM (2013) A Tumor suppressor complex with GAP activity for the Rag GTPases that signal amino acid sufficiency to mTORC1. *Science* 340: 1100-1106

Bartas M, Červeň J, Guziurová S, Slychko K, Pečinka P (2021) Amino Acid Composition in Various Types of Nucleic Acid-Binding Proteins. *Int J Mol Sci* 22

Baßler J, Hurt E (2019) Eukaryotic Ribosome Assembly. *Annu Rev Biochem* 88: 281-306

Ben-Sahra I, Manning BD (2017) mTORC1 signaling and the metabolic control of cell growth. *Curr Opin Cell Biol* 45: 72-82

Benjamin D, Colombi M, Moroni C, Hall MN (2011) Rapamycin passes the torch: a new generation of mTOR inhibitors. *Nat Rev Drug Discov* 10: 868-880

Bento-Abreu A, Jager G, Swinnen B, Rué L, Hendrickx S, Jones A, Staats KA, Taes I, Eykens C, Nonneman A *et al* (2018) Elongator subunit 3 (ELP3) modifies ALS through tRNA modification. *Hum Mol Genet* 27: 1276-1289

Bhat M, Robichaud N, Hulea L, Sonenberg N, Pelletier J, Topisirovic I (2015) Targeting the translation machinery in cancer. *Nat Rev Drug Discov* 14: 261-278

Bloomfield G, Kay RR (2016) Uses and abuses of macropinocytosis. *J Cell Sci* 129: 2697-2705

Borteçen T, Müller T, Krijgsveld J (2023) An integrated workflow for quantitative analysis of the newly synthesized proteome. *Nature Communications* 14: 8237

Boulias K, Greer EL (2023) Biological roles of adenine methylation in RNA. *Nat Rev Genet* 24: 143-160

Brugarolas J, Lei K, Hurley RL, Manning BD, Reiling JH, Hafen E, Witters LA, Ellisen LW, Kaelin WG, Jr. (2004) Regulation of mTOR function in response to hypoxia by REDD1 and the TSC1/TSC2 tumor suppressor complex. *Genes Dev* 18: 2893-2904

Brunn GJ, Hudson CC, Sekulić A, Williams JM, Hosoi H, Houghton PJ, Lawrence JC, Jr., Abraham RT (1997) Phosphorylation of the translational repressor PHAS-I by the mammalian target of rapamycin. *Science* 277: 99-101

Buttgereit F, Brand MD (1995) A hierarchy of ATP-consuming processes in mammalian cells. *Biochem J* 312 ( Pt 1): 163-167

Candiracci J, Migeot V, Chionh Y-H, Bauer F, Brochier T, Russell B, Shiozaki K, Dedon P, Hermand D (2019) Reciprocal regulation of TORC signaling and tRNA modifications by Elongator enforces nutrient-dependent cell fate. *Science Advances* 5: eaav0184

Chantranupong L, Wolfson RL, Orozco JM, Saxton RA, Scaria SM, Bar-Peled L, Spooner E, Isasa M, Gygi SP, Sabatini DM (2014) The Sestrins interact with GATOR2 to negatively regulate the amino-acid-sensing pathway upstream of mTORC1. *Cell Rep* 9: 1-8

Chen C, Tuck S, Byström AS (2009) Defects in tRNA Modification Associated with Neurological and Developmental Dysfunctions in Caenorhabditis elegans Elongator Mutants. *PLOS Genetics* 5: e1000561

Commisso C, Davidson SM, Soydaner-Azeloglu RG, Parker SJ, Kamphorst JJ, Hackett S, Grabocka E, Nofal M, Drebin JA, Thompson CB *et al* (2013) Macropinocytosis of protein is an amino acid supply route in Ras-transformed cells. *Nature* 497: 633-637

Condon KJ, Orozco JM, Adelmann CH, Spinelli JB, van der Helm PW, Roberts JM, Kunchok T, Sabatini DM (2021) Genome-wide CRISPR screens reveal multitiered mechanisms through which mTORC1 senses mitochondrial dysfunction. *Proc Natl Acad Sci U S A* 118

Crick FH (1966a) Codon--anticodon pairing: the wobble hypothesis. *J Mol Biol* 19: 548-555

Crick FH (1966b) The genetic code--yesterday, today, and tomorrow. *Cold Spring Harb Symp Quant Biol* 31: 1-9

Cunningham JT, Rodgers JT, Arlow DH, Vazquez F, Mootha VK, Puigserver P (2007) mTOR controls mitochondrial oxidative function through a YY1-PGC-1alpha transcriptional complex. *Nature* 450: 736-740

Dalla Venezia N, Vincent A, Marcel V, Catez F, Diaz JJ (2019) Emerging Role of Eukaryote Ribosomes in Translational Control. *Int J Mol Sci* 20

Das AT, Tenenbaum L, Berkhout B (2016) Tet-On Systems For Doxycycline-inducible Gene Expression. *Curr Gene Ther* 16: 156-167

de Almeida M, Hinterndorfer M, Brunner H, Grishkovskaya I, Singh K, Schleiffer A, Jude J, Deswal S, Kalis R, Vunjak M *et al* (2021) AKIRIN2 controls the nuclear import of proteasomes in vertebrates. *Nature* 599: 491-496

Delaunay S, Helm M, Frye M (2024) RNA modifications in physiology and disease: towards clinical applications. *Nature Reviews Genetics* 25: 104-122

Delaunay S, Rapino F, Tharun L, Zhou Z, Heukamp L, Termathe M, Shostak K, Klevernic I, Florin A, Desmecht H *et al* (2016) Elp3 links tRNA modification to IRES-dependent translation of LEF1 to sustain metastasis in breast cancer. *J Exp Med* 213: 2503-2523

Demichev V, Messner CB, Vernardis SI, Lilley KS, Ralser M (2020) DIA-NN: neural networks and interference correction enable deep proteome coverage in high throughput. *Nature Methods* 17: 41-44

Dever TE, Dinman JD, Green R (2018) Translation Elongation and Recoding in Eukaryotes. *Cold Spring Harb Perspect Biol* 10

Dever TE, Green R (2012) The elongation, termination, and recycling phases of translation in eukaryotes. *Cold Spring Harb Perspect Biol* 4: a013706

Dewez M, Bauer F, Dieu M, Raes M, Vandenhaute J, Hermand D (2008) The conserved Wobble uridine tRNA thiolase Ctu1–Ctu2 is required to maintain genome integrity. *Proceedings of the National Academy of Sciences* 105: 5459-5464

Düvel K, Yecies JL, Menon S, Raman P, Lipovsky AI, Souza AL, Triantafellow E, Ma Q, Gorski R, Cleaver S *et al* (2010) Activation of a metabolic gene regulatory network downstream of mTOR complex 1. *Mol Cell* 39: 171-183

Eberlé D, Hegarty B, Bossard P, Ferré P, Foufelle F (2004) SREBP transcription factors: master regulators of lipid homeostasis. *Biochimie* 86: 839-848

Fernández-Vázquez J, Vargas-Pérez I, Sansó M, Buhne K, Carmona M, Paulo E, Hermand D, Rodríguez-Gabriel M, Ayté J, Leidel S *et al* (2013) Modification of tRNA(Lys) UUU by elongator is essential for efficient translation of stress mRNAs. *PLoS Genet* 9: e1003647

Frias MA, Thoreen CC, Jaffe JD, Schroder W, Sculley T, Carr SA, Sabatini DM (2006) mSin1 Is Necessary for Akt/PKB Phosphorylation, and Its Isoforms Define Three Distinct mTORC2s. *Current Biology* 16: 1865-1870

Frye M, Harada BT, Behm M, He C (2018) RNA modifications modulate gene expression during development. *Science* 361: 1346-1349

Furuichi Y (2015) Discovery of m(7)G-cap in eukaryotic mRNAs. *Proc Jpn Acad Ser B Phys Biol Sci* 91: 394-409

Gingras AC, Gygi SP, Raught B, Polakiewicz RD, Abraham RT, Hoekstra MF, Aebersold R, Sonenberg N (1999) Regulation of 4E-BP1 phosphorylation: a novel two-step mechanism. *Genes Dev* 13: 1422-1437

Guertin DA, Stevens DM, Saitoh M, Kinkel S, Crosby K, Sheen JH, Mullholland DJ, Magnuson MA, Wu H, Sabatini DM (2009) mTOR complex 2 is required for the development of prostate cancer induced by Pten loss in mice. *Cancer Cell* 15: 148-159

Guertin DA, Stevens DM, Thoreen CC, Burds AA, Kalaany NY, Moffat J, Brown M, Fitzgerald KJ, Sabatini DM (2006) Ablation in Mice of the mTORC Components raptor, rictor, or mLST8 Reveals that mTORC2 Is Required for Signaling to Akt-FOXO and PKCα, but Not S6K1. *Developmental Cell* 11: 859-871

Haar EV, Lee S-i, Bandhakavi S, Griffin TJ, Kim D-H (2007) Insulin signalling to mTOR mediated by the Akt/PKB substrate PRAS40. *Nature Cell Biology* 9: 316-323

Hara K, Maruki Y, Long X, Yoshino K-i, Oshiro N, Hidayat S, Tokunaga C, Avruch J, Yonezawa K (2002) Raptor, a Binding Partner of Target of Rapamycin (TOR), Mediates TOR Action. *Cell* 110: 177-189

Hart T, Chandrashekhar M, Aregger M, Steinhart Z, Brown KR, MacLeod G, Mis M, Zimmermann M, Fradet-Turcotte A, Sun S *et al* (2015) High-Resolution CRISPR Screens Reveal Fitness Genes and Genotype-Specific Cancer Liabilities. *Cell* 163: 1515-1526

Hawer H, Hammermeister A, Ravichandran KE, Glatt S, Schaffrath R, Klassen R (2018) Roles of Elongator Dependent tRNA Modification Pathways in Neurodegeneration and Cancer. *Genes (Basel)* 10

Heras-Sandoval D, Pérez-Rojas JM, Hernández-Damián J, Pedraza-Chaverri J (2014) The role of PI3K/AKT/mTOR pathway in the modulation of autophagy and the clearance of protein aggregates in neurodegeneration. *Cellular Signalling* 26: 2694-2701

Hershey JW, Sonenberg N, Mathews MB (2012) Principles of translational control: an overview. *Cold Spring Harb Perspect Biol* 4

Hingorani SR, Wang L, Multani AS, Combs C, Deramaudt TB, Hruban RH, Rustgi AK, Chang S, Tuveson DA (2005) Trp53R172H and KrasG12D cooperate to promote chromosomal instability and widely metastatic pancreatic ductal adenocarcinoma in mice. *Cancer Cell* 7: 469-483

Hinnebusch AG (2014) The scanning mechanism of eukaryotic translation initiation. *Annu Rev Biochem* 83: 779-812

Holz MK, Ballif BA, Gygi SP, Blenis J (2005) mTOR and S6K1 mediate assembly of the translation preinitiation complex through dynamic protein interchange and ordered phosphorylation events. *Cell* 123: 569-580

Hsieh AC, Costa M, Zollo O, Davis C, Feldman ME, Testa JR, Meyuhas O, Shokat KM, Ruggero D (2010) Genetic dissection of the oncogenic mTOR pathway reveals druggable addiction to translational control via 4EBP-eIF4E. *Cancer Cell* 17: 249-261

Hsieh AC, Liu Y, Edlind MP, Ingolia NT, Janes MR, Sher A, Shi EY, Stumpf CR, Christensen C, Bonham MJ *et al* (2012) The translational landscape of mTOR signalling steers cancer initiation and metastasis. *Nature* 485: 55-61

Hsu PP, Sabatini DM (2008) Cancer Cell Metabolism: Warburg and Beyond. *Cell* 134: 703-707

Huang B, Johansson MJ, Bystrom AS (2005) An early step in wobble uridine tRNA modification requires the Elongator complex. *RNA* 11: 424-436

Hughes CS, Foehr S, Garfield DA, Furlong EE, Steinmetz LM, Krijgsveld J (2014) Ultrasensitive proteome analysis using paramagnetic bead technology. *Mol Syst Biol* 10: 757

Hurt E, Cheng J, Baßler J, Iwasa J, Beckmann R (2023) SnapShot: Eukaryotic ribosome biogenesis I. *Cell* 186: 2282-2282. e2281

Ingolia NT, Brar GA, Rouskin S, McGeachy AM, Weissman JS (2012) The ribosome profiling strategy for monitoring translation in vivo by deep sequencing of ribosome-protected mRNA fragments. *Nature Protocols* 7: 1534-1550

Inoki K, Zhu T, Guan K-L (2003) TSC2 Mediates Cellular Energy Response to Control Cell Growth and Survival. *Cell* 115: 577-590

Jacinto E, Loewith R, Schmidt A, Lin S, Rüegg MA, Hall A, Hall MN (2004) Mammalian TOR complex 2 controls the actin cytoskeleton and is rapamycin insensitive. *Nature Cell Biology* 6: 1122-1128

Jefferies HB, Reinhard C, Kozma SC, Thomas G (1994) Rapamycin selectively represses translation of the "polypyrimidine tract" mRNA family. *Proc Natl Acad Sci U S A* 91: 4441-4445

Kamphorst JJ, Nofal M, Commisso C, Hackett SR, Lu W, Grabocka E, Vander Heiden MG, Miller G, Drebin JA, Bar-Sagi D *et al* (2015) Human pancreatic cancer tumors are nutrient poor and tumor cells actively scavenge extracellular protein. *Cancer Res* 75: 544-553

Karlsborn T, Tukenmez H, Mahmud AK, Xu F, Xu H, Bystrom AS (2014) Elongator, a conserved complex required for wobble uridine modifications in eukaryotes. *RNA Biol* 11: 1519-1528

Kearse MG, Wilusz JE (2017) Non-AUG translation: a new start for protein synthesis in eukaryotes. *Genes Dev* 31: 1717-1731

Kim D-H, Sarbassov DD, Ali SM, King JE, Latek RR, Erdjument-Bromage H, Tempst P, Sabatini DM (2002) mTOR Interacts with Raptor to Form a Nutrient-Sensitive Complex that Signals to the Cell Growth Machinery. *Cell* 110: 163-175

Kim E, Goraksha-Hicks P, Li L, Neufeld TP, Guan KL (2008) Regulation of TORC1 by Rag GTPases in nutrient response. *Nat Cell Biol* 10: 935-945

Kim J, Kundu M, Viollet B, Guan K-L (2011) AMPK and mTOR regulate autophagy through direct phosphorylation of Ulk1. *Nat Cell Biol* 13: 132-141

Kim LC, Cook RS, Chen J (2017) mTORC1 and mTORC2 in cancer and the tumor microenvironment. *Oncogene* 36: 2191-2201

Kozak M (1989) The scanning model for translation: an update. *J Cell Biol* 108: 229-241

Ladang A, Rapino F, Heukamp LC, Tharun L, Shostak K, Hermand D, Delaunay S, Klevernic I, Jiang Z, Jacques N *et al* (2015) Elp3 drives Wnt-dependent tumor initiation and regeneration in the intestine. *J Exp Med* 212: 2057-2075

Laguesse S, Creppe C, Nedialkova DD, Prévot PP, Borgs L, Huysseune S, Franco B, Duysens G, Krusy N, Lee G *et al* (2015) A Dynamic Unfolded Protein Response Contributes to the Control of Cortical Neurogenesis. *Dev Cell* 35: 553-567

Lam YW, Lamond AI, Mann M, Andersen JS (2007) Analysis of nucleolar protein dynamics reveals the nuclear degradation of ribosomal proteins. *Curr Biol* 17: 749-760

Laplante M, Sabatini David M (2012) mTOR Signaling in Growth Control and Disease. *Cell* 149: 274-293

Laxman S, Sutter BM, Wu X, Kumar S, Guo X, Trudgian DC, Mirzaei H, Tu BP (2013) Sulfur amino acids regulate translational capacity and metabolic homeostasis through modulation of tRNA thiolation. *Cell* 154: 416-429

Lee S, Liu B, Lee S, Huang S-X, Shen B, Qian S-B (2012) Global mapping of translation initiation sites in mammalian cells at single-nucleotide resolution. *Proceedings of the National Academy of Sciences* 109: E2424-E2432

Leimkuhler S, Buhning M, Beilschmidt L (2017) Shared Sulfur Mobilization Routes for tRNA Thiolation and Molybdenum Cofactor Biosynthesis in Prokaryotes and Eukaryotes. *Biomolecules* 7

Li J, Kim Sang G, Blenis J (2014a) Rapamycin: One Drug, Many Effects. *Cell Metabolism* 19: 373-379

Li W, Xu H, Xiao T, Cong L, Love MI, Zhang F, Irizarry RA, Liu JS, Brown M, Liu XS (2014b) MAGeCK enables robust identification of essential genes from genome-scale CRISPR/Cas9 knockout screens. *Genome Biology* 15: 554

Lito P, Saborowski A, Yue J, Solomon M, Joseph E, Gadal S, Saborowski M, Kastenhuber E, Fellmann C, Ohara K *et al* (2014) Disruption of CRAF-mediated MEK activation is required for effective MEK inhibition in KRAS mutant tumors. *Cancer Cell* 25: 697-710

Loayza-Puch F, Rooijers K, Buil LC, Zijlstra J, Oude Vrielink JF, Lopes R, Ugalde AP, van Breugel P, Hofland I, Wesseling J *et al* (2016) Tumour-specific proline vulnerability uncovered by differential ribosome codon reading. *Nature* 530: 490-494

Long X, Lin Y, Ortiz-Vega S, Yonezawa K, Avruch J (2005) Rheb Binds and Regulates the mTOR Kinase. *Current Biology* 15: 702-713

Manning BD, Tee AR, Logsdon MN, Blenis J, Cantley LC (2002) Identification of the Tuberous Sclerosis Complex-2 Tumor Suppressor Gene Product Tuberin as a Target of the Phosphoinositide 3-Kinase/Akt Pathway. *Molecular Cell* 10: 151-162

Martina JA, Chen Y, Gucek M, Puertollano R (2012) MTORC1 functions as a transcriptional regulator of autophagy by preventing nuclear transport of TFEB. *Autophagy* 8: 903-914

Martineau Y, Azar R, Bousquet C, Pyronnet S (2013) Anti-oncogenic potential of the eIF4E-binding proteins. *Oncogene* 32: 671-677

McMahon M, Ruggero D (2018) A wobbly road to drug resistance in melanoma: tRNA-modifying enzymes in translation reprogramming. *EMBO J* 37

Merrick WC (2004) Cap-dependent and cap-independent translation in eukaryotic systems. *Gene* 332: 1-11

Michlits G, Jude J, Hinterndorfer M, de Almeida M, Vainorius G, Hubmann M, Neumann T, Schleiffer A, Burkard TR, Fellner M *et al* (2020) Multilayered VBC score predicts sgRNAs that efficiently generate loss-of-function alleles. *Nat Methods* 17: 708-716

Milton CK, Self AJ, Clarke PA, Banerji U, Piccioni F, Root DE, Whittaker SR (2020) A Genome-scale CRISPR Screen Identifies the ERBB and mTOR Signaling Networks as Key Determinants of Response to PI3K Inhibition in Pancreatic Cancer. *Mol Cancer Ther* 19: 1423-1435

Müller T, Kalxdorf M, Longuespée R, Kazdal DN, Stenzinger A, Krijgsveld J (2020) Automated sample preparation with SP3 for low-input clinical proteomics. *Mol Syst Biol* 16: e9111

Nagaraj N, Wisniewski JR, Geiger T, Cox J, Kircher M, Kelso J, Pääbo S, Mann M (2011) Deep proteome and transcriptome mapping of a human cancer cell line. *Mol Syst Biol* 7: 548

Nedialkova DD, Leidel SA (2015) Optimization of Codon Translation Rates via tRNA Modifications Maintains Proteome Integrity. *Cell* 161: 1606-1618

Nojima H, Tokunaga C, Eguchi S, Oshiro N, Hidayat S, Yoshino K, Hara K, Tanaka N, Avruch J, Yonezawa K (2003) The mammalian target of rapamycin (mTOR) partner, raptor, binds the mTOR substrates p70 S6 kinase and 4E-BP1 through their TOR signaling (TOS) motif. *J Biol Chem* 278: 15461-15464

Orth M, Metzger P, Gerum S, Mayerle J, Schneider G, Belka C, Schnurr M, Lauber K (2019) Pancreatic ductal adenocarcinoma: biological hallmarks, current status, and future perspectives of combined modality treatment approaches. *Radiation Oncology* 14: 141

Palm W (2019) Metabolic functions of macropinocytosis. *Philos Trans R Soc Lond B Biol Sci* 374: 20180285

Palm W, Park Y, Wright K, Pavlova NN, Tuveson DA, Thompson CB (2015) The Utilization of Extracellular Proteins as Nutrients Is Suppressed by mTORC1. *Cell* 162: 259-270

Palm W, Thompson CB (2017) Nutrient acquisition strategies of mammalian cells. *Nature* 546: 234-242

Pearce Laura R, Huang X, Boudeau J, Pawłowski R, Wullschleger S, Deak M, Ibrahim Adel FM, Gourlay R, Magnuson Mark A, Alessi Dario R (2007) Identification of Protor as a novel Rictor-binding component of mTOR complex-2. *Biochemical Journal* 405: 513-522

Pechincha C, Groessl S, Kalis R, de Almeida M, Zanotti A, Wittmann M, Schneider M, de Campos RP, Rieser S, Brandstetter M *et al* (2022) Lysosomal enzyme trafficking factor LYSET enables nutritional usage of extracellular proteins. *Science* 378: eabn5637

Peterson TR, Laplante M, Thoreen CC, Sancak Y, Kang SA, Kuehl WM, Gray NS, Sabatini DM (2009) DEPTOR is an mTOR inhibitor frequently overexpressed in multiple myeloma cells and required for their survival. *Cell* 137: 873-886

Peterson TR, Sengupta SS, Harris TE, Carmack AE, Kang SA, Balderas E, Guertin DA, Madden KL, Carpenter AE, Finck BN *et al* (2011) mTOR complex 1 regulates lipin 1 localization to control the SREBP pathway. *Cell* 146: 408-420

Porstmann T, Santos CR, Griffiths B, Cully M, Wu M, Leevers S, Griffiths JR, Chung YL, Schulze A (2008) SREBP activity is regulated by mTORC1 and contributes to Akt-dependent cell growth. *Cell Metab* 8: 224-236

Preiss T, Hentze MW (2003) Starting the protein synthesis machine: eukaryotic translation initiation. *Bioessays* 25: 1201-1211

Rapino F, Delaunay S, Rambow F, Zhou Z, Tharun L, De Tullio P, Sin O, Shostak K, Schmitz S, Piepers J *et al* (2018) Codon-specific translation reprogramming promotes resistance to targeted therapy. *Nature* 558: 605-609

Rapino F, Zhou Z, Roncero Sanchez AM, Joiret M, Seca C, El Hachem N, Valenti G, Latini S, Shostak K, Geris L *et al* (2021) Wobble tRNA modification and hydrophilic amino acid patterns dictate protein fate. *Nat Commun* 12: 2170

Rathert P, Roth M, Neumann T, Muerdter F, Roe J-S, Muhar M, Deswal S, Cerny-Reiterer S, Peter B, Jude J *et al* (2015) Transcriptional plasticity promotes primary and acquired resistance to BET inhibition. *Nature* 525: 543-547

Ratto E, Chowdhury SR, Siefert NS, Schneider M, Wittmann M, Helm D, Palm W (2022) Direct control of lysosomal catabolic activity by mTORC1 through regulation of V-ATPase assembly. *Nature Communications* 13: 4848

Rezgui VA, Tyagi K, Ranjan N, Konevega AL, Mittelstaet J, Rodnina MV, Peter M, Pedrioli PG (2013) tRNA tKUUU, tQUUG, and tEUUC wobble position modifications fine-tune protein translation by promoting ribosome A-site binding. *Proc Natl Acad Sci U S A* 110: 12289-12294

Ritchie ME, Phipson B, Wu D, Hu Y, Law CW, Shi W, Smyth GK (2015) limma powers differential expression analyses for RNA-sequencing and microarray studies. *Nucleic Acids Res* 43: e47

Rossiter NJ, Huggler KS, Adelmann CH, Keys HR, Soens RW, Sabatini DM, Cantor JR (2021) CRISPR screens in physiologic medium reveal conditionally essential genes in human cells. *Cell Metab* 33: 1248-1263 e1249

Roundtree IA, Evans ME, Pan T, He C (2017) Dynamic RNA Modifications in Gene Expression Regulation. *Cell* 169: 1187-1200

Roux PP, Ballif BA, Anjum R, Gygi SP, Blenis J (2004) Tumor-promoting phorbol esters and activated Ras inactivate the tuberous sclerosis tumor suppressor complex via p90 ribosomal S6 kinase. *Proceedings of the National Academy of Sciences* 101: 13489-13494

Sabatini DM (2017) Twenty-five years of mTOR: Uncovering the link from nutrients to growth. *Proc Natl Acad Sci U S A* 114: 11818-11825

Saikia M, Wang X, Mao Y, Wan J, Pan T, Qian SB (2016) Codon optimality controls differential mRNA translation during amino acid starvation. *Rna* 22: 1719-1727

Sancak Y, Bar-Peled L, Zoncu R, Markhard AL, Nada S, Sabatini DM (2010) Ragulator-Rag complex targets mTORC1 to the lysosomal surface and is necessary for its activation by amino acids. *Cell* 141: 290-303

Sancak Y, Thoreen CC, Peterson TR, Lindquist RA, Kang SA, Spooner E, Carr SA, Sabatini DM (2007) PRAS40 Is an Insulin-Regulated Inhibitor of the mTORC1 Protein Kinase. *Molecular Cell* 25: 903-915

Sanjana NE, Shalem O, Zhang F (2014) Improved vectors and genome-wide libraries for CRISPR screening. *Nature Methods* 11: 783-784

Saxton RA, Chantranupong L, Knockenhauer KE, Schwartz TU, Sabatini DM (2016) Mechanism of arginine sensing by CASTOR1 upstream of mTORC1. *Nature* 536: 229-233

Saxton RA, Sabatini DM (2017) mTOR Signaling in Growth, Metabolism, and Disease. *Cell* 168: 960-976

Schaffrath R, Leidel SA (2017) Wobble uridine modifications-a reason to live, a reason to die?! *RNA Biol* 14: 1209-1222

Scheidt V, Judes A, Bar C, Klassen R, Schaffrath R (2014) Loss of wobble uridine modification in tRNA anticodons interferes with TOR pathway signaling. *Microb Cell* 1: 416-424

Schimmel P (2018) The emerging complexity of the tRNA world: mammalian tRNAs beyond protein synthesis. *Nat Rev Mol Cell Biol* 19: 45-58

Sehgal SN (2003) Sirolimus: its discovery, biological properties, and mechanism of action. *Transplantation Proceedings* 35: S7-S14

Settembre C, Zoncu R, Medina DL, Vetrini F, Erdin S, Erdin S, Huynh T, Ferron M, Karsenty G, Vellard MC *et al* (2012) A lysosome-to-nucleus signalling mechanism senses and regulates the lysosome via mTOR and TFEB. *Embo j* 31: 1095-1108

Shi H, Chai P, Jia R, Fan X (2020) Novel insight into the regulatory roles of diverse RNA modifications: Re-defining the bridge between transcription and translation. *Molecular Cancer* 19: 78

Shu XE, Swanda RV, Qian SB (2020) Nutrient Control of mRNA Translation. *Annu Rev Nutr* 40: 51-75

Sung MK, Reitsma JM, Sweredoski MJ, Hess S, Deshaies RJ (2016) Ribosomal proteins produced in excess are degraded by the ubiquitin-proteasome system. *Mol Biol Cell* 27: 2642-2652

Suzuki T (2021) The expanding world of tRNA modifications and their disease relevance. *Nat Rev Mol Cell Biol* 22: 375-392

Tee AR, Fingar DC, Manning BD, Kwiatkowski DJ, Cantley LC, Blenis J (2002) Tuberous sclerosis complex-1 and -2 gene products function together to inhibit mammalian target of rapamycin (mTOR)-mediated downstream signaling. *Proceedings of the National Academy of Sciences* 99: 13571-13576

Terada N, Patel HR, Takase K, Kohno K, Nairn AC, Gelfand EW (1994) Rapamycin selectively inhibits translation of mRNAs encoding elongation factors and ribosomal proteins. *Proc Natl Acad Sci U S A* 91: 11477-11481

Thoreen CC, Chantranupong L, Keys HR, Wang T, Gray NS, Sabatini DM (2012) A unifying model for mTORC1-mediated regulation of mRNA translation. *Nature* 485: 109-113

Thoreen CC, Kang SA, Chang JW, Liu Q, Zhang J, Gao Y, Reichling LJ, Sim T, Sabatini DM, Gray NS (2009) An ATP-competitive mammalian target of rapamycin inhibitor reveals rapamycin-resistant functions of mTORC1. *J Biol Chem* 284: 8023-8032

Truitt ML, Ruggero D (2016) New frontiers in translational control of the cancer genome. *Nature Reviews Cancer* 16: 288-304

Tyanova S, Temu T, Cox J (2016) The MaxQuant computational platform for mass spectrometry-based shotgun proteomics. *Nature Protocols* 11: 2301-2319

Vézina C, Kudelski A, Sehgal SN (1975) Rapamycin (AY-22,989), a new antifungal antibiotic. I. Taxonomy of the producing streptomycete and isolation of the active principle. *J Antibiot (Tokyo)* 28: 721-726

Wan X, Harkavy B, Shen N, Grohar P, Helman LJ (2007) Rapamycin induces feedback activation of Akt signaling through an IGF-1R-dependent mechanism. *Oncogene* 26: 1932-1940

Wang T, Birsoy K, Hughes NW, Krupczak KM, Post Y, Wei JJ, Lander ES, Sabatini DM (2015) Identification and characterization of essential genes in the human genome. *Science* 350: 1096-1101

Wang T, Wei JJ, Sabatini DM, Lander ES (2014) Genetic screens in human cells using the CRISPR-Cas9 system. *Science* 343: 80-84

Wisniewski JR, Hein MY, Cox J, Mann M (2014) A "proteomic ruler" for protein copy number and concentration estimation without spike-in standards. *Mol Cell Proteomics* 13: 3497-3506

Wu T, Hu E, Xu S, Chen M, Guo P, Dai Z, Feng T, Zhou L, Tang W, Zhan L *et al* (2021) clusterProfiler 4.0: A universal enrichment tool for interpreting omics data. *Innovation (Camb)* 2: 100141

Wyant GA, Abu-Remaileh M, Frenkel EM, Laqtom NN, Dharamdasani V, Lewis CA, Chan SH, Heinze I, Ori A, Sabatini DM (2018) NUFIP1 is a ribosome receptor for starvation-induced ribophagy. *Science* 360: 751-758

Xu S, Zhan M, Jiang C, He M, Yang L, Shen H, Huang S, Huang X, Lin R, Shi Y *et al* (2019) Genome-wide CRISPR screen identifies ELP5 as a determinant of gemcitabine sensitivity in gallbladder cancer. *Nat Commun* 10: 5492

Yan G, Yang J, Li W, Guo A, Guan J, Liu Y (2023) Genome-wide CRISPR screens identify ILF3 as a mediator of mTORC1-dependent amino acid sensing. *Nat Cell Biol* 25: 754-764

Yang H, Rudge DG, Koos JD, Vaidialingam B, Yang HJ, Pavletich NP (2013) mTOR kinase structure, mechanism and regulation. *Nature* 497: 217-223

Ye J, Palm W, Peng M, King B, Lindsten T, Li MO, Koumenis C, Thompson CB (2015) GCN2 sustains mTORC1 suppression upon amino acid deprivation by inducing Sestrin2. *Genes Dev* 29: 2331-2336

Yoo H, Son D, Jang YJ, Hong K (2016) Indispensable role for mouse ELP3 in embryonic stem cell maintenance and early development. *Biochem Biophys Res Commun* 478: 631-636

Yu C, Luo D, Yu J, Zhang M, Zheng X, Xu G, Wang J, Wang H, Xu Y, Jiang K *et al* (2022) Genome-wide CRISPR-cas9 knockout screening identifies GRB7 as a driver for MEK inhibitor resistance in KRAS mutant colon cancer. *Oncogene* 41: 191-203

Yu Y, Yoon SO, Poulogiannis G, Yang Q, Ma XM, Villen J, Kubica N, Hoffman GR, Cantley LC, Gygi SP *et al* (2011) Phosphoproteomic analysis identifies Grb10 as an mTORC1 substrate that negatively regulates insulin signaling. *Science* 332: 1322-1326

Zhu Y, Orre LM, Zhou Tran Y, Mermelekas G, Johansson HJ, Malyutina A, Anders S, Lehtiö J (2020) DEqMS: A Method for Accurate Variance Estimation in Differential Protein Expression Analysis. *Mol Cell Proteomics* 19: 1047-1057

Zinshteyn B, Gilbert WV (2013) Loss of a conserved tRNA anticodon modification perturbs cellular signaling. *PLoS Genet* 9: e1003675

Zoncu R, Efeyan A, Sabatini DM (2011) mTOR: from growth signal integration to cancer, diabetes and ageing. *Nat Rev Mol Cell Biol* 12: 21-35